2002

The applications of laser spectroscopy in analytical chemistry and biochemistry: investigating the photophysics of hypericin and hypocrellin, as well as the structure of porcine fructose-1,6-bisphosphatase

Jin Wen
Iowa State University

The applications of laser spectroscopy in analytical chemistry and biochemistry: investigating the photophysics of hypericin and hypocrellin, as well as the structure of porcine fructose-1,6-bisphosphatase

by

Jin Wen

A dissertation submitted to the graduate faculty
in partial fulfillment of the requirements for the degree of
DOCTOR OF PHILOSOPHY

Major: Analytical Chemisty

Program of Study Committee:
Jacob W. Petrich, Major Professor
Mark S. Hargrove
Mei Hong
Victor S.-Y. Lin
Marc D. Porter

Iowa State University
Ames, Iowa
2002

UMI Number: 3061874

UMI Microform 3061874

ProQuest Information and Learning Company
300 North Zeeb Road
P.O. Box 1346
Ann Arbor, MI 48106-1346

Graduate College

Iowa State University

This is to certify that the doctoral dissertation of

Jin Wen

has met the dissertation requirements of Iowa State University

Signature was redacted for privacy.

Major Professor

Signature was redacted for privacy.

For the Major Program

Dedicated to my parents and my husband

TABLE OF CONTENTS

CHAPTER I: INTRODUCTION

General Introduction

Fluorescence is the phenomenon in which absorption of light of a given wavelength by a fluorophore is followed by the emission of light at longer wavelengths. There are three major advantages of fluorescence detection over other light-based investigation methods: high sensitivity (detection limit is as low as 10^{-15} mol·L^{-1}), high speed, and safety (samples are not affected or destroyed in the process, and no hazardous byproducts are generated). Fluorescence spectroscopy techniques have been developed during the past forty years, and the applications of these techniques have had a remarkable growth in the biological sciences in the past 20 years. Steady-state fluorescence spectroscopy and time-resolved fluorescence spectroscopy are two important research tools in biochemical and biophysical studies. Currently, the fluorescence techniques are also applied in areas such as environmental monitoring, clinical chemistry, DNA sequencing, genetic analysis, cell identification and etc.

Steady-state fluorescence spectroscopy and time-resolved fluorescence spectroscopy are the two major techniques used in my dissertation work. It is important to discuss briefly the basic principles of fluorescence spectroscopy [1, 2]. This discussion will be followed by a brief introduction of the major problems treated in this dissertation.

Fluorescence Spectroscopy

What happens after a photon excites a molecule originally in the ground state is usually illustrated by a Jablonski diagram (Figure 1.1). Molecules in excited vibrational states rapidly dissipate their excess vibrational energy and relax to the ground vibrational level in a given excited state. Internal conversion (typically a horizontal transition, *i.e.*

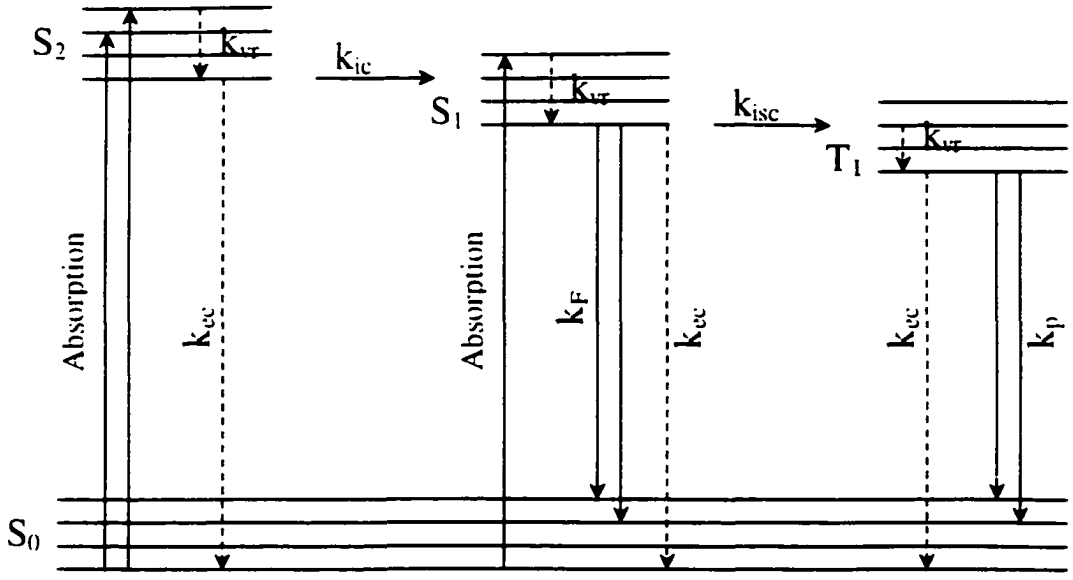

Figure 1.1 Jablonski diagram gives a picture of what would possible happen in a molecule after one photon absorbed. S_0 is singlet ground state, S_1 and S_2 are two possible singlet excited states, and T_1 is triplet excited state. The sublevels in each of the electronic states are vibrational states. The number of vibrational levels in different electronic states may vary. The rate of non-radiative transition (k_{nr}) is the sum of vibrational relaxation (k_{vr}), internal conversion (k_{ic}), external conversion (k_{ec}), and intersystem crossing (k_{isc}). k_F and k_P is the rate of fluorescence and rate of phosphorescence, respectively.

$S_1 \rightarrow S_2$), external conversion (*i.e.* energy transfer or collisions between the excited fluorophore and the solvent or other solute molecules), and intersystem crossing ($S_1 \rightarrow T_1$) are three types of nonradiative transitions. Fluorescence is a radiative transition between electronic states of the same multiplicity. Because internal conversion to S_1 and vibrational relaxation are more rapid processes than fluorescence, fluorescence usually occurs from the ground vibrational state of S_1 to various vibrational levels in S_0.

Quantum Yield

The fluorescence quantum yield or fluorescence quantum efficiency is the ratio of the number of photons emitted to the number absorbed. It can be expressed by the equation:

$$\Phi_F = \frac{k_F}{k_F + k_{nr}} \qquad (1\text{-}1)$$

Where k_F is the rate constant for fluorescence and k_{nr} is the sum of the rate constants for nonradiative processes, $k_{nr} = k_{ec} + k_{ic} + k_{isc}$ where k_{ec}, k_{ic} and k_{isc} are the rate constants for external conversion (ec), internal conversion (ic) and intersystem crossing (isc), respectively. The easiest way to estimate quantum yield of a fluorophore is by comparison with standards of known quantum yield.

$$\Phi_F = \Phi_R \frac{1-10^{-A_R}}{1-10^{-A}} \frac{\int F_F d\tilde{\nu}}{\int F_R d\tilde{\nu}} \frac{n^2}{n_R^2} \qquad (1\text{-}2)$$

Where Φ_R is the quantum yield of the standard, A is the absorbance at the excitation wavelength, n is the refractive index of the solvent and $\int F d\tilde{\nu}$ is the integral of the corrected emission spectrum. Usually, sample and standard are excited at the same wavelength so that it is not necessary to correct for the different excitation intensities for different wavelengths. Some of the most common used standards are listed in Table 1.1.

Fluorescence Lifetime

Besides quantum yield, fluorescence lifetime is another important characteristics of fluorophores. The fluorescence lifetime is the average time that a fluorophore spends in the excited state before emitting a photon of light and returning to the ground state. Most fluorescent materials (biological & chemical) have lifetimes in the range of picosecond (10^{-12} sec) to microsecond (10^{-6}sec). The lifetime of fluorophore is related to the rate constants with the following equation:

$$\tau_F \doteq (k_F + k_{nr})^{-1} \qquad (1\text{-}3)$$

Table 1.1 Quantum Yield Standards

Compound	Solvent	Φ_F	Reference
Tryptophan	Water	0.13	[3]
Hypericin	DMSO	0.32	[4]
Rhodamine 6G	Ethanol	0.94	[5]
Rhodamine 101	Ethanol	1.0	[6]
9,10-DPA[a]	Cyclohexane	0.95	[7]

[a] 9,10-DPA is 9,10-Diphenylanthracene

If there is no any nonradiative process, the lifetime is called intrinsic or natural lifetime (τ_n) and is given by:

$$\tau_n = 1/k_F \qquad (1\text{-}4)$$

Combine equations 1-1, 1-3 and 1-4, a relationship between quantum yield and lifetime is given by:

$$\Phi_F = \tau_F / \tau_n \qquad (1\text{-}5)$$

There are several direct or indirect methods to measure the fluorescence lifetime. Time-correlated single photon counting (TCSPC) is one of the popular methods used in time-domain lifetime measurement. The principle and instrumentation of TCSPC will be discussed in detail in Chapter II.

Fluorescence Quenching

Fluorescence intensity will be reduced by a wide variety of mechanisms. The processes that quench the fluorescence intensity include collision, energy transfer, charge

transfer, the emission being reabsorbed by the fluorophores in the solution and etc. The Stern-Volmer equation (1-6) is a well-known equation used to model the collisional quenching.

$$\frac{F_0}{F} = \frac{\tau_0}{\tau} = 1 + K_{SV}[Q] = 1 + k_q \tau_0 [Q] \qquad (1\text{-}6)$$

Where τ and τ_0 is the lifetime in the presence and absence of quencher, respectively, K_{SV} is the Stern-Volmer quenching constant, k_q is the biomolecular quenching constant, and [Q] is the quencher concentration. The Stern-Volmer equation is widely used to determine the accessibility of fluorophore (usually is tryptophan) in proteins in water. For example, if a tryptophan residue is buried inside the protein, an aqueous soluble quencher would not quench the intensity of fluorescence if it does not easily penetrate the protein; on the other hand, quenching occurs if the tryptophan residue is on the surface of the protein. Acrylamide and iodide are the two quencher commonly used because they do not denature the protein.

Fluorescence Resonance Energy Transfer (FRET)

Several nonradiative processes occur after a fluorophore absorbs a photon (Figure 1.1), fluorescence resonance energy transfer is one of the important processes. Energy transfer can occur when a donor's emission spectrum overlaps with an acceptor's absorption spectrum. This is not the result of emission from the donor being absorbed by the acceptor. There is no photon involved in FRET. The reason that FRET has become a valuable tool for studying biomoleculars is that the efficiency of energy transfer has a strong inverse dependence on the distance between the donor and acceptor [1]. Thus, the appearance of FRET is a highly specific indicator of the proximity of the two molecules. This led to the idea of using FRET efficiency as a "spectroscopic ruler" to measure molecular distances [8].

The concept of FRET was first introduced by Förster in 1948 [9]. The rate of energy transfer is given by Förster equation:

$$k_T = \frac{1}{\tau_D}\left(\frac{R_0}{r}\right)^6 \qquad (1\text{-}7)$$

Where τ_D is the lifetime of the donor in the absence of acceptor, R_0 is the Förster distance, and r is the distance between donor and acceptor. From the equation, one can easily conclude that when the donor-acceptor distance is equal to the Förster distance, the rate of energy transfer is equal to the radiative decay rate of donor in the absence of acceptor. The Förster distance (R_0) can be estimated from the donor's emission spectrum, acceptor's absorption spectrum and the quantum yield of donor [10]:

$$R_0 = 9.78\times10^3[\kappa^2 n^{-4}\Phi_D J]^{1/6} \qquad (1\text{-}8)$$

$$J = \int_0^\infty \frac{F_D(\tilde{\upsilon})\varepsilon_A(\tilde{\upsilon})}{\tilde{\upsilon}^4} d\tilde{\upsilon} \qquad (1\text{-}9)$$

κ^2 is the dipole-dipole orientation factor and it is usually assumed to be 2/3, n is the refractive index of the solvent, Φ_D is the fluorescence quantum yield of the donor, $F_D(\tilde{\upsilon})$ is the corrected emission spectrum of donor with its area normalized to unity in a wavenumber unit, $\varepsilon_A(\tilde{\upsilon})$ is the acceptor molar extinction coefficient at wavenumber $\tilde{\upsilon}$. The unit of Förster distance obtained from equation (1-8) is Å. The Förster distance is typically in the range of 20 ~ 60 Å.

Fluorescence Anisotropy

When polarized light is used to excite fluorophores in an isotropic solution, only those whose electric dipoles are aligned parallel to the plane of polarization of the incident

beam absorb the light. Before the absorption of light, the fluorophores are oriented randomly in the solution, the selective absorption results in a partially oriented population of fluorophores and in partially polarized fluorescence emission. The dipole orientation of the emission is parallel to the transition moment of each molecule. If the molecules are unable to rotate during the lifetime of the excited state, then the plane of polarization of the fluorescence will be parallel to that of the exciting light. However, if the fluorophores are able to rotate within this time period, then the degree of polarization will diminished with time. The emission is depolarized by a number of phenomena. Rotational diffusion is one major cause. Anisotropy measurement provides information on the size and shape of proteins or the rigidity of various molecular environments. Fluorescence anisotropy measurement will be discussed in Chapter II.

Hypericin and Hypocrellin

Hypericin (4,5,7,4',5',7'–hexahydroxy 2,2'dimethyl-meso naphthodianthrone) is a naturally occurring polycyclic aromatic dianthraquinone (Figure 1.2). It can be extracted from plants of the *Hypericum perforatum*, commonly known as St. John's wort.

The healing properties of St. John's Wort have long been known. Throughout the ancient world the Greeks used it as a skin balm and it figured prominently in prechristian celtic rituals, both for magical purposes and as a calming agent. Now in the twenty first century St. John's Wort is still exerting its medicinal qualities as a natural herbal remedy for depression. In the late 1980s, Meruelo et al. reported that hypericin and pseudohypericin inactivated or blocked the reproduction of certain retroviruses in mice [11]. This led to speculation that those compounds might have the similar effect to human retroviruses, like HIV (human immunodeficiency virus) that causes acquired immunodeficiency syndrome

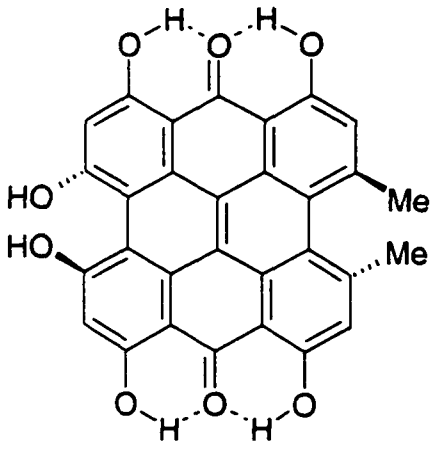

(a)

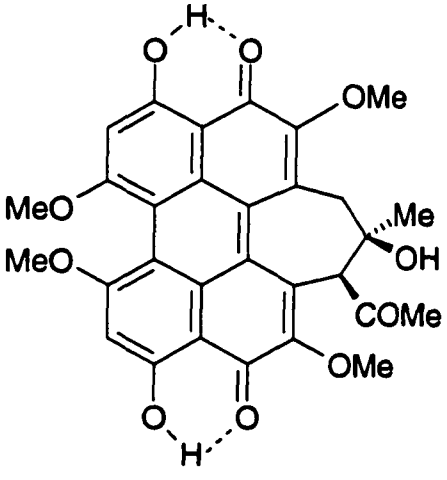

(b)

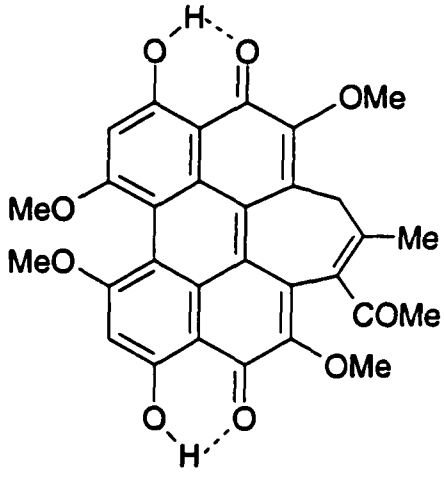

(c)

Figure 1.2 Structure of (**a**) hypericin, (**b**) hypocrellin A, and (**c**) hypocrellin B.

(AIDS). Recent research results showed that hypericin could destroy the equine infectious anemia virus (EIAV) and the related human immunodeficiency virus [12-16]. Besides the clinical and pre-clinical studies toward hypericin, the relevant chemical, physical and biological characterizations were carried out by several researchers [17-20]. Several studies showed that the presence of light is important for the antiviral and antitumor activities of hypericin [21-23]. However, the molecular basis of this mechanism is still not well understood. Several mechanisms have been suggested including light-induced acidification [24], singlet oxygen [25], free radical and superoxide [26], and excited-state H-atom transfer [27].

Hypocrellin, a naturally occurring polycyclic quinone found in a kind of mold (*Hypocrella bambusae*) common in China, is another exciting potential photodynamic therapy (PDT) agent. Hypocrellin includes hypocrellin A and hypocrellin B (Figure 1.2). Like hypericin, hypocrellin also displays significant light-induced antiviral activity against enveloped lentiviruses such as HIV [28, 29].

The structural similarities of hypericin and hypocrellin have been the basis for performing comparative studies on them. Notably, they acidify the surrounding media in the presence of light [24, 30]. Unlike hypericin, which maintains measurable virucidal activity at low oxygen level, hypocrellin absolutely requirs oxygen for its antiviral activity [22]. The study of the primary photophysics of hypericin and hypocrellin show that they both display excited-state intramolecular H-atom transfer. The time constant in hypericin is ~10ps [31], does not depend on viscosity, and depends only very weakly on solvent [32]. The transfer rate in hypocrellin has a strong dependence on the solvent viscosity and the time constant ranges from 10ps to 250ps in the solvent studied [33]. A ~10ps component is also detected

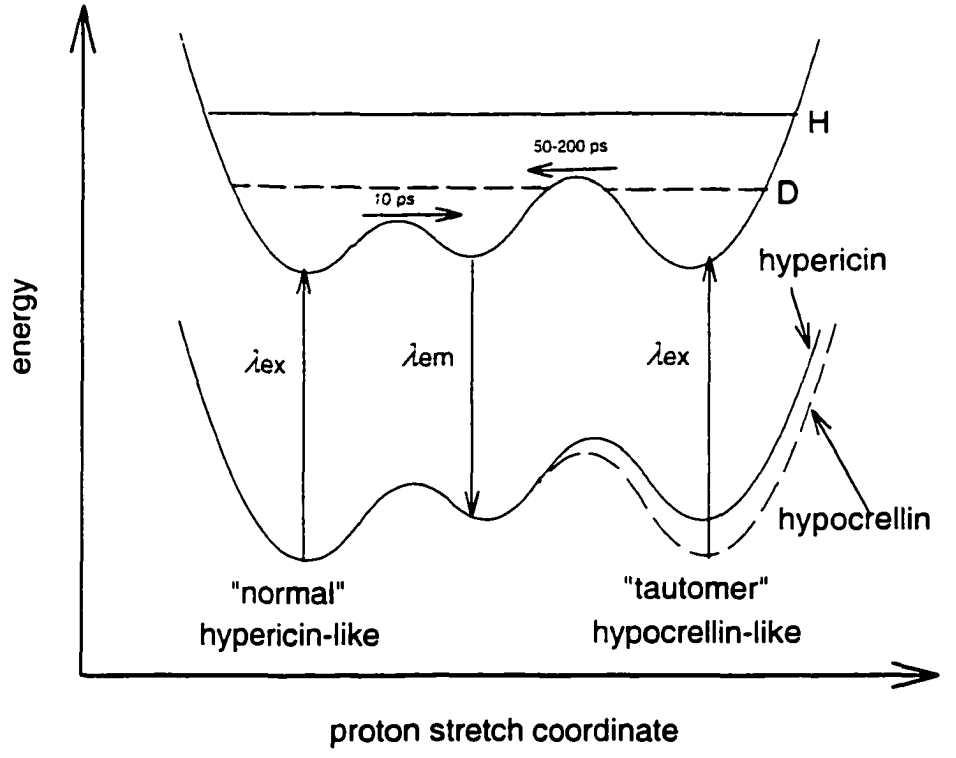

Figure 1.3 Unified picture depicting the ground- and excited-state potential energy surfaces for hypericin-like and hypocrellin-like molecules as a function of the proton stretch coordinate. The right-hand side of the ground-state potential energy surface indicates that the hypericin double tautomer is not populated in the ground state, whereas the hypocrellin A double tautomer is populated. On the excited-state surface, the zero-point vibrational levels for an OH---O or an OD---O system are depicted. The height of the zero-point level with respect to the barrier in the proton stretch coordinate determines whether an isotope effect will be observed. The third potential potential well, the middle of the figure represents either another possible tautomeric form or some other intermediate between, for example, the normal and the double tautomer species of hypericin. The arrows in the diagram are meant to remind the reader of the time constants for the H-atom transfer processes in hypericin and hypocrellin. One should not identify the proton coordinate for the reaction coordinate in this system [34].

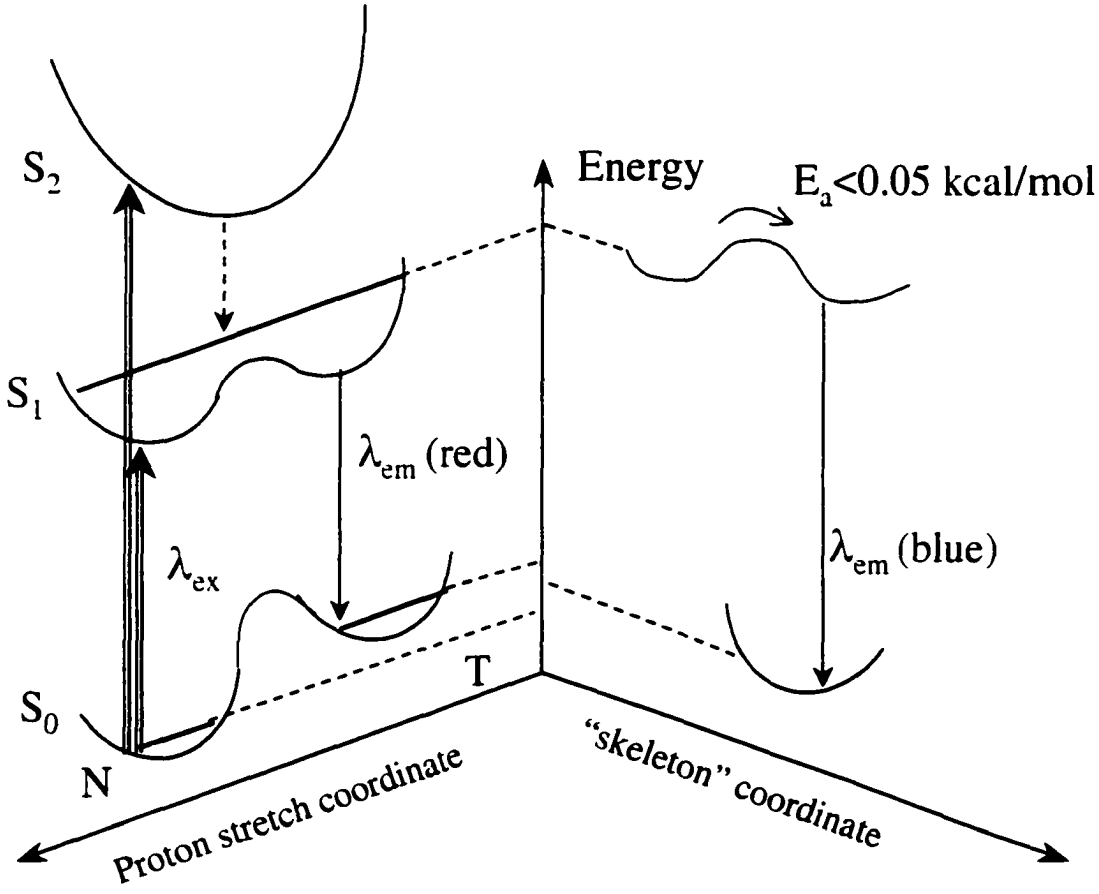

Figure 1.4 Generalized potential energy surface rationalizing the 10ps H-atom transfer in hypericin (and hypocrellin A, in which case N and T are interchanged). The absence of an isotope effect for this component indicates that the zero point vibrational level lies above the barrier in the proton coordinate and that the reaction coordinate for the H-atom transfer cannot be identified with the proton coordinate. Trapping the system in the tautomer well is effected by a low amplitude conformational change in the "skeleton" coordinate. This diagram attempts to provide a plausible explanation of how a rise in "blue" emission can occur by making the energy difference between the ground and excited state double tautomer larger in the skeleton coordinate than in the proton coordinate [33].

for hypocrellin in viscous solvents such as octanol and ethylene glycol [35]. The H-atom transfer is not concerted in hypericin [36].

During the past several years, the Petrich group has undertaken the task of unravelling the excited-state primary photophysical processes of hypericin and hypocrellin, and of making an effort to produce a unified picture of the hypericin and hypocrellin photophysics (Figure 1.3 and Figure 1.4). This hypothesis is based on the observation that under certain conditions a ~10ps component is resolved in hypocrellin photophysics which is comparable to that observed in hypericin.

Antiviral Activity of Hypericin and Hypocrellin

Hypericin and hypocrellin are two kinds of natural occurring photosensitizers. The mechanism by which hypericin (or hypocrellin) inactivate HIV infectivity is not clear. Generally it is believed that photosensitization processes involve molecules having a high triplet yield. Both hypericin and hypocrellin have a large triplet yield, 0.70 for hypericin in ethanol [4] and 0.83 for hypocrellin A in benzene [37], respectively. Two general photoreactions involving the triplet state of a photosensitizer are recognized toward the phototheraputic mechanism of hypericin and hypocrellin [38], *i.e.* type I and type II, which are illustrated in Figure 1.5. In type II process, the interaction of the triplet state of photosensitizer with the ground triplet state of molecular oxygen leads to a production of singlet oxygen, which is a highly reactive species. In type I, the triplet state of photosensitizer reacts with substrate by H-atom transfer or electron transfer to form radical species, *i.e.* superoxide anion.

In addition to those two types of well-known mechanisms, researchers in Iowa State University have proposed an alternative origin of the photoinduced virucidal activity of

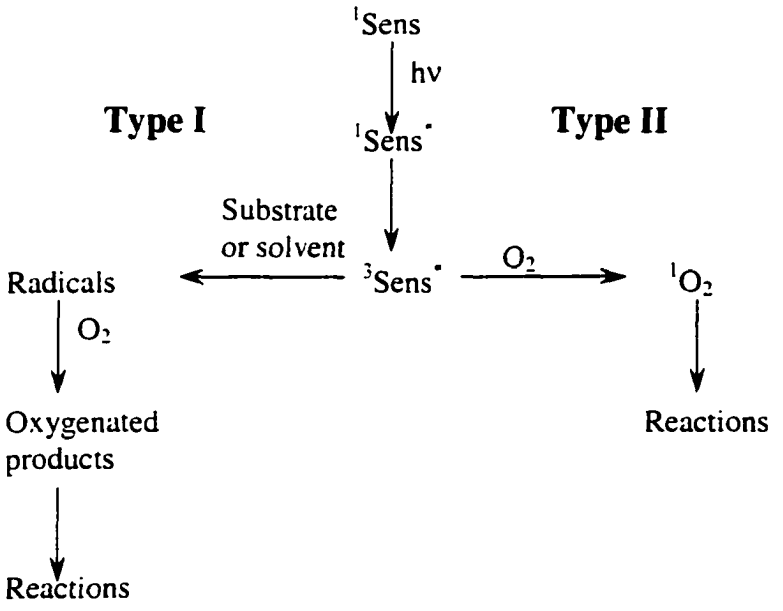

Figure 1.5 Type I and Type II photosensitization processes.

hypericin [24, 39]. Both hypericin and hypocrellin were observed a pH decrease in cells after the illumination. This pH drop effect is due to the excited state H-atom transfer from the photosensitizer to its environment. It is argued that the virucidal activity of hypericin (or hypocrellin) is related to its ability to acidify its environment [19, 40].

The comparative studies of nine perylenequinones, including hypericin and hypocrellin, conducted by Diwu and co-workers [41] reveal that the quantum yield of singlet oxygen formation is not sufficient to explain the reported antiviral activities of these molecules. Some studies suggest that hypericin does not require oxygen for its antiviral activity [19, 24, 42]. All those results support the idea that there are pathways parallel to those involving molecular oxygen for light-induced antiviral activity in hypericin, thus, light induced pH drop could be taken into account as one of the possible reasons. Also, the type I

and type II photoprocesses might be affected by the pH drop in a way to generate reactive species that can exist under acidic environment [30].

Photodynamic Therapy (PDT) and Molecular Flashlight

Photodynamic therapy (PDT) is a promising treatment for some types of cancer and other nonmalignant conditions. It is based on the discovery that certain drugs known as photosensitizing agents can kill one-celled organisms by exposure of the tissue to visible nonthermal light (400-700nm). In PDT, first a drug called a photosensitizer is administered to the patient, usually by injection. The photosensitizer alone is harmless and has no effect on either healthy or abnormal tissue. However, when light (often from a laser) is directed onto tissue containing the drug, the drug becomes activated and the tissue is rapidly destroyed, but only precisely where the light has been directed. Thus, by careful application of the light beam, the technique can be targeted selectively to the abnormal tissue [43].

Most photosensitive molecules have a heterocyclic ring structure similar to that of chlorophyll or hemoglobin. Light energy is captured in the form of photons and the energy is transferred to other molecules resulting in the liberation of short-lived energetic species that interact with biological systems and produce tissue damage [44]. An ideal photosensitizer must be biologically stable, photochemically efficient, selectively retained in the target tissue relative to surrounding normal tissue and should have minimal toxicity other than to the treated area. Hematoporphyrin and its derivatives are the most commonly used photosensitizer [45-48], but they have significant side effects. Thus many other sensitizers have been synthesized and studied, namely, phthalocyanines [49], mesotetra(hydroxyphenyl) porphyrins [50], 5-aminolevulinic acid [51], texaphyrins [52], benzoporphyrin derivative monoacid ring A [53] and etc.

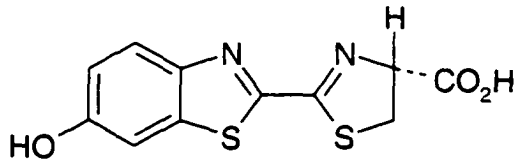

(a)

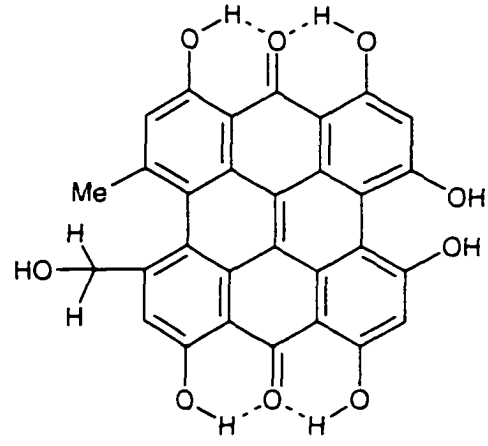

(b)

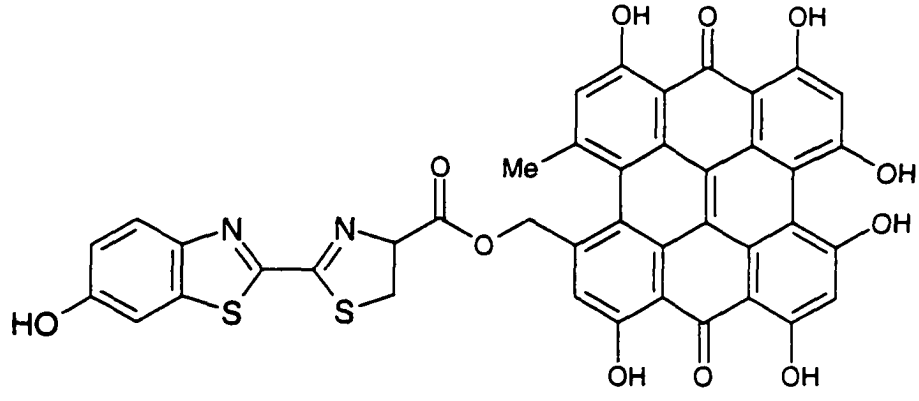

(c)

Figure 1.6 Structure of (**a**) luciferin, (**b**) pseudo hypericin, and (**c**) hypericin-luciferin tethered molecule.

An advantage of PDT is that it causes minimal damage to healthy tissue. However, the traditional method of exciting the photosensitizers is to illuminate the target area by introducing fiber optics [54, 55] or to depend on external light sources to penetrate the tissue efficiently enough to excite the chromophore [55-57]. The first of these methods is invasive and only effective for localized tumors. The latter depends critically on the absorption spectrum of the photosensitizer and the spectrum intensity, and penetration efficiency of the external light source.

Scientists at Iowa State University have proposed an alternative method called the "molecular flashlight". The photosensitizer, hypericin, is excited by inducing a chemiluminescent reaction in the patient [42, 58]. They have demonstrated that the chemiluminescence produced by the reaction of luciferin and the enzyme luciferase is sufficient to induce the antiviral activity of hypericin in vitro [58]. Recently they synthesized a molecule containing hypericin and luciferin moieties joined by a tether (Figure 1.6), and studied some of its biological and photophysical properties. The results of this study showed that the antiviral activity of the tethered molecule is equivalent to that of pseudohypericin (Figure 1.6), which is the base molecule for the synthesis of the tethered species.

Enzymatic Role of the Loop (52-72) in Porcine Fructose-1,6-bisphosphatase

Fructose 1,6-bisphosphatase (FBPase) is a primary control point in gluconeogenesis (synthesis of carbohydrate from noncarbohydrate material) and is important in the regulation of blood glucose. FBPase catalyzes the hydrolysis of fructose-1,6-bisphosphatate to fructose 6-phosphate and inorganic phosphate. FBPase is a homotetramer, each unit contains 335 residues [59] and the molecular weight of each unit is 37,000. The enzyme requires divalent cations (Mg^{2+}, Mn^{2+}, or Zn^{2+}), and the rates of reaction vary sigmoidally with metal ion

concentration (Hill coefficient of 2) [60-62]. The enzyme has two allosteric sites, an activator site for monovalent cations and an inhibitor site for AMP. The active site of the enzyme accommodates the substrate fructose-1,6-bisphosphatate and two divalent metal ion subsites. Binding of AMP and one of the divalent metal ions is mutually exclusive and this is the basis of enzyme regulation. In addition, fructose-2,6-bisphosphatate binds in the substrate site and inhibits the enzyme synergistically with AMP. FBPase exists in at least two conformational states called R and T [63, 64]. Binding of AMP at allosteric site located 28 Å from the nearest active site stabilizes the inactive T-state.

FBPase consists an important loop (residues 52-72) that is involved in the catalytic function. A proposed model for allosteric regulation involving loop 52-72 was graphically demonstrated in Figure 1.7 [65]. The loop is engaged in active R-state, while disengaged in the inactive T-state. After coordination of divalent cation (*i.e.* Mg^{2+}) and binding of fructose-1,6-bisphosphatae substrate, the loop 52-72 closes onto the active site. This loop closure brings together the amino acids that are critical for catalysis and determine the fate of the substrate. The engaged loop 52-72 allows Asn^{64} to hydrogen bond with the side chain of Glu^{98}, which putatively works in concert with Asp^{74} as a catalytic base. The engaged loop 52-72 also stabilizes the hydrogen bond of Asp^{68} with Arg^{276} [65]. When AMP binds to loop 22-27, which connects helix H1 and H2, interactions between subunits C1 and c4 could displace helix H2. The small displacement of helix H2 putatively disengages loop 52-72 from the rest of the tetramer, which in turn perturbs Asp^{74} and Glu^{98} (catalytic base tandem) [65].

Dissertation Organization

Chapter II in this dissertation introduces two major experiment systems utilized for this work and will be described in detail: time-correlated single photon counting and 30-Hz

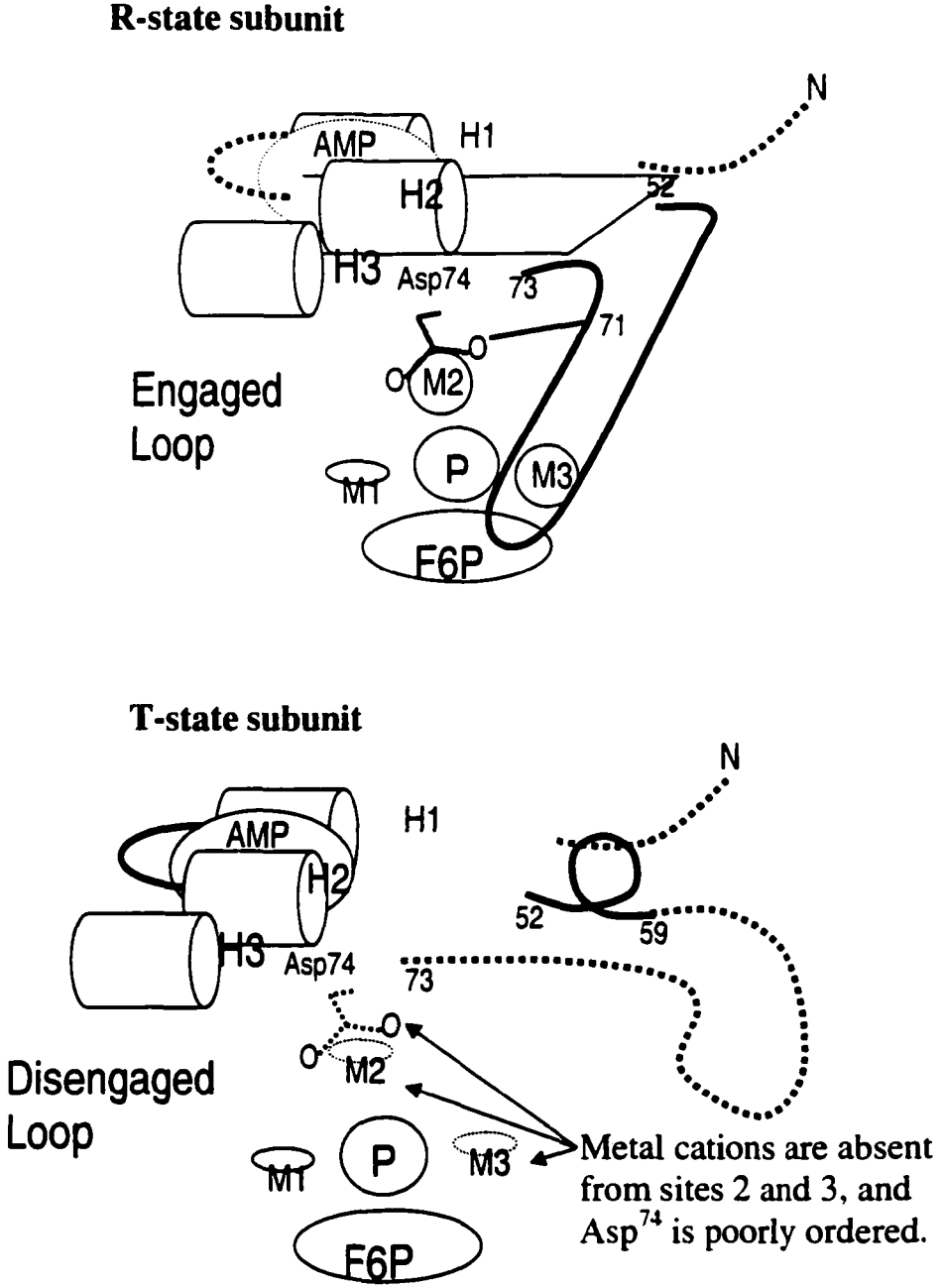

Figure 1.7 Scheme for allosteric regulation of FBPase catalysis. The engaged conformation of loop 52-72 (top) and the AMP-bound state (bottom) are antagonistic. Dashed lines represent poorly ordered structure.

pump-probe transient absorption spectrometer. Chapter III to VII contain individually published papers or papers submitted for publication. Chapter IV (Environment of Tryptophan 57 in Studied by Time-resolved Fluorescence and Site-directed Mutagenesis) presents the work on structural studies of porcine fructose-1,6-bisphosphatase by using state-of-the-art fluorescence techniques. Chapter III (Photophysics of Hypericin and Hypocrellin A in Complex with Subcellular Components: Interactions with Human Serum Albumin). Fluorescence lifetime and anisotropy measurement, fluorescence quantum yield and energy transfer measurement were performed by Jin Wen. Chapter V (Multidimensional Reaction Coordinate for the Excited-state H-atom Transfer in Perylene Quinones: Importance of the 7-Membered Ring in Hypocrellin A and B) and Chapter VI (Coupling of Large-Amplitude Side Chain Motions to the Excited-state H-Atom Transfer of Perylene Quinones: Application of Theory and Experiment to Calphostin C) discuss the photophysics of hypericin and hypocrellins, and give a simple model to describe their photoprocesses occurring in hypocrellins. In chapter V, steady-state measurement, transient absorption measurement were performed by Jin Wen. In chapter VI, Jin Wen performed the steady-state measurements and the transient absorption measurements. Chapter VII (Towards the Molecular Flashlight: Preparation, properties, and Photophysics of a Hypericin-luciferin Tethered Molecule) is a research note that has been accepted by *Photochemistry and Photobiology*. It discusses the synthesis method of a hypericn-luciferin tethered molecule and compares its photophysical and photobiological characterizations in both organic solvent and micelles that mimic the environment in living cells. Chapter VIII gives general conclusions for the whole dissertation.

References:

1. Lakowicz, J. R. *Principles of fluorescence spectroscopy*: 2nd ed.; Kluwer Academic/Plenum: New York, **1999**.
2. Ingle, J. D.; Crouch, S. R. *Spectrochemical analysis*: Prentice Hall: Englewood Cliffs, N.J., **1988**.
3. Chen, R. F. (1967) Fluorescence quantum yields of tryptophan and tyrosine. *Anal. Lett.* **1**, 35-42.
4. Jardon, P.; Lazorchak, N.; Gautron, R. (1986) Laser spectroscopic study of the first triplet state by Hypericin. *J. Chim. Phys. Phys.-Chim. Biol.* **83**, 311-315.
5. Fischer, M.; Georges, J. (1996) Fluorescence quantum yield of Rhodamine 6G in ethanol as a function of concentration using thermal lens spectrometry. *Chem. Phys. Lett.* **260**, 115-118.
6. Karstens, T.; Kobs, K. (1980) Rhodamine B and rhodamine 101 as reference substances for fluorescence quantum yield measurements. *J. Phys. Chem.* **84**, 1871-1872.
7. Mardelli, M.; Olmsted, J., III (1977) Calorimetric determination of the 9,10-diphenylanthracene fluorescence quantum yield. *J. Photochem.* **7**, 277-285.
8. Stryer, L. (1978) Fluorescence energy transfer as a spectroscopic ruler. *Annu. Rev. Biochem.* **47**, 819-846.
9. Föster, T. (1948) Intermolecular energy migration and fluorescence. *Ann. Phys. (Leipzig)* **2**, 55-75.
10. Fleming, G. R. *Chemical applications of ultrafast spectroscopy*; Oxford University Press ; Clarendon Press: New York, Oxford [Oxfordshire], **1986**.
11. Meruelo, D.; Lavie, G.; Lavie, D. (1988) Therapeutic agents with dramatic antiretroviral activity and little toxicity at effective doses: aromatic polycyclic diones hypericin and pseudohypericin. *Proc. Natl. Acad. Sci. U. S. A.* **85**, 5230-5234.
12. Piscitelli, S. C.; Burstein, A. H.; Chaitt, D.; Alfaro, R. M.; Falloon, J. (2000) Indinavir concentrations and St John's wort. *Lancet* **355**, 547-548.
13. Lenard, J.; Rabson, A.; Vanderoef, R. (1993) Photodynamic inactivation of infectivity of human immunodeficiency virus and other enveloped viruses using

hypericin and rose bengal: Inhibition of fusion and syncytia formation. *Proc. Natl. Acad. Sci. U. S. A.* **90**, 158-162.

14. Gulick, R. M.; McAuliffe, V.; Holden-Wiltse, J.; Crumpacker, C.; Liebes, L.; Stein, D. S.; Meehan, P.; Hussey, S.; Forcht, J.; Valentine, F. T. (1999) Phase I studies of hypericin, the active compound in St. John's wort, as an antiretroviral agent in HIV-infected adults: AIDS clinical trials group protocols 150 and 258. *Ann. Intern. Med.* **130**, 510-514.
15. Degar, S.; Prince, A. M.; Pascual, D.; Lavie, G.; Levin, B.; Mazur, Y.; Lavie, D.; Ehrlich, L. S.; Carter, C.; Meruelo, D. (1992) Inactivation of the human immunodeficiency virus by hypericin: evidence for photochemical alterations of p24 and a block in uncoating. *AIDS Res. Hum. Retroviruses* **8**, 1929-1936.
16. Carpenter, S.; Kraus, G. A. (1991) Photosensitization is required for inactivation of equine infectious anemia virus by hypericin. *Photochem. Photobiol.* **53**, 169-174.
17. Andreoni, A.; Colasanti, A.; Colasanti, P.; Mastrocinque, M.; Riccio, P.; Roberti, G. (1994) Laser photosensitization of cells by hypericin. *Photochem. Photobiol* **59**, 529-533.
18. English, D. S.; Zhang, W.; Kraus, G. A.; Petrich, J. W. (1997) Excited-State Photophysics of Hypericin and Its Hexamethoxy Analog: Intramolecular Proton Transfer as a Nonradiative Process in Hypericin. *J. Am. Chem. Soc.* **119**, 2980-2986.
19. Fehr, M. J.; Carpenter, S. L.; Petrich, J. W. (1994) The role of oxygen in the photoinduced antiviral activity of hypericin. *Bioorg. Med. Chem. Lett.* **4**, 1339-1344.
20. Miskovsky, P.; Sureau, F.; Chinsky, L.; Wheeler, G. V.; Turpin, P. Y., Spectrosc. Biol. Mol., Eur. Conf., 6th, **1995**, 539-540.
21. Blank, M.; Mandel, M.; Hazan, S.; Keisari, Y.; Lavie, G. (2001) ANTI-cancer activities of hypericin in the dark. *Photochem. Photobiol.* **74**, 120-125.
22. Park, J.; English, D. S.; Wannemuehler, Y.; Carpenter, S.; Petrich, J. W. (1998) The role of oxygen in the antiviral activity of hypericin and hypocrellin. *Photochem. Photobiol.* **68**, 593-597.

23. Wills, N. J.; Park, J.; Wen, J.; Kesavan, S.; Kraus, G. A.; Petrich, J. W.; Carpenter, S. (2001) Tumor cell toxicity of hypericin and related analogs. *Photochem. Photobiol.* **74**, 216-220.

24. Fehr, M. J.; McCloskey, M. A.; Petrich, J. W. (1995) Light-Induced Acidification by the Antiviral Agent Hypericin. *J. Am. Chem. Soc.* **117**, 1833-1836.

25. Hadjur, C.; Jeunet, A.; Jardon, P. (1994) Photosensitization by hypericin: electron spin resonance (ESR) evidence for the formation of singlet oxygen and superoxide anion radicals in an in vitro model. *J. Photochem. Photobiol. B* **26**, 67-74.

26. Weiner, L.; Mazur, Y. (1992) EPR studies of hypericin. Photogeneration of free radicals and superoxide. *J. Chem. Soc. Perkin Trans* **2**, 1439-1442.

27. Das, K.; English, D. S.; Petrich, J. W. (1997) Deuterium Isotope Effect on the Excited-State Photophysics of Hypocrellin: Evidence for Proton or Hydrogen Atom Transfer. *J. Phys. Chem. A* **101**, 3241-3245.

28. Hudson, J. B.; Zhou, J.; Chen, J.; Harris, L.; Yip, L.; Towers, G. H. N. (1994) Hypocrellin, from Hypocrella bambusae, is phototoxic to human immunodeficiency virus. *Photochem. Photobiol.* **60**, 253-255.

29. Meruelo, C.; Degar, S.; Nuria, A.; Mazur, Y.; Lavie, D.; Levin, B.; Lavie, G. In *Natural Products as Antiviral Agents*; Chu, K., Cutler, H. G., Eds.: New York, **1992**, pp 91-119.

30. Chaloupka, R.; Sureau, F.; Kocisova, E.; Petrich, J. W. (1998) Hypocrellin A photosensitization involves an intracellular pH decrease in 3T3 cells. *Photochem. Photobiol.* **68**, 44-50.

31. Gai, F.; Fehr, M. J.; Petrich, J. W. (1994) Role of Solvent in Excited-State Proton Transfer in Hypericin. *J. Phys. Chem.* **98**, 8352-8358.

32. Gai, F.; Fehr, M. J.; Petrich, J. W. (1994) Observation of Excited-State Tautomerization in the Antiviral Agent Hypericin and Identification of Its Fluorescent Species. *J. Phys. Chem.* **98**, 5784-5795.

33. Petrich, J. W. (2000) Excited-state intramolecular H-atom transfer in nearly symmetrical perylene quinones: hypericin, hypocrellin, and their analogues. *Int. Rev. Phys. Chem.* **19**, 479-500.

34. Das, K.; Smirnov, A. V.; Snyder, M. D.; Petrich, J. W. (1998) Picosecond Linear Dichroism and Absorption Anisotropy of Hypocrellin: Toward a Unified Picture of the Photophysics of Hypericin and Hypocrellin. *J. Phys. Chem. B* **102**, 6098-6106.

35. Das, K.; English, D. S.; Fehr, M. J.; Smirnov, A. V.; Petrich, J. W. (1996) Excited-State Processes in Polycyclic Quinones: The Light-Induced Antiviral Agent, Hypocrellin, and a Comparison with Hypericin. *J. Phys. Chem.* **100**, 18275-18281.

36. Park, J.; Datta, A.; Chowdhury, P. K.; Petrich, J. W. (2001) Is the excited-state H-atom transfer in hypericin concerted? *Photochem. Photobiol.* **73**, 105-109.

37. Diwu, Z.; Lown, J. W. (1992) Photosensitization by anticancer agents. 12. Perylene quinonoid pigments, a novel type of singlet oxygen sensitizer. *J. Photochem. Photobiol., A* **64**, 273-287.

38. Diwu, Z. (1995) Novel therapeutic and diagnostic applications of hypocrellins and hypericins. *Photochem. Photobiol* **61**, 529-539.

39. Fehr, M. J.; Carpenter, S. L.; Wannemuehler, Y.; Petrich, J. W. (1995) Roles of Oxygen and Photoinduced Acidification in the Light-Dependent Antiviral Activity of Hypocrellin A. *Biochemistry* **34**, 15845-15848.

40. Gai, F.; Fehr, M. J.; Petrich, J. W. (1993) Ultrafast excited-state processes in the antiviral agent hypericin. *J. Am. Chem. Soc.* **115**, 3384-3385.

41. Hudson, J. B.; Imperial, V.; Haugland, R. P.; Diwu, Z. (1997) Antiviral activities of photoactive perylenequinones. *Photochem. Photobiol.* **65**, 352-354.

42. Kraus, G. A.; Zhang, W.; Fehr, M. J.; Petrich, J. W.; Wannemuehler, Y.; Carpenter, S. (1996) Research at the Interface between Chemistry and Virology: Development of a Molecular Flashlight. *Chem. Rev.* **96**, 523-535.

43. Ackroyd, R.; Kelty, C.; Brown, N.; Reed, M. (2001) The history of photodetection and photodynamic therapy. *Photochem. Photobiol.* **74**, 656-669.

44. Weishaupt, K. R.; Gomer, C. J.; Dougherty, T. J. (1976) Photoradiation therapy. 3. Identification of singlet oxygen as the cytotoxic agent in photo-inactivation of a murine tumor. *Cancer Res.* **36**, 2326-2329.

45. Lipson, R. L.; Baldes, E. J.; Olsen, A. M. (1961) Use of a derivative of hematoporphyrin in tumor detection. *J. Natl. Cancer Inst.* **26**, 1-12.

46. Leonard, J. R.; Beck, W. L. (1971) Hematoporphyrin fluorescence: an aid to diagnosis of malignant neoplasms. *Laryngoscope* **81**, 365-372.

47. Benson, R. C., Jr.; Farrow, G. M.; Kinsey, J. H.; Cortese, D. A.; Zincke, H.; Utz, D. C. (1982) Detection and localization of in situ carcinoma of the bladder with hematoporphyrin derivative. *Mayo Clin. Proc.* **57**, 548-555.

48. Lytle, A. C.; Dunn, J. B.; Paspa, P. M.; Doiron, D. R.; Balchum, O. J. (1990) Fluorescence video endoscopic system for early cancer detection. *Proc. SPIE-Int. Soc. Opt. Eng.* **1200**, 466-475.

49. Bown, S. G.; Tralau, C. J.; Smith, P. D. C.; Akdemir, D.; Wieman, T. J. (1986) Photodynamic therapy with porphyrin and phthalocyanine sensitization: quantitative studies in normal rat liver. *Br. J. Cancer* **54**, 43-52.

50. Berenbaum, M. C.; Hall, G. W.; Hoyes, A. D. (1986) Cerebral photosensitization by hematoporphyrin derivative. Evidence for an endothelial site of action. *Br. J. Cancer* **53**, 81-89.

51. Divaris, D. X. G.; Kennedy, J. C.; Pottier, R. H. (1990) Phototoxic damage to sebaceous glands and hair follicles of mice after systemic administration of 5-aminolevulinic acid correlates with localized protoporphyrin IX fluorescence. *Am. J. Pathol.* **136**, 891-897.

52. Rockson, S. G.; Kramer, P.; Razavi, M.; Szuba, A.; Filardo, S.; Fitzgerald, P.; Cooke, J. P.; Yousuf, S.; De Vault, A. R.; Renschler, M. F.; Adelman, D. C. (2000) Photoangioplasty for human peripheral atherosclerosis: Results of a phase I trial of photodynamic therapy with motexafin lutetium (antrin). *Circulation* **102**, 2322-2324.

53. Bressler, N. M. (2001) Photodynamic therapy of subfoveal choroidal neovascularization in age-related macular degeneration with verteporfin: Two-year results of 2 randomized clinical trials-TAP report 2. *Arch. Ophthalmol. (Chicago)* **119**, 198-207.

54. Marijnissen, J. P. A.; Versteeg, J. A. C.; Star, W. M.; Van Putten, W. L. J. (1992) Tumor and normal tissue response to interstitial photodynamic therapy of the rat R-1 rhabdomyosarcoma. *Int. J. Radiat. Oncol., Biol., Phys.* **22**, 963-972.

55. Kriegmair, M.; Baumgartner, R.; Lumper, W.; Waidelich, R.; Hofstetter, A. (1996) Early clinical experience with 5-aminolevulinic acid for the photodynamic therapy of superficial bladder cancer. *Br. J. Urol.* **77**, 667-671.

56. Xie, X.; Hudson, J. B.; Guns, E. S. (2001) Tumor-specific and photodependent cytotoxicity of hypericin in the human LNCaP prostate tumor model. *Photochem. Photobiol.* **74**, 221-225.

57. Dougherty, T. J.; Gomer, C. J.; Henderson, B. W.; Jori, G.; Kessel, D.; Korbelik, M.; Moan, J.; Peng, Q. (1998) Photodynamic therapy. *J. Natl. Cancer Inst.* **90**, 889-905.

58. Carpenter, S.; Fehr, M. J.; Kraus, G. A.; Petrich, J. W. (1994) Chemiluminescent activation of the antiviral activity of hypericin: a molecular flashlight. *Proc. Natl. Acad. Sci. U. S. A.* **91**, 12273-12277.

59. Marcus, F., Edelstein, I., Reardon, I., and Heinrikson, R. L. (1982) Complete amino acid sequence of pig kidney fructose-1,6-bisphosphatase. *Proc. Natl. Acad. Sci. U.S.A.* **79**, 7161-7165.

60. Stone, S. R., and Fromm, H. J. (1980) Investigations of the kinetic mechanism of bovine liver fructose-1,6-bisphosphatase. *Biochemistry* **19**, 620-625.

61. Liu, F., and Fromm, H. J. (1988) Interaction of fructose-2,6-bisphosphate and AMP with fructose-1,6-bisphosphatase as studied by nuclear magnetic resonance spectroscopy. *J. Biol. Chem.* **263**, 9122-9128.

62. Nimmo, H. G., and Tipton, K. F. (1975) The effect of pH on the kinetics of beef-liver fructose bisphosphatase. *Eur. J. Biochem.* **58**, 567-574.

63. Shyur, L.-F., Aleshin, A. E., Honzatko, R. B., and Fromm, H. J. (1996) Biochemical properties of mutant and wild-type fructose-1,6-bisphosphatases are consistent with the coupling of intra- and intersubunit conformational changes in the T- and R-state transition. *J. Biol. Chem.* **271**, 33301-33307.

64. Zhang, Y., Liang, J.-Y., Huang, S. and Lipscomb, W. N. (1994) Toward a mechanism for the allosteric transition of pig kidney fructose-1,6-bisphosphatase. *J. Mol. Biol.* **244**, 609-624.

65. Choe, J.-Y., Poland, B. W., Fromm, H. J., and Honzatko, R. B. (1998) Role of a dynamic loop in cation activation and allosteric regulation of recombinant porcine fructose-1,6-bisphosphatase. *Biochemistry* **33**, 11441-11450.

CHAPTER II: EXPERIMENTAL APPARATUS

Time-Correlated Single Photon Counting (TCSPC)

1) Apparatus

Time-correlated single photon counting is a widely-used technique by photochemist and photobiologist to measure fluorescence lifetimes on the picosecond to nanosecond timescales. The principle of TCSPC and the descriptions of various experimental setups have been discussed in detail by several researchers [1, 2]. In this chapter, I will discuss the TCSPC setup in our laboratory and several of its applications.

A schematic of the apparatus is shown in Figure 2.1 [3]. A Coherent 701 rhodamine 6G dye laser is pumped with about 1W of 532nm radiation from a Coherent Antares 76-s CW mode-locked Nd:YAG laser. The dye laser is cavity-dumped at 3.8MHz. The output wavelength of the dye laser is adjustable in the range between 560nm and 620nm. The full width at half maximum (FWHM) of the pulses is about 10ps. Ultraviolet (UV) excitation wavelengths (between 280nm and 310nm) are achieved by focusing the dye laser pulses with a lens onto a potassium dihydrogen phosphate crystal (KDP). Fluorescence is collected at right angles through a polarizer mounted at 54.7° relative to the excitation polarization, then passed through cutoff filters or a monochromator and detected with a Hamamatsu R3890u-50 microchannel plate photomultiplier tube (MCP-PMT). Data are stored in a Norland 5500 multichannel analyzer (MCA), then transferred and analyzed with a personal computer.

The time-scale of the experiment is set with an Ortec 457 time-to-amplitude converter (TAC). The trigger, usually the output from the microchannel plate amplified by a pre-amplifier, is routed through a discriminator to serve as a "start" signal to initiate charging of

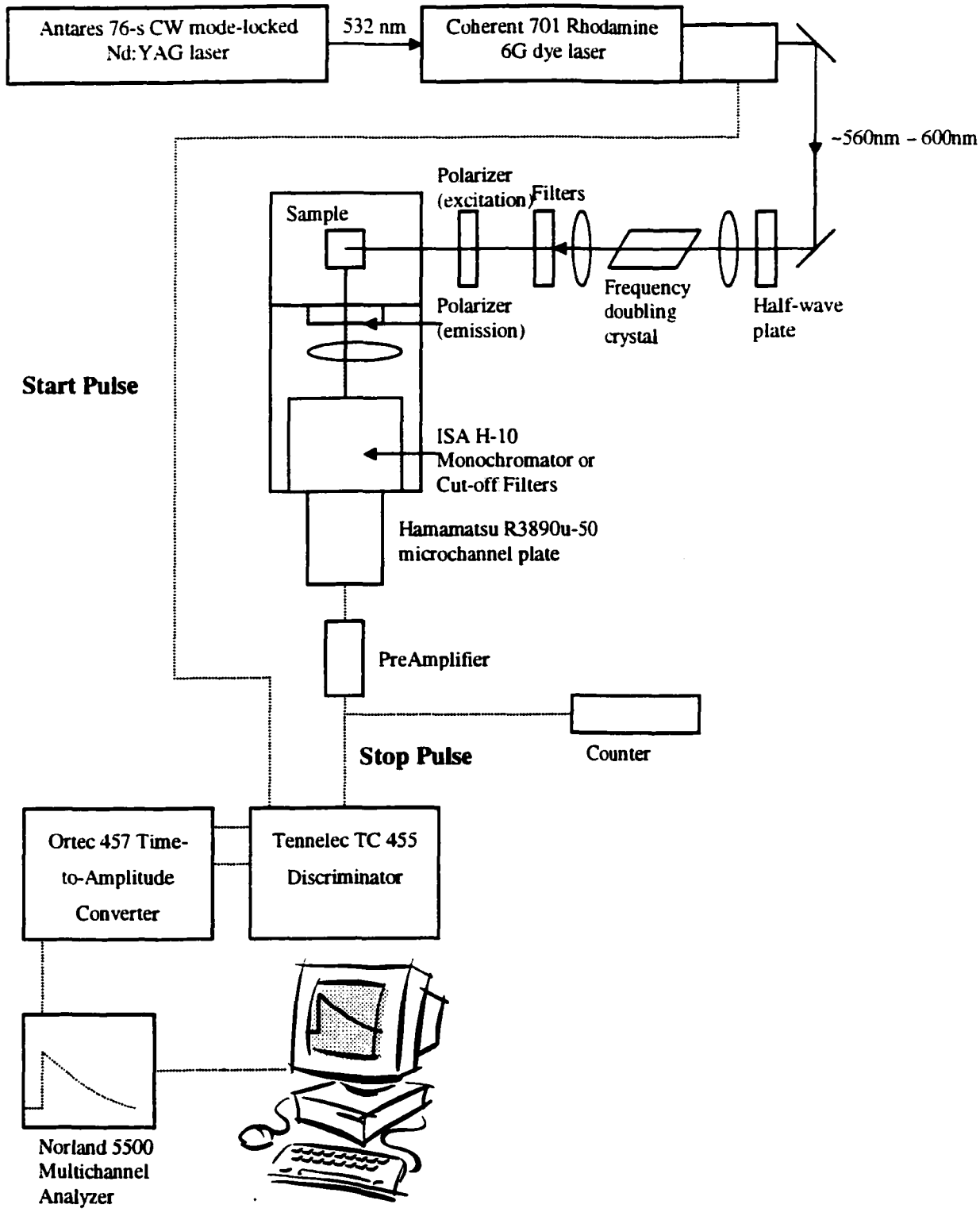

Figure 2.1 Time-correlated single photon counting apparatus

a capacitor within the TAC. The output from the cavity dumper driver provides a "stop" signal to stop the charging ramp in the TAC. A pulse is then output from the TAC, the amplitude of which is proportional to the charge on the ramp and hence the time between "start" and "stop". The time difference between two separate pulses from the cavity dumper is fixed and so a "decay time" is represented by the pulse amplitude from the TAC. The TAC is run in this "inverted mode" so that each detected photon is counted. It takes a finite time to reset the voltage ramp, and if the TAC was started by each laser trigger many counts would be lost while the TAC was reset. A count is stored in the MCA in an address corresponding to the pulse amplitude output from the TAC.

The time resolution of TCSPC depends on the jitter of detection electronics. Although the width of the laser pulse is about 7ps, the FWHM of the instrument function is about 150ps. Therefore, TCSPC is not possible to detect the ultrafast photophysical events.

2) Nonlinear Least-Squares Fitting

An important aspect of the TCSPC experiment is the analysis of the decays. The measured decay I(t) is the convolution of the instrument response function L(t') and the δ-pulse response function G(t-t')[2].

$$I(t) = L(t') \otimes G(t-t') \qquad (2\text{-}1)$$

$$= \int_0^t L(t)G(t-t')dt'$$

The fitting process is as follows: 1) Determine a mathematical model. The δ-pulse response function G(t-t') is normally represented with a single or multi exponentials. We always start with the simplest model, a single exponential. If this does not give a good fit, we will try

double or triple exponentials. 2) Estimate the initial values. Most fitting programs require a guess value for each parameter in the expression. The program runs iteratively until some set of criteria or tolerance is reached. "The goal of data analysis is to obtain the parameter values which provide the best match between the measured decay I(t) and the calculated decay $I_c(t)$ using the assumed parameter values." [4]

The most common algorithm used in TCSPC data analysis is Nonlinear Least-Squares Analysis, which is a mathematical procedure for finding a best fitting curve to a given set of points by minimizing the sum of the squares of deviations of the data points from the fitted curve. A parameter χ^2, called chi-squared, is calculated for each iteration:

$$\chi^2 = \sum_{i=n_1}^{n_2} \frac{1}{\sigma_i^2}[I(t_i) - I_c(t_i)]^2 = \sum_{i=n_1}^{n_2} \frac{[I(t_i) - I_c(t_i)]^2}{I(t_i)} \qquad (2\text{-}2)$$

σ_i is the error for data point. In TCSPC, the error is the square root of the number photon counts. Hence, $\sigma_i^2 = I(t_i)$. n_1 and n_2 are the first and last channels of region chosen for analysis. In an ideal fit, the fitted curve passes through each data point, and the χ^2 is zero. For a real situation, some data points are fit well, having a small (less than 1) ratio of deviation to error, and other data points are fit poorly, having a large (greater than 1) ratio of deviation to error. Statistically, a good fit will contain both. Therefore, on average we expect the value of each term in the sum equals 1 and the $\chi 2$ equals the number of data points. It is not convenient to interpret χ^2 in this function because it depends on the number of data points. Thus, a reduced χ^2 is more commonly used. The expression of reduced χ^2 is as follows:

$$\chi_R^2 = \frac{\chi^2}{n_2 - n_1 + 1 - p} \qquad (2\text{-}3)$$

where χ^2, n_1 and n_2 are as defined above, and p is the number of variable parameters in the fitting function. The value of χ_R^2 is expected to be unity if there is no systematic error.

The steps to judge the goodness of a fit are: 1) visual comparison of the measured data and calculated data, which should be good matched. 2) visual examination of calculated residuals which should be randomly distributed around zero. 3) χ_R^2 should be close to 1. Values of χ_R^2 less than 1.2 generally indicate an acceptable fit.

3) Time-Resolved Anisotropy Analysis

The TCSPC can also be used to measure the time-resolved anisotropy. In time-resolved anisotropy measurement, the apparatus setup is almost the same as we described in Figure 2.1 except for a few of differences: 1) The analyzer polarizer is controlled by a motor to rotate between 0 degree and 90 degree in a given interval (e.g. every 2 minutes). 2) Two decays are recorded on the MCA, one corresponding to the decay of molecules whose electric dipoles are parallel to the polarization of incident beam (recorded when the polarizer is at 0 degree), the other corresponding to the decay of molecules whose electric dipoles are perpendicular to the polarization of excitation beam (recorded when the polarizer is at 90 degree).

Rotational diffusion of fluorophores is a major cause of fluorescence depolarization. The Perrin equation [2] gives the relationship between anisotropy r, initial anisotropy r_0, fluorescence lifetime decay time τ_F and rotational relaxation time τ_r:

$$\frac{1}{r} = \frac{1}{r_0}\left[1 + \frac{3\tau_F}{\tau_r}\right] \qquad (2\text{-}4)$$

where anisotropy r can be calculated by the following equation:

$$r = \frac{I_{\parallel} - I_{\perp}}{I_{\parallel} + 2I_{\perp}} \tag{2-5}$$

Here $I_{\parallel}$ and $I_{\perp}$ are the fluorescence intensity components parallel and perpendicular to the plane of polarization of incident beam.

The rotational relaxation time τ_r can be recovered from time-resolved anisotropy measurement. In time-resolved anisotropy measurement, the time dependent decays of the parallel (||) and perpendicular ($\perp$) components are given by:

$$\begin{aligned} I_{\parallel} &= e^{-t/\tau_F}(1 + 2r_0 e^{-t/\tau_r}) \\ I_{\perp} &= e^{-t/\tau_F}(1 - r_0 e^{-t/\tau_r}) \end{aligned} \tag{2-6}$$

So the time dependent anisotropy, r(t) is given by:

$$\begin{aligned} r(t) &= [I_{\parallel}(t) - I_{\perp}(t)] / [I_{\parallel} + 2I_{\perp}(t)] \\ &= r_0 e^{-t/\tau_r} \end{aligned} \tag{2-7}$$

r(t) depends only on the rotational relaxation time τ_r, while the total fluorescence intensity depends only on fluorescence decay time τ_F ($F(t) = 3\ e^{-t/\tau_F}$), so that τ_F and τ_r can be separated and recovered respectively.

Anisotropy decays can be used to estimate the mobility of a fluorophore. An interesting application is a fluorophore attached onto a bulky molecule like protein. Here the diffusion of fluorophore is modeled to be restricted to a cone of half angle (θ_C). The cone angle is related to the order parameter by:

$$\frac{r_\infty}{r_0} = S^2 = [\frac{1}{2}(\cos\theta_C)(1 + \cos\theta_C)]^2 \tag{2-8}$$

where r_0 is the initial anisotropy when time is 0 and r_∞ is the limiting anisotropy. When the cone angle is 90 degree, S^2 is zero, which indicates a freely rotating fluorophore, and S^2 with a value of 1 indicates a totally restricted motion of fluorophore, which indicates that the fluorophore is rotated with protein. If the anisotropy decay is fit to a double exponentials, $r(t) = r_1(0)\exp(-t/\tau_{r1}) + r_2(0)\exp(-t/\tau_{r2})$, then $r_0 = r_1(0) + r_2(0)$, and r_∞ is the fit of the slow time component of anisotropy decay.

30 Hz Pump-Probe Transient Absorption Spectrometer

1) Apparatus

Unlike TCSPC, the time resolution of this system is determined by the laser pulse width. This system is fast enough to monitor any photophysical events happened in picosecond timescale, for example excited state H-atom transfer. The details of the spectrometer will be discussed as well as the pump-probe experiment itself. Figure 2.2 [5] describes the basic set up of the experiment.

A Coherent Model 76-s Antares laser is used as the "mother" laser to pump all the other lasers. The second harmonic output of the Antares, with a power of ~1.5 W at 532nm, is used to pump a Coherent model 702-1 dye laser, while a portion of fundamental (1064nm) of Antares is seeded into a continuum model RGA60 30Hz regenerative amplifier (regen), which amplifies a 100ps 200nJ pulse to approximately 200mJ at 1064nm. The output of regenerative amplifier is produced via second harmonic generation in a KDP crystal at 532nm with a power of ~40mJ / pulse. The repetition rate of the output is 30Hz. The dye laser, which is pumped by the Antares, is used in conjunction with a saturable absorber to produce 1nJ 1ps pulses at 76MHz. The lasing medium is Rhodamine 6G in ethylene glycol

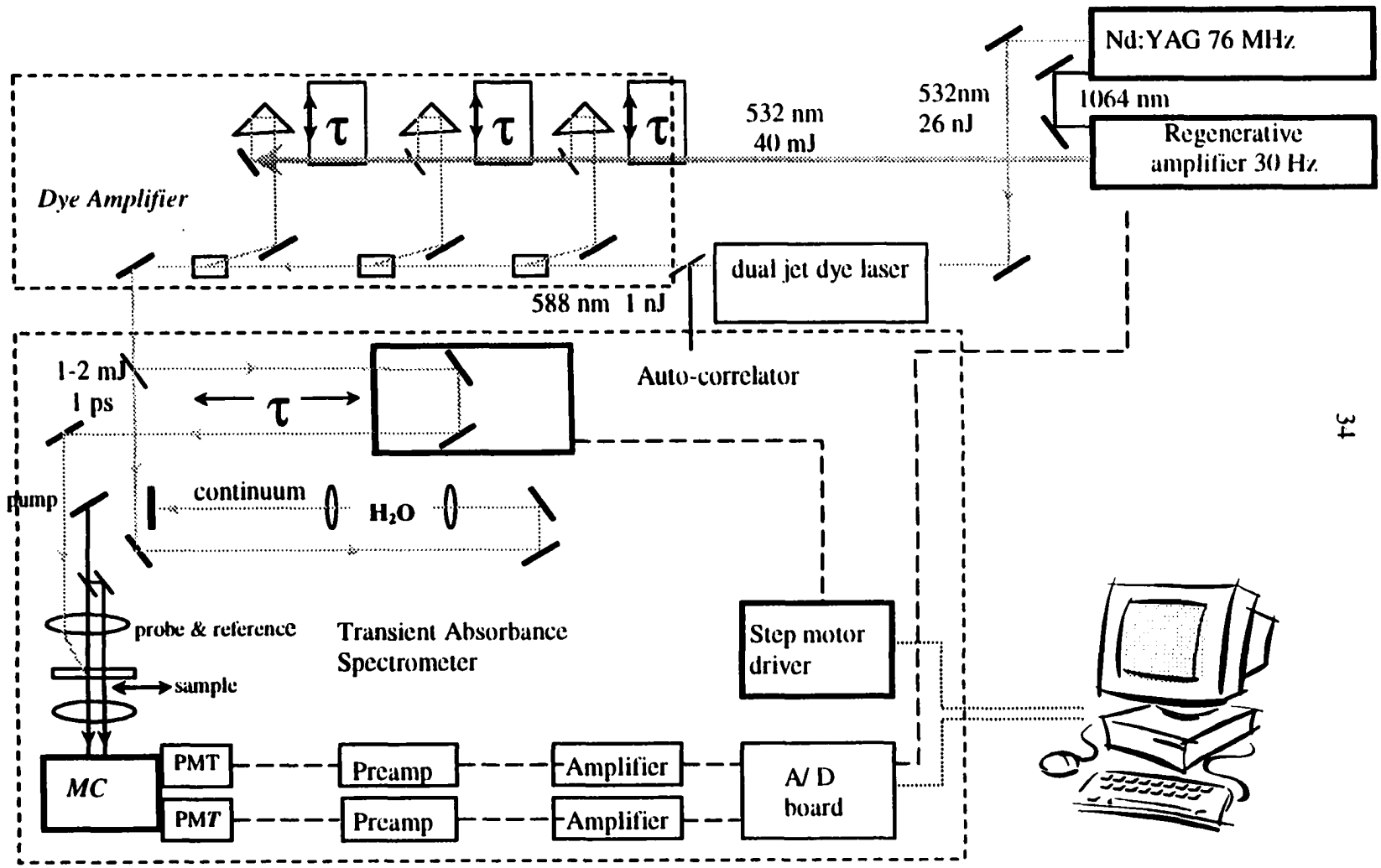

Figure 2.2 30Hz Pump-Probe Transient Absorption Spectrometer

and the saturable absorber is DODCI in ethylene glycol. Shortening of 100ps pulses to ~7ps in the dye laser is due to the increasing gain on the rising edge of the dye pulse, followed by rapid depletion of the gain at the peak of the dye pulse[1]. The saturable absorber inside the dye laser cavity will further shorten the pulse width to ~1ps with absorbing the leading edge of the pulse. At this point, the pulses from the dye laser are sufficiently short, but their low power excludes the performance of nonlinear optical effects, such as white light continuum generation. A dye amplifier followed the dye laser is used to produce high-energy pulses. The dye amplifier contains three dye cells full of Kiton Red. The amplification is obtained when the pulse from regenerative amplifier and the pulse from the dye laser enter the dye cell at the same time and they overlap spatially. The gain is on the order of 10^6 and the energy of each pulse is ~2mJ.

The amplified pulses are split into two parts. One part travels through a translation stage that is controlled by a computer through an IEEE interface. This part is known as "pump". The other part is focused into a cuvette of water to produce the white light continuum. This part is known as "probe". Because the probe is white light, it allows the probing range across the whole spectrum from blue to red. The probe is split into two spots both hitting the sample cell, entering the monochromator slit and detected by two PMTs respectively. The pump is directed to reach the sample cell at the same spot as one of the probe spot at 45° relative to the probe and finally is blocked to avoid it reaching the detector.

2) Pump-Probe experiment

Because the pump and the probe pulses travel through different paths and the pump pulse is on a translation stage, the timing between two pulses may vary. If the probe pulse enters the sample before the pump pulse (before time zero), no reactions or dynamics will be

observed. Time zero occurs when the pump and probe beam travel the same distance and enter the sample at the same time. If the probe pulse enters the sample after the pump pulse (after time zero), the probe beam will interrogate the change induced in the sample by the pump pulse. There are three kinds of phenomena:

1) *Bleaching*: this occurs when probing in the region where there is ground state absorption of the sample. Some ground state sample molecules are promoted to the excited state by the pump pulses, thus there are fewer ground state molecules to absorb the probe pulses which results in an increase in transmission of the probe beam in comparison to before time zero.
2) *Stimulated emission*: this occurs when probing in the region where there is fluorescence of the sample. Some molecules are promoted to the excited state by the pump pulses. When the energy of the probe pulse equals the difference between the excited state energy and the ground state energy, it can coherently stimulate the emission of photons from the upper levels. The result of stimulated emission is an increase in transmission of the probe beam in comparison to before time zero.
3) *Excited state absorption*: this occurs when the probe pulse is absorbed by the excited state of the sample. When this occurs, a decrease in transmission of the probe beam would be observed.

As described above, when an increase of transmission is observed in the experiment, there are two possible processes that can happen: ground state bleaching and stimulated emission. If the probe pulse is in the spectral region where there is only ground state absorption, then the trace monitored corresponds to the ground state bleaching. If the probe pulse is in the

spectral region where there is only fluorescence of the sample, then the trace corresponds to the stimulated emission. If the probe pulse in the spectral region where the absorption and emission spectra overlap, then the trace is complicated, might be only due to one process or both.

3) Data Analysis

Kinetic traces are collected as a change in transmission (I_t/I_0) of probe versus stage delay time. Because the sample population is directly proportional to the change in absorbance, the trace is first converted to the change of probe absorbance versus stage delay time by the relation:

$$A = -\log (I_t / I_0) \qquad (2\text{-}9)$$

Then the rise time of a kinetic trace is determined by the convolution of the probe and pump pulses.

A standard, Nile blue in ethanol, is usually used to determine the width of the pulse. Because the pump and the probe pulses have identical pulse width and are shortened by a saturable absorber, the pulse can be approximately modeled by a double-sided exponential. The fitting procedure is as follows: 1) estimate the width of the pulse by measuring the rising edge of the standard, 2) generate a series of double sided exponential pulses, 3) fit the standard trace by convolution with pulses of various widths until a satisfactory fit has been obtained, 4) after finding the good pulse, this pulse is used to fit the kinetic trace obtained in the experiment.

References:

1. Fleming, G. R. *Chemical applications of ultrafast spectroscopy*; Oxford University Press ;Clarendon Press: New York Oxford [Oxfordshire], **1986**.

2. O'Connor, D. V.; Phillips, D. *Time-correlated single photon counting*; U.S. ed.: Academic Press: Orlando, Fla., **1984**.

3. Ashby, K. D. *The laser in biophysical and analytical chemistry: Investigating biophysical processes and dynamics, as well as analytical techniques, as applied to systems of biological and chemical relevance*, Iowa State University, Ames, 2000.

4. Lakowicz, J. R. *Principles of fluorescence spectroscopy*; 2nd ed.; Kluwer Academic/Plenum: New York, **1999**. p119

5. Fehr, M. J. *Photophysics and mechanism of photoinduced antiviral action of the natural products, hypericin and hypocrellin A*, Iowa State University, Ames, 1995.

CHAPTER III: PHOTOPHYSICS OF HYPERICIN AND HYPOCRELLIN A IN COMPLEX WITH SUBCELLULAR COMPONENTS: INTERACTIONS WITH HUMAN SERUM ALBUMIN

A paper published in *Photochemistry and Photobiology*[1]

Kaustuv Das[2], Alexandre V. Smirnov[2], Jin Wen[2], Pavol Miskovsky[3] and Jacob W. Petrich[2,4]

Abbreviations: HSA, human serum albumin; HIV, human immunodeficiency virus; DMSO, dimethylsulfoxide; LBO, lithium triborate; BBO, β-barium borate; SNARF, carboxy-seminaphthorhodafluor-1; BCECF, 2′-7′-*bis*(carboxyethyl)5-carboxyfluorescein; Poly dG-dC, polydeoxyguanylic-deoxycytidylic acid; Brij-35, polyoxyethylene 23 lauryl ether; AOT dioctyl sulfosuccinate.

Abstract

Time-resolved fluorescence and absorption measurements are performed on hypericin complexed with human serum albumin, HSA, (1:4, 1:1, and ~5:1 hypericin:HSA complexes). Detailed comparisons with hypocrellin A/HSA complexes (1:4 and 1:1) are made. Our results are consistent with the conclusions of previous studies indicating that hypericin binds

---

[1] Reprinted with permission of *Photochemistry and Photobiology*,**1999**, 69(6), 633-645

[2] Department of Chemistry, Iowa State University, Ames, IA 50011-3111 USA

[3] Department of Biophysics, Safarik University, 041 54 Kosice, SLOVAKIA

[4] To whom correspondence should be addressed

to HSA by means of a specific hydrogen bonded interaction between its carbonyl oxygen and the N_1-H of the tryptophan residue in the II A subdomain of HSA. (They also indicate that some hypericin binds nonspecifically to the surface of the protein.) A single-exponential rotational diffusion time of 31 ns is measured for hypericin bound to HSA, indicating that it is very rigidly held. Energy transfer from the tryptophan residue of HSA to hypericin is very efficient and is characterized by a critical distance of 94 Å, from which we estimate a time constant for energy transfer of $\sim 3 \times 10^{-15}$ s. Although it is tightly bound to HSA, hypericin is still capable of executing excited-state intramolecular proton (or hydrogen atom) transfer in the ~5:1 complex, albeit to a lesser extent than when it is free in solution. It appears that the proton transfer process is completely impeded in the 1:1 complex. The implications of these results for hypericin (and hypocrellin A) are discussed in terms of the mechanism of intramolecular excited-state proton transfer, the mode of binding to HSA, and the light-induced antiviral and antitumor activity.

Introduction

Hypericin and hypocrellin A (Figure 3.1) are naturally occurring polycyclic quinones that have gained great interest recently owing to their light-induced biological activity [1-5]. They display virucidal activity against several types of viruses, including the human immunodeficiency virus (HIV) [6-9], as well as antiproliferative and cytotoxic effects on tumor cells [10-12]. Hypericin is also a potent antidepressant [13-15], exhibits light-dependent inhibition of protein kinase C (PKC) [16,17], and is reported to possess numerous other types of biological behavior [19-23]. Hypericin, like other anticancer drugs, also induces apoptosis [11,23,24].

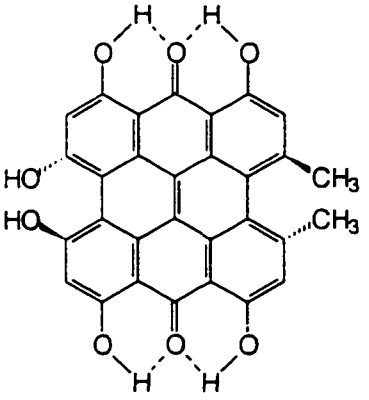

Hypericin

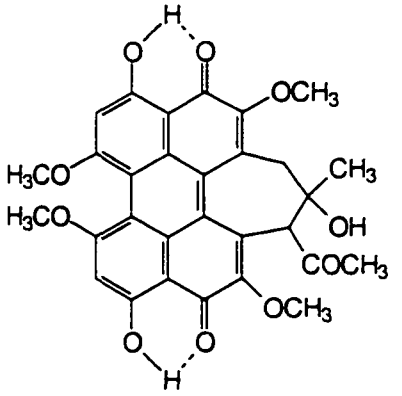

Hypocrellin A

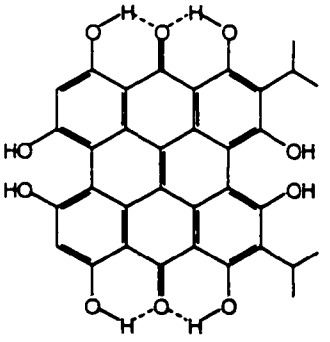

Stentorin chromophore

Figure 3.1 Two-dimensional structures of hypericin, hypocrellin A, and the stentorin chromophore.

Owing to this important biological activity, over the past few years we have been studying the photophysics of hypericin and hypocrellin [25-35]. By means of H/D substitution, investigation of methoxy analogs, and complementary studies using both transient absorption and fluorescence upconversion spectroscopies, we have unambiguously demonstrated that the major primary photophysical process in hypericin and hypocrellin A in organic solvents is excited-state intramolecular proton or hydrogen atom transfer. Considerable effort was required to demonstrate this fact owing to the unusual mirror image

symmetry between absorption and emission spectra, the lack of an H/D isotope effect on the proton transfer reaction in hypericin, and the occasional consideration of this ultrafast reaction in terms of equilibrium Förster-cycle type calculations [36].

We have suggested that the labile protons resulting from the intramolecular proton transfer reaction may be important for understanding the light-induced biological activity of hypericin and hypocrellin A. Notably, hypericin and hypocrellin A acidify their surroundings upon light absorption [37-39]. The role of photogenerated protons takes on significance in the context of the growing body of literature implicating changes in pH with inhibition of virus replication [40], antitumor activity [41,42], and apoptosis [43,44,45]. For example, comparative studies for nine perylenequinones, including hypericin, provide evidence that the quantum yield of singlet oxygen formation is not sufficient to explain the reported antiviral activities of these molecules and that other structural features of perylenequinones are involved [46]. In fact, the quantum yield of singlet oxygen from hypericin is much less than had initially been presumed. Recently, Jardon and coworkers have revised their earlier estimation of a singlet oxygen quantum yield of 0.73 [47,48], essentially equal to the triplet yield, to 0.35 in ethanol and less than 0.02 in water [49]. Based on this result, mechanisms involving only oxygen clearly cannot explain all the activity of hypericin.

We had previously reported that hypericin does not require oxygen for its antiviral activity [5,18,34]. This conclusion was based on an inability to estimate accurately low oxygen levels in our virus samples. Our most recent results indicate that while antiviral pathways independent of oxygen may exist, the role of oxygen in this activity is significant, although it seems to differ for hypericin and hypocrellin A. The ability of photogenerated

protons to enhance the activity of activated oxygen species [39] is still considered to be of importance [50]. De Witte and coworkers have also recently considered the relative role of oxygen in the phototoxicity of hypericin against A431 human skin carcinoma cells [51].

Although numerous studies dealing with the biological and photophysical properties of hypericin have been performed, the mechanism and site of action of hypericin at the cellular level is still unclear. Thus a better understanding of the interaction of hypericin with various possible cellular targets (membranes, proteins or nucleic acids) is essential for a determination of its function in biological systems. For human T47D mammary tumor cells, it has been shown that hypericin immediately associates with cell membrane and also localizes in the cytoplasm and nucleus after a long-time incubation (3 hr 30min) [52]. And recently a study of hypericin in fetal rat neurons was performed, employing both fluorescence imaging and subnanosecond time resolution, that indicated localization in the membrane as well as in the nucleus [53].

Human serum albumin (HSA) is a transport protein in the blood plasma. It binds a wide variety of substances, such as metals, fatty acids, amino acid, hormones, and a large number of therapeutic drugs [54]. Because of its clinical and pharmaceutical importance, the interaction of HSA with a variety of ligands has been studied [55,56]. HSA consists of six helical subdomains and its polypeptide back bone is formed by 585 amino acids. HSA has two major binding sites denoted IIA and IIIA according to the subdomains where they occur. The interaction of hypericin with HSA has been studied by various groups [57,58-60]. Hypericin in aqueous physiological solution is aggregated [61], and binding with albumin helps to solubilize it in monomeric form, which is believed to be important for virucidal

action [62]. Burel and Jardon have also noted that the photodynamic properties of hypericin are greatly diminished when it is aggregated [63].

Previous studies have suggested that the binding site of hypericin was in the III A subdomain of the protein, where the hypericin is not completely shielded from the outer environment [59.60]. Recent surface enhanced Raman (SERS) and resonance Raman (RR) studies, however, identify the binding site as the II A subdomain, where the binding occurs through an interaction between the carbonyl oxygen of hypericin and the N_1-H of the single tryptophan residue (W214) in the protein [57].

In this article we discuss the results of time-resolved fluorescence and absorption measurements of hypericin and hypocrellin A bound to HSA. An important problem that arises in the course of this investigation is understanding the nature of the complex that hypericin forms with subcellular components, in particular, HSA. Is this binding specific, that is, directed to a particular target site, or nonspecific? What nonradiative processes are induced upon binding? As will be seen, drastically different degrees of nonexponential fluorescence decay are observed for hypericin and hypocrellin A when they interact with HSA. In order to respond to these questions, hypericin was investigated in complex with other biological macromolecules whose binding interactions would be expected to present a considerable spectrum of variability with respect to that of HSA, namely poly dG-dC, Brij-35 micelles, and myoglobin.

Materials and Methods

Hypericin, hypocrellin A, and the pH probes SNARF, and BCECF were purchased from Molecular Probes, and were used as received. Human serum albumin (99%, essentially

fatty acid and globulin free), horse heart myoglobin (minimum 90%, lyophilized, essentially salt free), polydeoxyguanylic-deoxycytidylic acid (Poly dG-dC), Brij-35 (polyoxyethylene 23 lauryl ether), and AOT (dioctyl sulfosuccinate) were purchased from Sigma and were used as received.

Preparation of the hypericin-albumin and hypericin-myoglobin complexes. HSA and myoglobin solutions of 1.5×10^{-5} M concentration were prepared in 10-mM phosphate buffer (pH 7). A concentrated solution of hypericin in DMSO was added to the protein solution in microliter quantities so as to obtain a final DMSO concentration of ~ 0.8% and a final hypericin concentration of 4.0×10^{-6} M. The HSA/hypericin and myoglobin/hypericin complexes were equilibrated for 12 hours in the dark.

For steady-state spectra and time-resolved fluorescence studies we initially prepared a complex whose stoichiometry was 1:4 hypericin:HSA where the concentration of HSA was 1.5×10^{-5} M; and that of hypericin, 4.0×10^{-6} M. We also prepared 1:1 complexes where both the HSA and the hypericin concentrations were about 4.0×10^{-6} M. Both the 1:4 and the 1:1 hypericin:HSA complexes gave the same results in the fluorescence lifetime and anisotropy decay experiments..

For time-resolved absorption measurements, in order to obtain a measurable signal from the bound hypericin, it was necessary to increase the hypericin concentration to 7.0×10^{-5} M while keeping HSA at 1.5×10^{-5} M. This provided an ~5:1 hypericin:HSA complex. Attempts to make a 1:4 hypericin:HSA complex with [HSA] = 3.0×10^{-4} M and [hypericin] = 7.0×10^{-5} M resulted in aggregation of HSA. Furthermore, keeping [HSA] = 1.0×10^{-4} M in an attempt to make a 4:1 hypericin:HSA complex with [hypericin] = 4.0×10^{-4} M resulted

in aggregation of hypericin. Finally a 1:1 hypericin:HSA complex was prepared where the concentration of each was 7×10^{-5} M. The association constant between hypericin and HSA has been given as 7.5×10^{5} M^{-1} [58] and 1.3×10^{7} M^{-1} [62].

Preparation of the hypericin-poly dG-dC complex. Ten units (one unit when dissolved in 1 mL buffer gives an absorbance of 1 at 260 nm in a 1 cm cell) of poly dG-dC was dissolved in 1 mL of 10 mM phosphate buffer (pH 7) by stirring for 24 hours. A concentrated solution of hypericin in DMSO was added in microliter amounts in order to obtain a final hypericin concentration of 3.0×10^{-6} M and a final DMSO concentration of 0.5%. The solution was stirred for 24 hours in the dark before performing experiments. Attempts to increase the concentration of hypericin for transient absorption experiments resulted in aggregation, so that pump-probe studies could not be performed.

Preparation of hypericin in micelles. To a concentrated (1.25×10^{-3} M) solution of Brij-35 in water a concentrated solution of hypericin in DMSO was added so as to have a final hypericin concentration of 2.0×10^{-6} M.

Time-resolved studies. Steady-state absorption spectra were obtained on a Perkin Elmer Lambda 18 double-beam UV-vis spectrophotometer with 1-nm resolution. Steady-state fluorescence spectra were obtained on a SPEX Fluoromax with a 4-nm band pass, corrected for detector response. The apparatus for time-correlated single-photon counting and the 30-Hz pump-probe transient absorption spectrometer are described in detail elsewhere [25-27]. Fluorescence decays are collected for a maximum of 10,000 counts in the peak channel. The polarized fluorescence traces used to obtain fluorescence anisotropy decay parameters were collected to a maximum of 20,000 counts in the peak channel.

Fluorescence upconversion. The fluorescence upconversion apparatus is based on a homemade Ti:sapphire laser [64] producing pulses of less than 50 fs fwhm at a repetition rate as high as 90 MHz. The Ti:sapphire oscillator is pumped by an intracavity frequency-doubled Nd:YVO_4 continuous-wave laser (Millennia V, Spectra Physics) and produces tunable (750-850 nm) pulses which are precompensated for group velocity dispersion with a pair of glass prisms and a gold mirror. The fundamental beam is frequency doubled by a type-I, 1.0-mm LBO crystal from Super Optronics. These frequency-doubled excitation pulses, which typically were centered about 414 nm, are separated from the fundamental by a 400-nm dielectric mirror. To precompensate for group velocity dispersion a pair of quartz prisms oriented at Brewster's angle is used before focusing into the sample with 15 cm convex lens with anti-reflection coating for 400 nm. In order to reduce energy losses during precompensation a 400-nm zero-order quartz half-waveplate is used to minimize reflections at air-prism interfaces. The polarization orientation of the excitation light is then adjusted to the desired angle by another similar half-waveplate. For room temperature measurements, the sample was circulated in 1 mm flow cell by means of a dye laser pump with voltage-controlled rotation speed. The excitation light is removed from fluorescence by a 450-nm long-pass filter. The residual fundamental pulses are used as the gate to upconvert the fluorescence, which is collected with an LMH-10x microscope objective (OFR Precision Optical Products) coated for near infrared transmission. They are then focused by a 15-cm quartz lens onto a type-I 0.4-mm BBO crystal (cut at 31° and mounted by Quantum Technology, Inc.). The polarization of both excitation and gate beams is controlled with a set of zero-order half-wave plates coated for 400 and 800 nm respectively. The upconverted signal is sent directly into a H10 (8 nm/mm) monochromator (Jobin Yvon/Spex Instruments

S.A. Group) coupled to a Hamamatsu R760 photomultiplier equipped with UG11 UV-pass filter and operated at maximum sensitivity. The photomultiplier output is amplified with two stages (total by a factor of 25) by a Stanford Research Systems SR-445 DC-300 MHz amplifier with input terminated at 500 Ω and carefully calibrated after a long (1-2 hours) warm-up. Photon arrival events are registered with SR400 gated photon counter operated in CW mode with threshold level of 100-120 mV. At each delay step signal is obtained by averaging 3-5 samples collected for 1 s each. To reduce fluctuations due to laser flicker or sample instability (e.g. air bubbles in the flow cell) data are resampled if significant relative standard deviation or relative drift is detected. This approach also helps eliminate errors in data transmission lines. A translation stage (Klinger Scientific) with a resolution of 1 step/μm or 10 microsteps/μm is used to delay gate pulses and is controlled by a computer via an IEEE interface and Klinger Scientific CD-4 motor driver. The instrument response function is obtained by collecting a cross correlation function of the second harmonic and the fundamental (with the long-pass filter removed): The resulting third harmonic intensity is plotted against delay time. Cross correlation functions typically have a fwhm of 280-300 fs and for time scales greater 20 ps are assumed to be delta-function like. All curves were fit and deconvoluted from the instrument response function using an iterative convolute-and-compare nonlinear least-squares algorithm.

Average pump power was about 40-60 mW as measured at the second prism for precompensation. Spectral resolution was limited by the bandwidth of the upconversion crystal (BBO) and was estimated to be ±3 nm.

A sample of a total volume of ~10 ml was constantly pumped through a 1-mm quartz flow cell by a dye circulator. All experiments excluding sample preparation were performed in a dark room.

An attempt was made to prepare a chromophore in buffer solution to serve as a reference sample for HSA complexes. Unfortunately, hypericin emission is efficiently quenched in the absence of the hydrophobic environment provided by the protein, and the quantum yield was not sufficient to obtain a reasonable signal. Hypocrellin A was essentially nonfluorescent both with and without the protein, which is why no fluorescence upconversion results for hypocrellin A are reported here.

Attempts to observe light-induced acidification. Light induced pH drops by hypericin have been observed in different environments such as vesicles and 3T3 cells [37-39]. We have employed the pH probes SNARF (Molecular Probes) to see if there is any light induced pH drops of hypericin bound to HSA. For the pH drop experiments, the solution was purged with argon for at least 30 minutes (argon was flowed gently over the top of the solution so as to prevent the formation of bubbles). The solutions are illuminated by the fluorimeter for 10 minutes at 550 nm (4-nm band pass). The hypericin/HSA complex was studied in pure water with and without buffer; but the SNARF spectra remained unchanged after illumination.

Consequently, a control experiment was performed to determine if there was any light induced pH drop of hypericin in a reverse micellar system in the absence of HSA. The system studied in this case was hypericin in n-heptane/AOT/water reverse micelles; and the pH probe used was SNARF. The concentration of AOT used was 0.5 M, and the amount of water added was 200 μL. The concentration of hypericin and SNARF were 2.2×10^{-6} M and 6.4×10^{-6} M. The solution was kept in the dark and purged with argon for one hour before

illumination. The second harmonic of the Nd-YAG (532 nm) was used to illuminate the solution, and the power was a few microwatts. The composite fluorescence spectrum of hypericin and SNARF was recorded as soon as it was illuminated by the laser light and five minutes after. The two spectra showed no change in relative intensity, and consequently showed no indication of a light-induced pH change.

Results

Steady-state Spectra

Figures 3.2a and 3.3 present the fluorescence excitation spectra of hypericin in DMSO and in sulfuric acid (where the carbonyl groups are protonated). These differ in a number of ways. First, the sulfuric acid spectrum is red shifted with respect to that of DMSO. Secondly, the relative intensity of the 400-500 nm region of the sulfuric acid spectrum has increased considerably with respect to the DMSO spectrum. The emission spectrum in sulfuric acid is also red shifted compared to that in DMSO.

For purposes of comparison, Figures.3.2a and 3.4 present the steady-state excitation and emission spectra of hypericin in complex with HSA and poly dG-dC, along with the spectrum in DMSO. In complex with HSA and with poly dG-dC, the excitation spectrum of hypericin is closer to that in sulfuric acid than in DMSO. The emission spectra are also red shifted, though not as much as in sulfuric acid.

The fluorescence quantum yield of hypericin/HSA (1:4) is 0.18, compared to 0.35 for hypericin in DMSO [32]. The emission intensity of hypericin/poly dG-dC is very much weaker. The changes in the hypericin excitation spectra induced upon binding it to either HSA or poly dG-dC can be interpreted in terms of an interaction through its carbonyl oxygen if the above comparisons with the sulfuric acid spectra are justified. This interpretation is

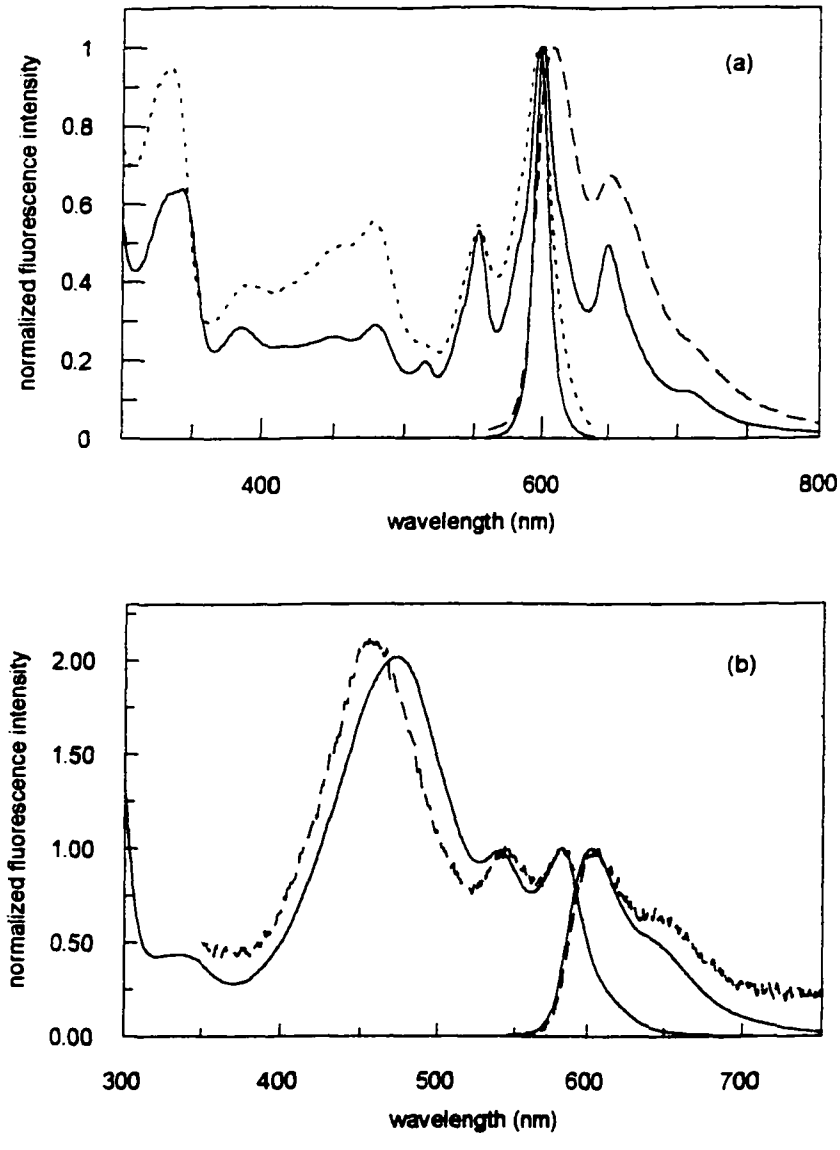

Figure 3.2 (a) Fluorescence excitation (λ_{em} = 650 nm) and emission (λ_{ex} = 550 nm) spectra of hypericin in HSA (1:4 complex, [HSA] = $1.5x10^{-5}$(M) and [hyp] = $7x10^{-6}$ (M), dotted line) and in DMSO (solid line).

(b) Fluorescence excitation (λ_{em} = 650 nm for DMSO and 600 nm for HSA) and emission(λ_{ex} = 414 nm) spectra of hypocrellin A in HSA (1:1 complex, [HSA]=[hypocrellin] = $3.6x10^{-6}$ (M), dotted line) and in DMSO (solid line). Greater noise in these data indicates considerably higher quenching efficiency as compared to hypericin/HSA complex.

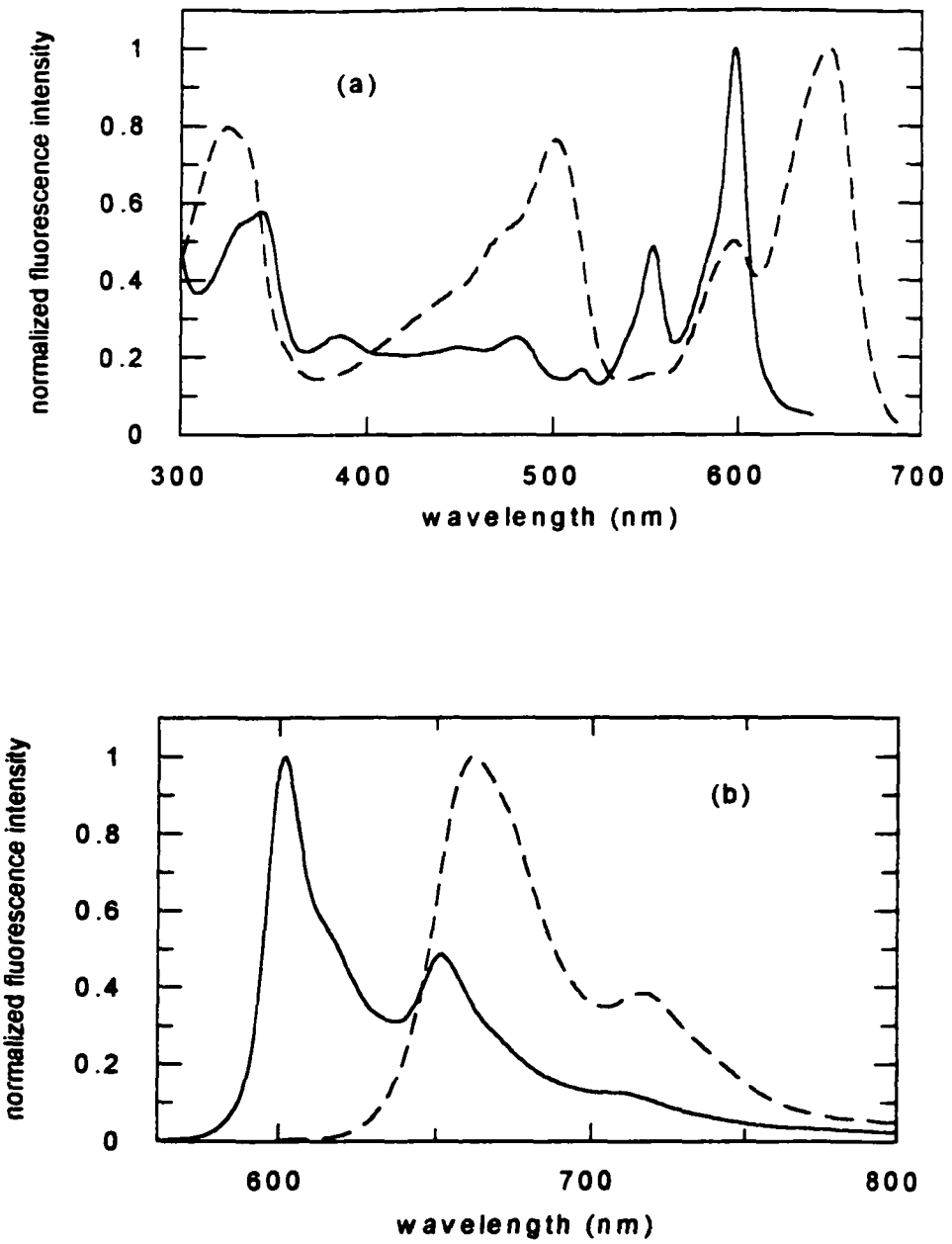

Figure 3.3 (a) Fluorescence excitation spectra of hypericin in sulfuric acid (λ_{em} = 750 nm, dotted line) and in DMSO (λ_{em} = 650 nm, solid line).

(b) Fluorescence emission spectra (λ_{ex} = 550 nm) of hypericin in sulfuric acid (dotted line) and in DMSO (solid line).

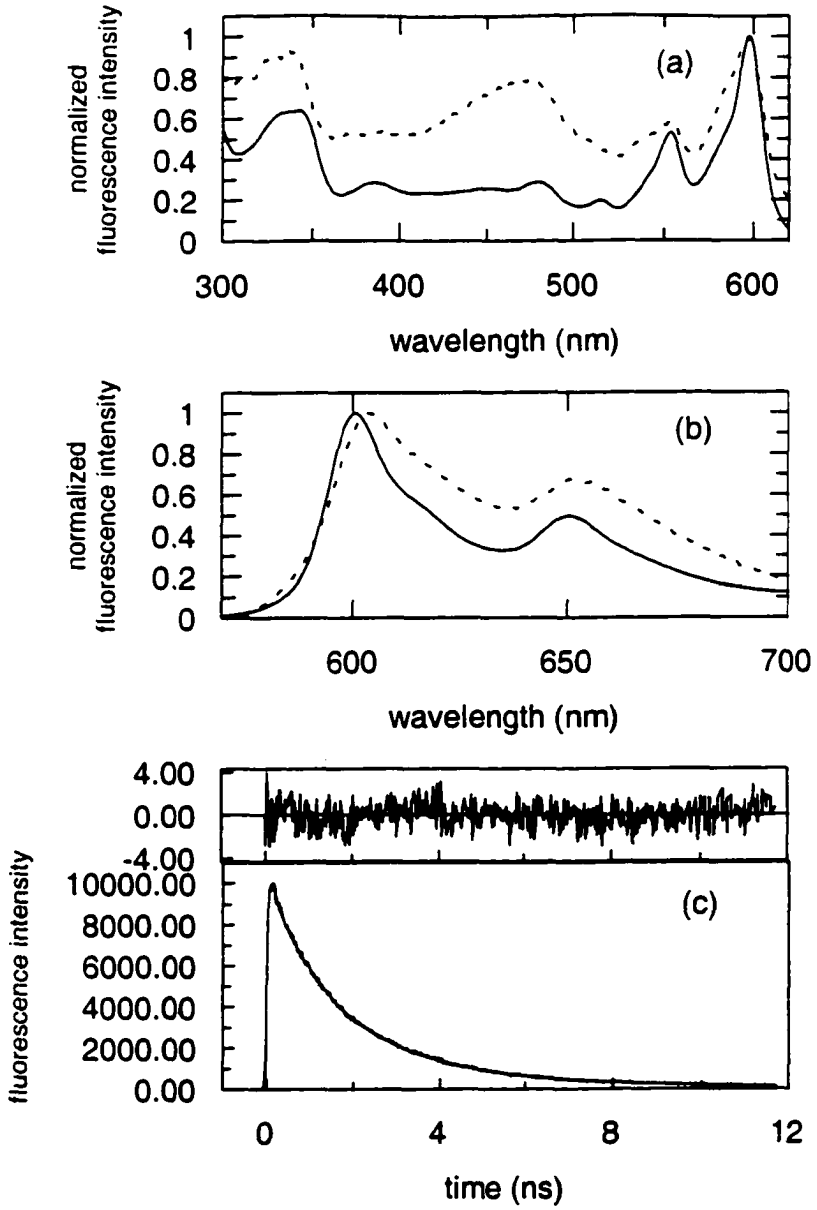

Figure 3.4 (a) Fluorescence excitation spectra (λ_{em} = 650 nm) of hypericin in poly dG-dC (dotted line) and in DMSO (solid line).

(b) Fluorescence emission spectra (λ_{ex} = 550 nm) of hypericin in poly dG-dC (dotted line) and in DMSO (solid line).

(c) Fluorescence decay of hypericin bound to poly dG-dC: λ_{ex} = 570nm; $\lambda_{em} \geq$ 610nm, χ^2 = 1.30.

consistent with Raman studies which suggest that the carbonyl oxygen of hypericin interacts with the N_1-H of the single tryptophan residue present in II A subdomain of HSA [57]. Raman studies also suggest that the hypericin interaction occurs via its carbonyl and *peri* hydroxyl groups with the N_7 nitrogen of the guanine residue in poly dG-dC [57,65-67]. The reduction of the fluorescence quantum yield of hypericin/HSA with respect to that in DMSO may be due to the H-bonding interaction of the carbonyl oxygen with the tryptophan residue, or a part of hypericin is projected outside of the protein, exposed to the solvent, or may be due to both. Similarly, in nucleic acid the very low emission can probably be accounted for greater interaction with the guanine residue, and/or greater exposure to the solvent. (It may be argued that the reduction of the fluorescence quantum yield of hypericin noted above is due to the formation of hypericin aggregates. At the micromolar concentrations used for the hypericin/HSA spectra, there was no evidence in the absorption spectra for aggregate formation. We did not, however, have enough nucleic acid to obtain a properly corrected absorption spectrum of the nucleic acid complex.)

Fluorescence Lifetime and Anisotropy Decay of Hypericin and Hypocrellin A in Complex with HAS

Tryptophan 214 of HSA. The fluorescence and fluorescence anisotropy decay parameters of the tryptophan of HSA are presented in Tables 3.1 and 3.2. In HSA, the tryptophan residue has a nonexponential fluorescence decay, which is best described by a sum of three exponentials. Its anisotropy decay is best characterized by a double exponential. These results are consistent with those obtained by other workers [68]. The double exponential anisotropy decay of the tryptophan can thus be interpreted as arising from both rapid restricted local depolarizing motions and the overall rotational diffusion of the protein. The

Table 3.1. Fluorescence lifetime parameters[a].

Sample	a_1	τ_1 (ps)	a_2	τ_2 (ps)	a_3	τ_3 (ps)
tryptophan in HSA[b]	0.29±0.01	363±30	0.23±0.02	2607±200	0.47±0.04	7787±500
tryptophan in hypericin/HSA complex[b]	0.32±0.03	296±45	0.29±0.01	2300±100	0.39±0.03	7720±470
hypericin in hypericin/HSA complex[c]	0.51±0.01	2850±350	0.49±0.01	5000±580		
hypocrellin A in hypocrellin/HSA complex[c]	0.4 (0.41)	89 (51)	0.25 (0.12)	540 (490)	0.35 (0.47)	1500 (1450)
hypericin in myoglobin[c]	0.33	180	0.27	1600	0.40	5800
hypericin in Brij-35 micelles[c]	0.05	1000	0.95	6500		
hypericin in poly dG-dC[c]	0.37	32	0.43	1300	0.20	3400

[a] Fluorescence lifetimes were fit to a sum of up to three exponentially decaying components and had the form: $F(t) = a_1 \exp(-t/\tau_1) + a_2 \exp(-t/\tau_2) + a_3 \exp(-t/\tau_3)$. The absence of values for a_3 and τ_3 implies that the lifetime was adequately described by a double exponential decay. $\chi^2 \leq 1.3$ for all data presented in the Table.

[b] For excitation and detection of the emission of the tryptophan residue of HSA, λ_{ex} = 288 nm, λ_{em} = 300-400 nm.

[c] For excitation and detection of hypericin and hypocrellin A, λ_{ex} = 570 nm, $\lambda_{em} \geq 610$ nm. Both 1:4 and 1:1 hypericin:HSA complexes gave identical results. Data shown here are for the 1:4 complex. For hypocrellin A, data for both 1:4 and 1:1 complexes are shown. The values in parentheses are those for the 1:1 complex.

Table 3.2. Fluorescence anisotropy parameters[a].

sample	r_1	τ_{r1} (ps)	r_2	τ_{r2} (ps)
tryptophan in HSA[b]	0.07±0.01	920±40	0.12±0.01	28000±3000
hypericin in HSA[c]	0.32±0.01	31000±4000		
hypocrellin A in HSA[c]	0.10 (0.14)	252 (165)	0.05 (0.12)	31000 (31000)
hypericin in Brij-35 micelles[c]	0.13	860	0.17	4700
hypericin in EtOH/MeOH(1:1)[c,d]	0.35±0.01	83±10		

[a] Fluorescence anisotropy decays were fit to a sum of up to two exponentially decaying components and had the form: $F(t) = r_2 \exp(-t/\tau_{r1}) + r_2 \exp(-t/\tau_{r2})$. The absence of values for r_2 and τ_{r2} implies that the lifetime was adequately described by a single exponential decay.

[b] For excitation and detection of the emission of the tryptophan residue of HSA, λ_{ex} = 288 nm, λ_{em} =300 - 400 nm.

[c] For excitation and detection of hypericin and hypocrellin A, λ_{ex} = 570 nm, $\lambda_{em} \geq 610$ nm. Both 1:4 and 1:1 hypericin:HSA complex gave identical results. Data shown here are for the 1:4 complex. For hypocrellin A, data for both 1:4 and 1:1 complexes are shown. The values in parentheses are those for the 1:1 complex.

[d] Reference 31.

relative contributions of these two effects are related by the order parameter, S^2, from which can be calculated a hypothetical semi cone angle in which the tryptophan diffuses. For probes attached to globular proteins, the order parameter, S^2, is a model independent measure of the extent to which restricted motion can occur: $S^2 = [r(t)/r(0)] \exp(t/\tau_r) = r(0^+)/r_{eff}(0)$, where τ_r and $r(0^+)$ are determined by the fit of the long-time behavior of the anisotropy decay

(the overall protein reorientation or tumbling) to a single exponential and are equivalent to τ_2 and $r_2(0)$, respectively (69). $r_{eff}(0) = r_1(0) + r_2(0)$. For the tryptophan residue in HSA, $S^2 = 0.8 \pm 0.01$. The order parameter can be related to a hypothetical cone semiangle, θ_0, within which the transition dipole moment can diffuse: $S = (1/2)\cos\theta_0 (1 + \cos\theta_0)$. For the tryptophan residue in HSA, $\theta_0 = 30 \pm 1^o$.

Hypericin. In comparison, hypericin has a single-exponential fluorescence decay of ~5.5 ns in all nonaqueous pure solvents. Bound to HSA (for both 1:4 and 1:1 complexes), however, its fluorescence decay is best described by a double exponential with a short component of ~2.5 ns (Figure 3.5 and Table 3.1). In order to understand what induces the nonexponential decay, hypericin was also studied in Brij-35 micelles and in complex with the protein myoglobin. In both cases, the resulting fluorescence decay is nonexponential. In the case of myoglobin, where hypericin can bind only to the surface of the protein, the decay is best described by a triple exponential (Table 3.1). Thus, in HSA the presence of this short component may arise from new nonradiative decay processes for a subset of hypericin molecules in the binding pocket, protruding into the solvent, or bound to the surface of the protein, or both.

The polarized fluorescence decay curves of hypericin bound to HSA are given in Figure 3.5. The limiting value for the anisotropy, r(0), for hypericin bound to the protein is 0.32 (Table 3.2). The anisotropy decay is single exponential and ~400-fold longer than that for the free molecule (31 ns in the protein as compared to ~80 ps in a 1:1 ethanol/methanol mixture [31]). This large rotational time constant is obviously a signature of the overall protein motion, thus indicating that hypericin is very rigidly bound to HSA. The anisotropy decay of hypericin bound to HSA must be considered carefully in light of the lifetime data

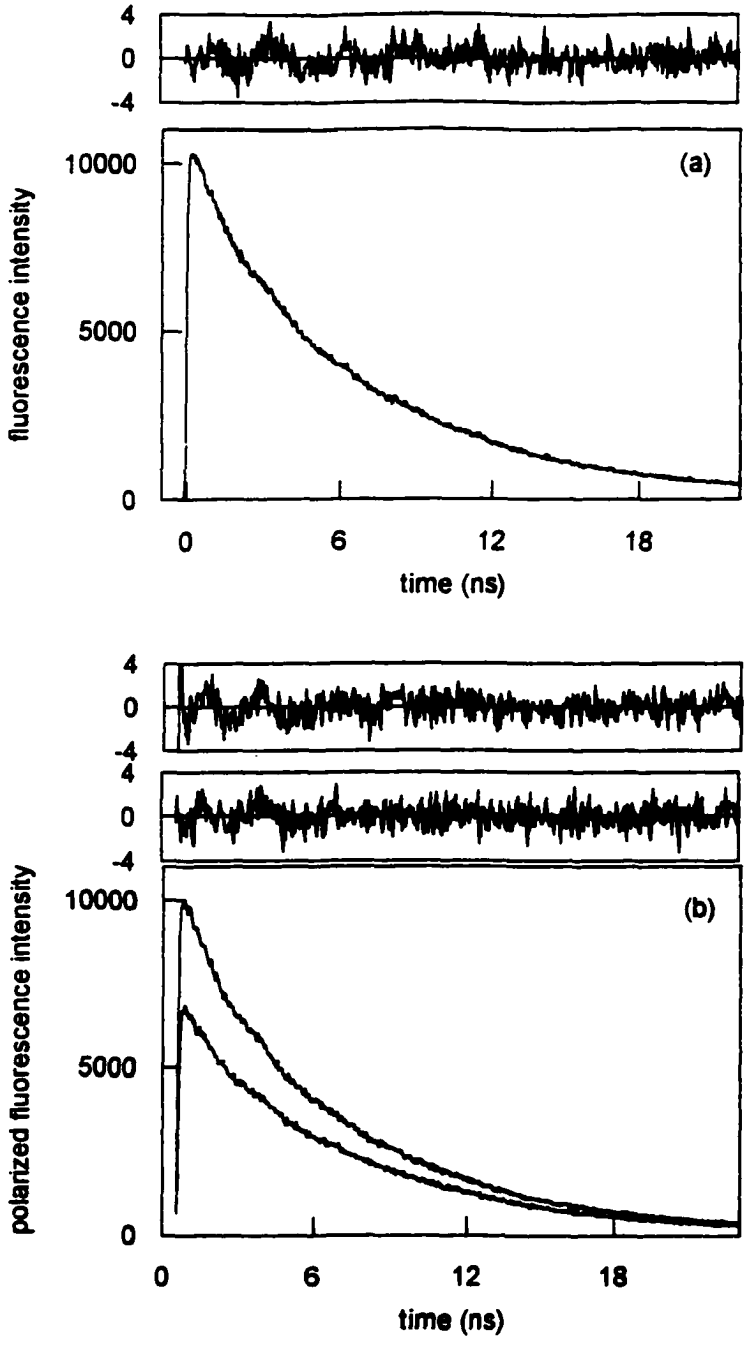

Figure 3.5 (a)Fluorescence decay of hypericin bound to HSA: $\lambda_{ex} = 570$ nm; $\lambda_{em} \geq 610$ nm, $\chi^2 = 1.10$.

(b) Fluorescence anisotropy decay of hypericin bound to HSA: $\lambda_{ex} = 570$ nm; $\lambda_{em} \geq 610$ nm, $\chi^2 = 1.12$. (The anisotropy decay is independent of the stoichiometry of the complex. Data not shown. See Table 3.2).

discussed immediately above. Chromophores bound to proteins that exhibit no rapid restricted motion (with an apparatus providing ~50 ps time resolution) are extremely rare. The example of the single tryptophan residue buried in the interior of *Pseudomonas aeruginosa* azurin is one example [70]. The surfaces should be much less rigid and more disordered than the interiors. In addition, the surfaces are exposed to interactions with solvent. Consequently, the fluorescence anisotropy decay of the single surface exposed tryptophan residue in *Alcaligenes faecalis* azurin does exhibit rapid restricted motion, as is expected [70]. We thus conclude that the single-exponential anisotropy decay of 31 ns for hypericin bound to HSA arises from hypericin molecules rigidly held in the binding pocket, but in sufficiently different conformations to experience different nonradiative interactions with neighboring amino acid residues. If there are surface-bound hypericin molecules, the signal-to-noise ratio of our experiment is not sufficient to detect them in the anisotropy decay.

Bound to poly dG-dC, the fluorescence intensity of hypericin was too low to permit time-resolved polarization studies. However, the time-resolved fluorescence (Figure 3.4c) shows a nonexponential decay, which can be best fit by a sum of three exponentials (Table 3.1).

Hypocrellin A. The effects of aqueous solvation and of binding to HSA on the fluorescence anisotropy decay and lifetime of hypocrellin A are illustrated in Figs.3.6 and 3.7. There are considerable differences with respect to hypericin:

1) The fluorescence lifetime and anisotropy decays of the hypocrellin A/HSA complex depend on stoichiometry. Different kinetics are obtained for the 1:4 and the 1:1 complexes (Figure 3.6 and Tables 3.1 and 3.2). Most notable are the relative

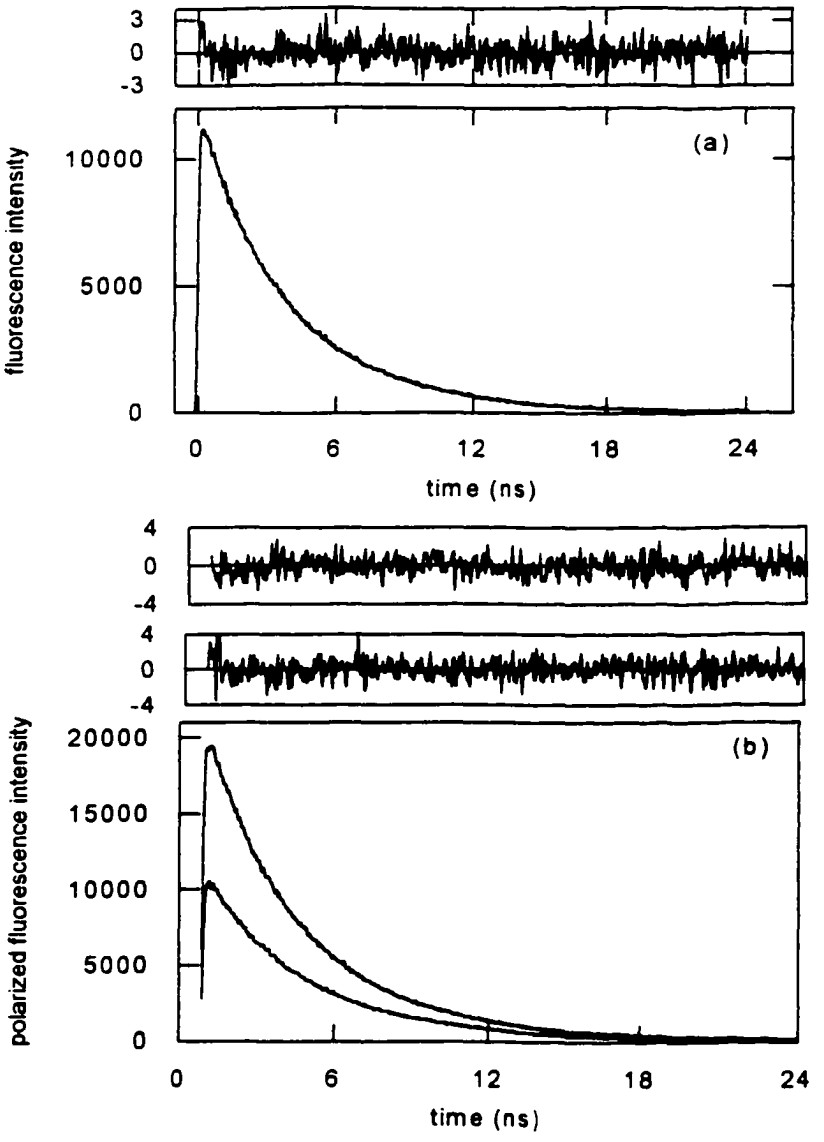

Figure 3.6 (a) Fluorescence anisotropy decay of hypocrellin A/HSA (1:4) in buffer. A fit to a double exponential yields r(t) = 0.10 exp(-t/0.25 ns) + 0.12 exp(-t/31 ns), χ^2 = 1.05. A fit of the lifetime to a triple exponential yields F(t) = 0.35 exp(-t/ 1.5ns) + 0.25 exp(-t/0.54 ns) + 0.40 exp(-t/0.09 ns), χ^2 = 1.0 (data not shown). The order parameter for this complex (1:4) is 0.54 and the half angle is 35.8°. See Table 3.2.

(b) Fluorescence anisotropy decay of hypocrellin A/HSA (1:1) in buffer. A fit to a double exponential yields r(t) = 0.14 exp(-t/0.17 ns) + 0.05 exp(-t/31 ns), χ^2 = 1.08. A fit of the lifetime to a triple exponential yields F(t) = 0.47 exp(-t/1.45ns) + 0.12 exp(-t/0.49 ns) + 0.41 exp(-t/0.05 ns), χ^2 = 1.15 (data not shown). The order parameter for this complex (1:1) is 0.28 and the half angle is 50.2°. See Table 3.2.

amplitudes of the shorter and 31-ns components of the anisotropy decays. Such an effect is not apparent for the hypericin/HSA complexes.

2) The steady-state absorption spectrum of hypocrellin A is much less sensitive to the presence of water than that of hypericin (compare Figs.3.7a and 3.8a), as measured by the perturbation of the lowest energy transition upon addition of water.
3) The fluorescence lifetime of hypocrellin A is much less sensitive to the presence of water that that of hypericin (Figs.3.7c and 3.8c).
4) The fluorescence decay of hypocrellin A bound to HSA is more similar to that of hypocrellin A in a 1% DMSO solution compared to hypericin bound to HSA (Figs. 3.7b and 3.8b).

Based on these fluorescence results, it is difficult to determine with any degree of certainty to what extent and in what manner hypocrellin binds to HSA. For example, the fluorescence lifetime data in mixed DMSO/water solutions clearly indicate that hypocrellin is much more hydrophilic than is hypericin. We tentatively suggest that hypocrellin is aggregating nonspecifically at the surface of the protein.

Investigating Ultrafast Excited-state Processes by Transient Pump-probe Absorption and Fluorescence Upconversion Techniques

Hyperici: Transient absorption. In pump-probe transient absorption experiments, we have discovered that stimulated emission can be induced from the excited state of hypericin in the region of 600-660 nm [25-27]. This stimulated emission grows with a time constant of 6-10 ps in all solvents, except sulfuric acid, where it appears within the duration of our laser

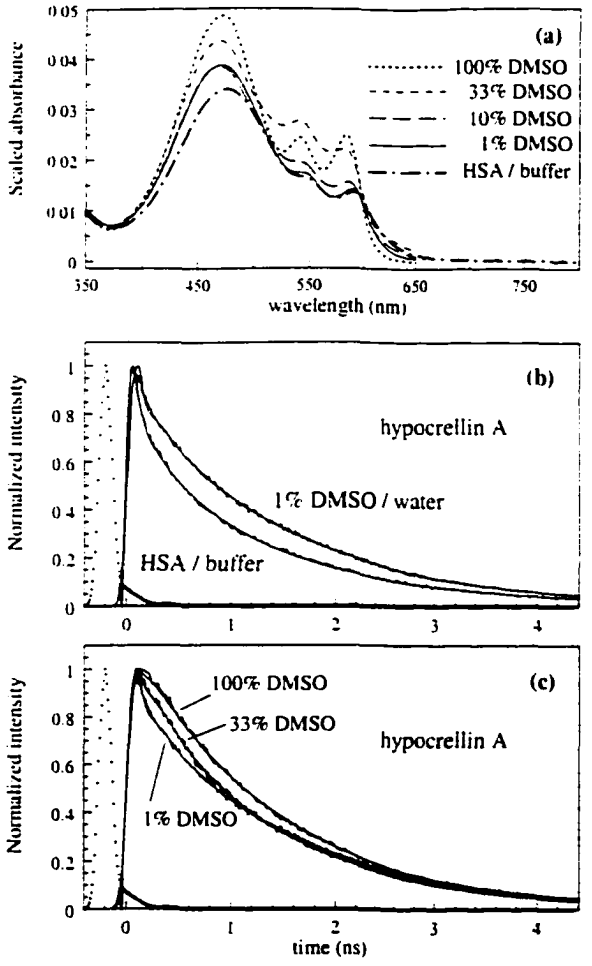

Figure 3.7 (a) Absorbance spectra of hypocrellin A in 1:1 mixture with HSA in buffer (solid) and in DMSO/water mixtures of various proportions: 1% (dotted), 10% (long dashed), 33% (short dashed) and 100% DMSO (dash-dot). These spectra were scaled to compensate for slightly different chromophore concentration.

(b) Comparison of normalized lifetime decay traces in mixture with HSA (1:1 ratio) and in 1% DMSO/water solution. F(t) = 0.985exp(-t/4.2 ps)+0.002exp(-t/235 ps)+0.013exp(-t/1450 ps) for 1% DMSO. F(t) = 0.55exp(-t/63 ps)+0.19exp(-t/644 ps)+0.26exp(-t/1620 ps) for HSA/buffer solution.

(c) Normalized lifetime decay traces of hypocrellin A in DMSO/water mixtures of different proportions. F(t) = 0.97exp(-t/4.2 ps)+0.02exp(-t/235 ps)+0.01exp(-t/1450 ps) for 1% DMSO. F(t) = 0.83exp(-t/1.2 ps)+0.03exp(-t/363 ps)+0.13exp(-t/1335ps) for 33% DMSO. F(t) = 1.00 exp(-t/1310 ps) for 100% DMSO. The instrument response function is shown by the dotted line. It is also artificially shifted with respect to the fluorescence decays.

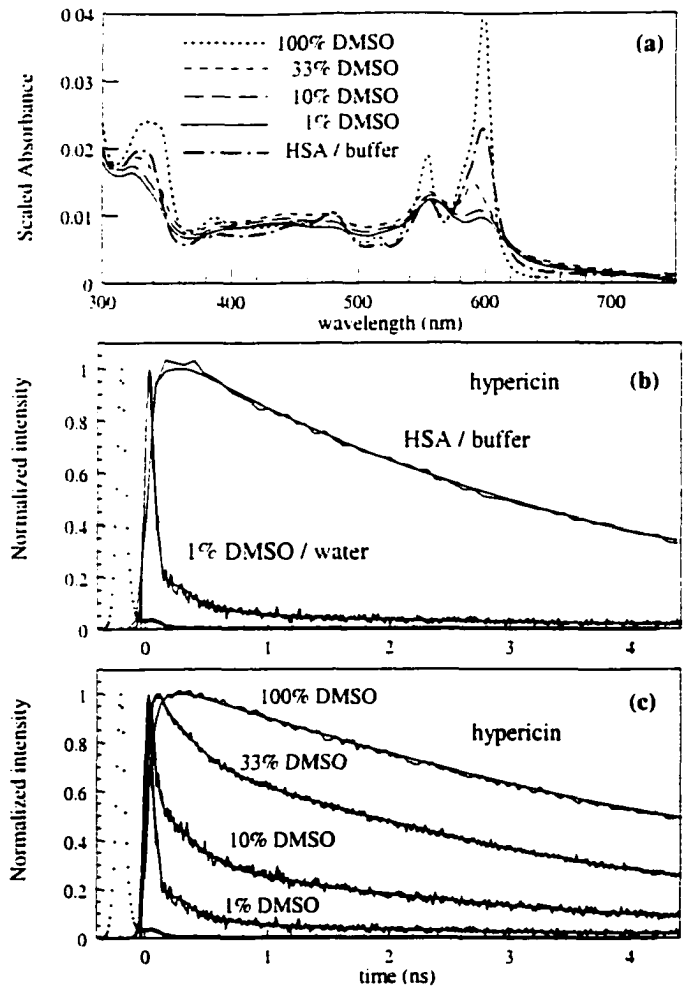

Figure 3.8 (a) Absorbance spectra of hypericin in 1:1 mixture with HSA in buffer (dash-dotted) and in DMSO/water mixtures of various proportions: 1% (solid), 10% (long dashed), 33% (short dashed) and 100% DMSO (dotted). These spectra were scaled to compensate for slightly different chromophore concentration.

(b) Comparison of normalized lifetime decay traces of hypericin with HSA (1:1 ratio) and in 1% DMSO/water solution. F(t) = 0.96exp(-t/12 ps)+0.03exp(-t/304 ps)+0.01exp(-t/3680ps) for 1% DMSO. F(t) = 0.75exp(-t/3050 ps)+0.25exp(-t/5770 ps) for HSA/buffer solution.

(c) Normalized lifetime decay traces of hypericin in DMSO/water mixtures of different proportions. is shown in the insert. F(t) = 0.96exp(-t/12 ps)+0.03exp(-t/304 ps)+0.01exp(-t/3680ps) for 1% DMSO. F(t) = 0.91exp(-t/1.4 ps)+0.05exp(-t/264 ps)+0.04exp(-t/3380ps) for 10% DMSO. F(t) = 0.41exp(-t/190 ps)+0.59exp(-t/3870ps) for 33% DMSO. F(t) = 1.00 exp(-t/5580 ps) for 100% DMSO. The instrument response function is shown by the dotted line. It is also artificially shifted with respect to the fluorescence decays.

pulses. We have argued that this transient is a signature of excited-state intramolecular proton (or hydrogen atom) transfer between the hydroxyl groups *peri* to the carbonyl. This interpretation has been confirmed in numerous experiments involving hypericin analogs [32,33] and by the fluorescence upconversion technique [34]. Figure 3.9 presents the stimulated emission transients of hypericin in sulfuric acid, DMSO and in ~5:1 and 1:1 complexes with HSA.

The curves are distinctly different; and when the transients in DMSO and the protein are normalized and fit globally, the amplitude for the rise time of hypericin is smaller in HSA (0.36) than in DMSO (0.65) for the ~5:1 complex. It is thus possible to interpret these results as indicating that the excited-state proton or hydrogen atom transfer of hypericin is partially reduced, but not stopped completely, when it is complexed with HSA: i.e., that while one of the carbonyl groups is complexed to the N_1-H of the tryptophan residue, the other one is free to execute excited-state proton transfer. Because the ratio of hypericin to HSA in this experiment is approximately 5 to 1, the possibility that the observed kinetics are a superposition of intramolecular proton transfer reactions of surface-bound hypericin and pocket-bound hypericin cannot be unambiguously excluded. For example, it may be argued that the transient in Figure 3.9c represents at least two different populations of hypericin molecules: those in which intramolecular proton transfer is completely inhibited because they are pocket bound and one of their carbonyls is coordinated to the N-H proton; and those that are bound to the surface and free to execute intramolecular proton transfer.

In order to investigate this possibility, the 1:1 complex of hypericin and HSA was investigated. In the 1:1 complex, the rising component disappears, indicating that the intramolecular proton transfer process has been impeded.

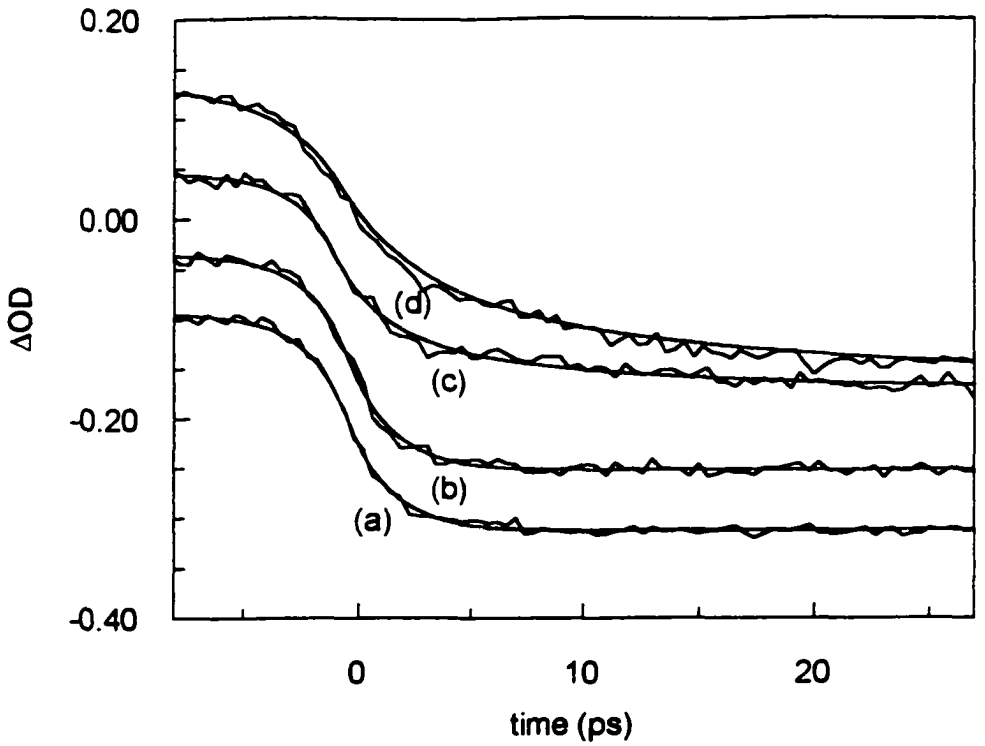

Figure 3.9 Transient absorption traces of hypericin in different environments. The traces are normalized to the maximum absorption in the figure. λ_{pump} = 588 nm; λ_{probe} = 600 nm.
(a) Sulfuric acid: $\Delta A(t)/\Delta A_{max} = -1.0 \exp(-t/\infty)$.
(b) HSA: $\Delta A(t)/\Delta A_{max} = -1.0 \exp(-t/\infty)$; 1:1 complex, [HSA] = [hyp] = 7×10^{-5} M
(c) HSA: $\Delta A(t)/\Delta A_{max} = -0.36$ [exp(-t/6.0 ps)– 1] - 0.64; ~1:5 complex; [HSA] = 1.5×10^{-5} M; [hyp] = 7×10^{-5} M
(d) DMSO: $\Delta A(t)/\Delta A_{max} = -0.65$ [exp(-t/6.0 ps)– 1] - 0.35.

Fluorescence upconversion of the 1:1 complex. Because of the possibility that the rising component was obscured in the 1:1 complex by the presence of other absorbing species or because the signal-to-noise ratio was insufficient, we searched for the rising component with the fluorescence upconversion technique, which measures only emission. Figures 3.10 and 3.11 present fluorescence upconversion traces of the 1:1 hypericin/HSA complex at two different emission wavelengths, 606 and 653 nm, corresponding to the first two maxima of the emission spectrum of the hypericin/HSA complex (Figure 3.2a). On the

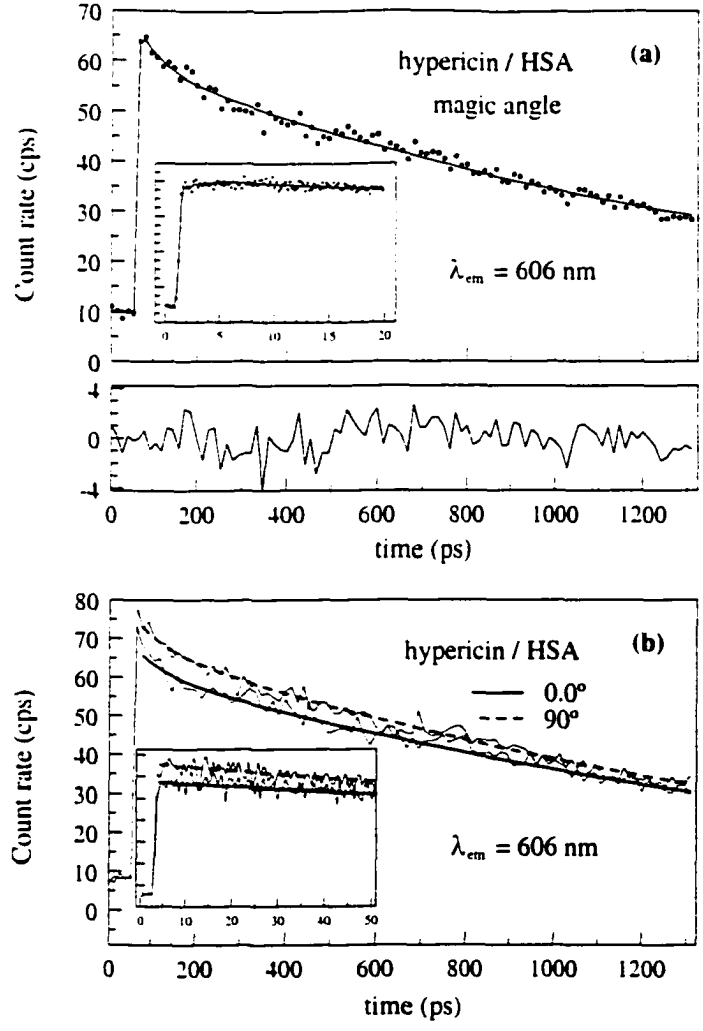

Figure 3.10 (a) Fluorescence upconversion at the "magic angle" of 1:1 hypericin:HSA complex, [HSA] = 1×10^{-4} M, λ_{ex} = 414 nm, λ_{em} = 606 nm. A fit to double exponential yields: F(t) = 0.12 exp(-t/50 ps) + 0.88 exp(-t/1320 ps). The 50-ps component is not observed with the limited resolution afforded by time correlated single photon counting measurements. The insert shows results obtained on a 20 ps time scale.

(b) Parallel and perpendicular fluorescence upconversion traces of the 1:1 hypericin:HSA complex, λ_{ex} = 414 nm, λ_{em} = 606 nm. Anisotropy decay fit with a single decaying component yields r(t) = -0.03 ± 0.01 exp(-t/2 ± 1 ns). The large relative error is due to the small value of limiting anisotropy at this excitation wavelength. The insert shows results obtained on a 20 ps time scale. That a value of ~2 ns instead of 31 ns (Table 3.2) is obtained is a result of collecting the data on a full scale of only 1.3 ns.

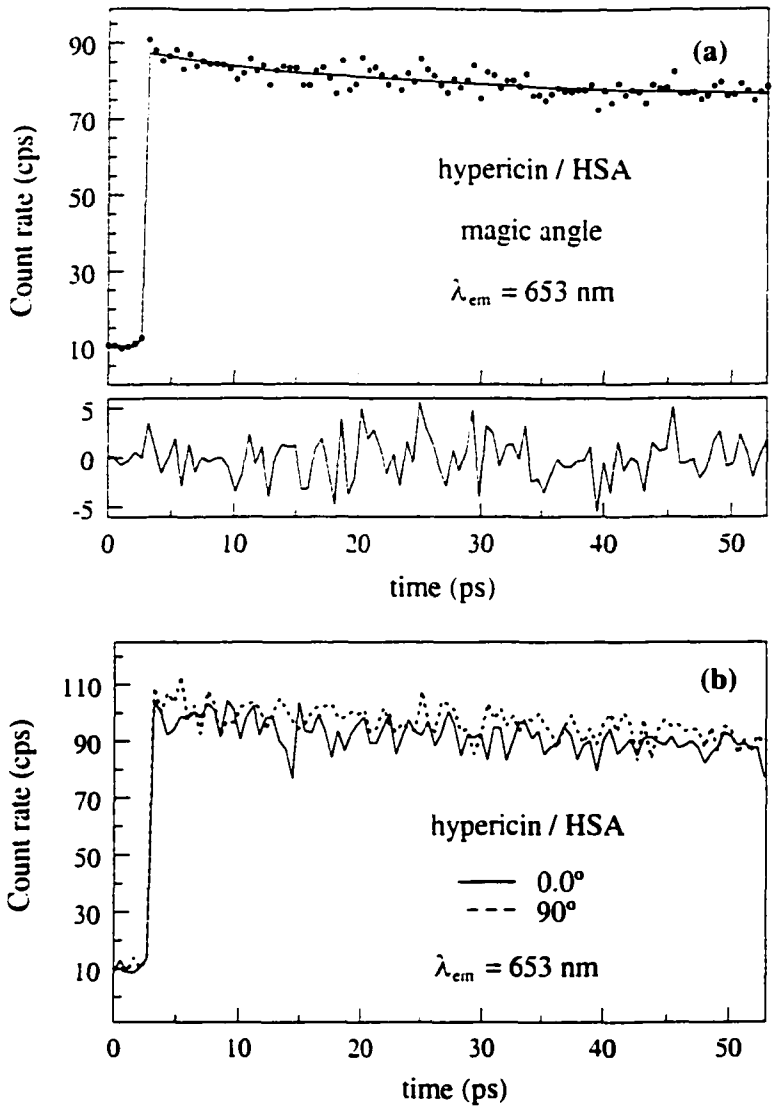

Figure 3.11 (a) Fluorescence upconversion at the "magic angle" of 1:1 hypericin:HSA complex, [HSA] = $1x10^{-4}$ (M); λ_{ex} = 414 nm, λ_{em} = 653 nm.

(b) Parallel and perpendicular fluorescence upconversion traces of the 1:1 hypericin:HSA complex, λ_{ex} = 414 nm, λ_{em} = 653 nm. These data were collected on the short timescale only.

shortest time scales investigated (20 ps full scale) there was no evidence for a rising component in the fluorescence signal, confirming the conclusions obtained from the transient

absorption measurements, that intramolecular proton transfer is impeded in the 1:1 hypericin/HSA complex.

Hypocrellin A. Because the fluorescence of hypocrellin A is so strongly quenched in the complex with HSA (Figures 3.6 and 3.7), it was impractical to obtain upconversion data. Transient absorption experiments with the 1:1 complex give no indication of excited-state proton transfer and only indicate a rapid decay of an excited state (~32 ps), consistent with the photon counting data (Figures 3.6 and 3.7).

Energy Transfer in the HSA Complexes

Between the tryptophan of HSA and hypericin . The emission spectrum of tryptophan overlaps the hypericin absorption spectrum, thus providing the possibility of energy transfer from tryptophan to hypericin. The total integrated emission intensity of the tryptophan residue in albumin is greater when there is no hypericin complexed to it. The ratio of the integrated emission intensity of tryptophan (after correcting for the inner filter effect due to hypericin absorption) without and with hypericin is 1.5, i.e. there is a 33% decrease in the integrated emission intensity. Figure 3.12 presents the corrected emission spectra of the tryptophan emission in the presence and in the absence of hypericin. The ratio of the integrated emission of hypericin at two wavelengths, 295 and 550 nm, was determined as follows [69]:

$$\frac{\Phi_F(\lambda_1)}{\Phi_F(\lambda_2)} = \frac{1-10^{-A(\lambda_2)}}{1-10^{-A(\lambda_1)}} \frac{\int_0^\infty I_{em}(\lambda_1,\tilde{\nu})d\tilde{\nu}}{\int_0^\infty I_{em}(\lambda_2,\tilde{\nu})d\tilde{\nu}} \frac{c(\lambda_1)}{c(\lambda_2)} \qquad (3-1)$$

where, $A(\lambda_i)$ is the absorbance (optical density) at the excitation wavelength, λ_i, $I_{em}(\lambda_i, \tilde{\nu})$ is the emission intensity at the excitation wavelength λ_i and $c(\lambda_i)$ is a correction factor taking into account fluctuations of the excitation intensity. The integrated emission (fluorescence quantum yield) of hypericin is 0.36 in DMSO and 0.53 when it is complexed with HSA (in this latter case, correction is made for the "inner filter effect" due to tryptophan absorption at

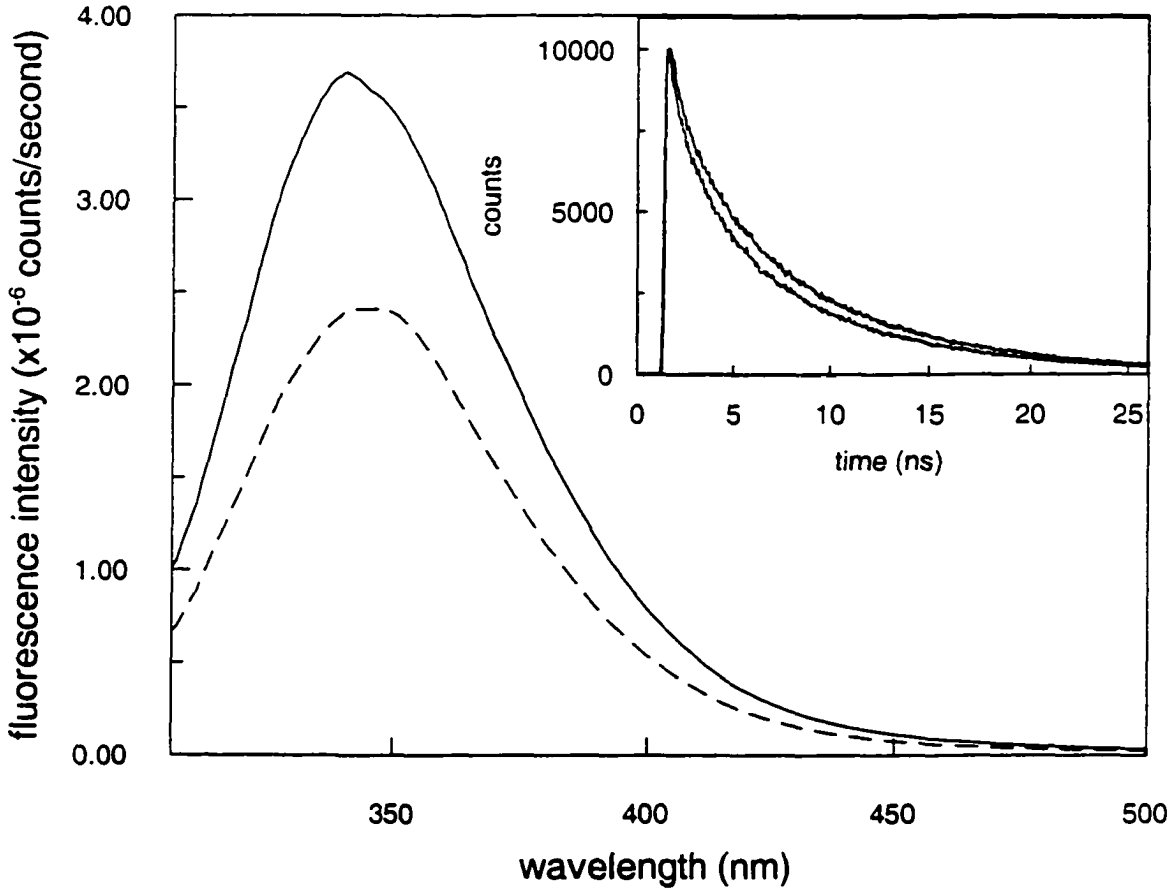

Figure 3.12 Corrected tryptophan emission of HSA in the presence (dashed line) and in the absence (solid line) of hypericin. Inset: Decay curve of the tryptophan residue of HSA in the absence (top) and in the presence (bottom) of hypericin. λ_{ex} = 288 nm; 300 ≤ λ_{em} ≤ 400 nm.

295 nm). Thus there is a 47% increase in the integrated emission of hypericin when excited at 295 nm, in the presence of albumin. This is in fair agreement with the percentage decrease of tryptophan emission. The fluorescence decay curves for tryptophan in the presence and in absence of hypericin are clearly different (Figure 3.12). The tryptophan residue in HSA has an emission maximum at 340 nm (compared to that of tryptophan in buffer at 352 nm) and the emission maximum has a slight red shift (342 nm) when complexed with hypericin. The quantum yield of tryptophan in HSA is 0.12 as compared to that of 0.18 for tryptophan in water at pH 7 [69,71]. The average fluorescence lifetime of tryptophan in HSA decreases by 14% when hypericin is bound (data not shown). We were, however, unable to see any rise in the time resolved fluorescence of hypericin when exciting at 295 nm. This may be probably due to a very fast energy transfer that cannot be resolved with our instrument or whose amplitude is small compared to the prompt fluorescence arising from the direct excitation of the hypericin. Such a rapid energy transfer can explain our inability to observe a rise time in fluorescence emission of hypericin in our time-correlated single-photon-counting experiments.

In order to determine the efficiency of this energy transfer, we estimated the so-called critical distance. The efficiency of the nonradiative energy transfer in a Förster energy transfer mechanism is determined by, among other things, R_0, the critical distance at which the rate of energy transfer is equal to the inverse of the fluorescent lifetime of the donor.

$$k_{ET} = \frac{1}{\tau_F}\left(\frac{R_0}{R}\right)^6 \qquad (3-2)$$

$$R_0^6 = \frac{9000(\ln 10)\Phi_D}{128\pi^5 n^4 N}\frac{2}{3}\int_0^\infty F_D(\tilde{\nu})\varepsilon_A(\tilde{\nu})\tilde{\nu}^{-4}d\tilde{\nu} \qquad (3-3)$$

In the above equations k_{ET} is the rate of energy transfer, τ_F is the average lifetime of the tryptophan donor (3.4 ns), R is the distance of separation between the donor and acceptor, n is the index of refraction of the medium, N is Avogadro's number, Φ_D is the fluorescence quantum yield of the tryptophan donor (0.12), $F_D(\tilde{\nu})$ is the donor emission normalized to unit area on wavenumber scale, and $\varepsilon_A(\tilde{\nu})$ is the decadic molar extinction coefficient (in $L^{-1}mol^{-1}cm^{-1}$) on a wavenumber scale. R_0 calculated for the tryptophan-hypericin complex is 94 Å. This large value for R_0 is not surprising because there is a high degree of spectral overlap (Figure 3.13). Assuming the actual distance between these molecules to be 10 Å (center to center) the rate for energy transfer is $3.8 \times 10^{14} s^{-1}$ (3×10^{-15} s). In order to resolve the energy transfer between tryptophan and hypericin, the two chromophores would need to be separated by 55 Å: such a separation, given the parameters of the calculation, yields an energy transfer time of 50 ps. We thus conclude that energy transfer between tryptophan and hypericin is too rapid to be observed with our apparatus. (We note that if the donor and acceptor are in physical contact, a Förster dipole-dipole mechanism may not be a quantitatively appropriate model for the energy transfer.)

If we assume that even in the 1:4 hypericin:HSA complex hypericin is nonspecifically bound to the surface of HSA (which is in agreement with the nonexponential fluorescence decay of hypericin in this complex) as well as specifically coordinated to the tryptophan residue, a range of energy transfer times are expected. These can only be crudely estimated since even though a published structure for HSA exists [72,73], its coordinates have not been deposited in any data bank of which we are aware. The dimensions of HSA are approximately $30 \times 80 \times 80$ Å. If we assume for a case of nonspecific binding that the tryptophan and hypericin lie on opposite extremes of the HSA the energy transfer time will

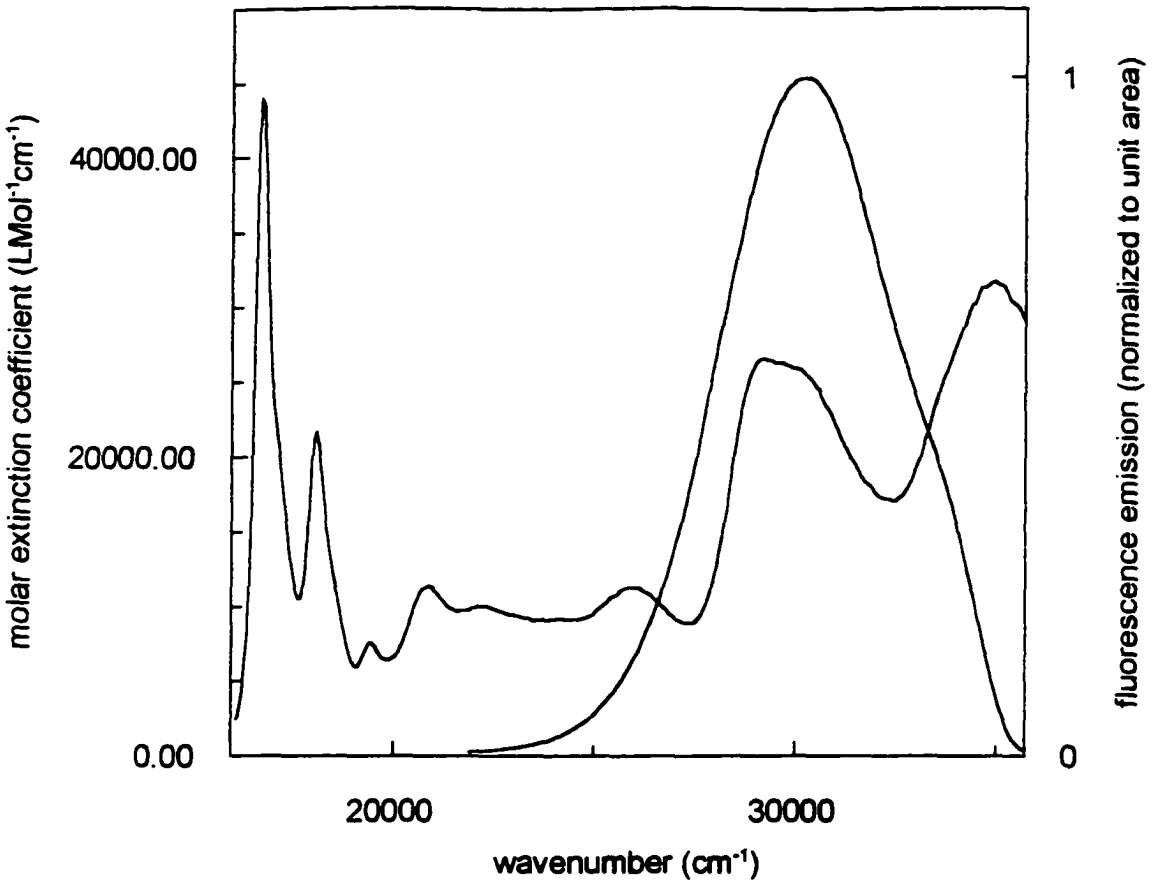

Figure 3.13 Spectral overlap between hypericin absorption and the tryptophan emission from HSA (in phosphate buffer at pH 7 and 22°C).

be 0.4 ps at 30 Å and 790 ps at 80 Å. If all the hypericin molecules had a 10-Å center-to-center distance from tryptophan, it is expected that a negligible amount of tryptophan fluorescence be observed. Since this is not the case, we conclude that there is nonspecific binding of hypericin to HSA even in the 1:4 hypericin:HSA complex.

Between the tryptophan of HSA and hypocrellin A . We have no evidence for energy transfer from tryptophan to hypocrellin. In a 1:1 complex, the quantum yield of hypocrellin only increases 6%, which is negligible within the margin of error. In a 1:4 hypocrellin/ HSAcomplex, the hypocrellin quantum yield decreases by 28%, which implies aggregation

of hypocrellin. These results are again consistent with hypocrellin A binding to the surface of HSA in a nonspecific manner.

Discussion and Conclusions

A comparison of the steady-state spectra of hypericin in DMSO and sulfuric acid and in complex with HSA and poly dG-dC suggests that there is a strong interaction of the hypericin carbonyl group with the latter two macromolecules. Specific interactions of hypericin with DNA and its model compounds were studied by surface enhanced and resonance Raman spectroscopy [57,65-67]. The results indicate that there is a specific site interaction between the terminal hydroxyl and carbonyl groups of hypericin and the guanine residues in DNA probably through the N_7 atom. Raman studies also indicate that the carbonyl oxygen of hypericin interacts with the tryptophan residue in the II A sub domain of HSA. This interaction is suggested to occur via hydrogen bonding between the N_1-H of the tryptophan and the carbonyl oxygen of hypericin [57].

As indicated above, there are several important differences in the interactions of hypericin and hypocrellin A with HSA. It is reasonable to conclude from the 31-ns single-exponential fluorescence anisotropy decay of the HSA/hypericin complex and the fact that the form of this decay is independent of the stoichiometry of the complex (Figure 3.6), that the majority of hypericin binds rigidly and specifically in the IIA subdomain of HSA. On the other hand, not only is there a rapidly decaying component of ~150-250 ps in the anisotropy of the hypocrellin/HSA complex, but the form of the decay depends on the stoichiometry of the complex (Figure 3.6). The order parameters for the hypocrellin/HSA complex are ≤ 0.5

(as opposed to 1 for the hypericin/HSA complex) and indicate, along with the other data, that the majority of hypocrellin that binds to HSA binds to the more fluid-like exterior.

A comparison of the fluorescence properties of hypericin and hypocrellin in complex with HSA and in DMSO/water mixtures indicates that hypocrellin is more hydrophilic than hypericin, which is consistent with the above interpretation of the anisotropy data for hypocrellin binding largely to the HSA surface in a nonspecific manner. That there is no energy transfer from the HSA tryptophan to hypocrellin and that in the case of the 1:4 hypocrellin/HSA complex the fluorescence quantum yield of hypocrellin actually decreases when the tryptophan is excited strongly suggests that hypocrellin is aggregated at the surface of HSA.

In the 1:4 hypericin/HSA complex, it is very likely that some hypericin binds to the surface; but the fact that hypericin's lifetime in the complex is so much longer than that of hypocrellin's (Figures 3.7b and 3.8b) indicates that these surface-bound molecules are not aggregated. Also, hypericin's ability to execute excited-state intramolecular proton transfer in this complex (Figure 3.9c) indicates that these surface-bound molecules are not aggregated—assuming aggregation most likely occurs end-to-end, so that the hydroxyl and carbonyl groups of neighboring hypericin molecules are mutually blocked [61]. Note that there is no evidence for intramolecular excited state proton transfer for the hypocrellin/HSA complex in any stoichiometry. Study of the hypericin/HSA complex may also provide significant insight into the nature of the proton transfer reaction itself. If the specific binding interaction of hypericin to HSA is such as indicated in the Raman experiments (i.e., by coordinating one carbonyl group of hypericin and hence prohibiting it from accepting the neighboring hydroxyl proton), then the absence of intramolecular proton transfer in the 1:1

complex (Figures 3.9b, 3.10, 3.11) indicates that proton transfer cannot occur independently in the "top" or "bottom" of the molecule; and, consequently, that the proton transfer is a concerted event involving both ends of hypericin. It is also possible that the rigid binding of hypericin to HSA prohibits it from any intramolecular conformational change [74] that accompanies the proton transfer reaction and that this also is responsible for the absence of intramolecular proton transfer in the complex.

Finally, an important problem raised by this study is understanding the nature of the nonradiative processes induced upon binding hypericin to proteins, DNA, or micelles. In all the model systems to which hypericin is bound, nonexponential fluorescence decay is induced (Table 3.1). This question has been raised by Song and coworkers [75-76] in the context of another system that is very similar to that of hypericin, namely the stentorin chromophore (Figure 3.1). Stentorin serves as the primary photosensor in the single cell ciliate, *Stentor coeruleus*. Proton transfer has been suggested as a possible primary photoprocess in triggering the light signal transduction chain in *Stentor coeruleus*. The stentorin chromophore is covalently linked to an ~50 kDa apoprotein. Bound to the protein, in water, this chromophore exhibits a very short-lived nonexponential fluorescence decay that is dominated (~95%) by an 8-ps component. Song and coworkers have shown that the long-lived hypericin fluorescence can be efficiently quenched by electron acceptors such as benzoquinone [77,78] and they have proposed that excited-state electron transfer of the stentorin chromophore to disulfide bonds in the protein result in photooxidation of the stentorin chromophore (HO—ST—OH) to oxystentorin (O = ST = O) and the loss of two protons by the following mechanism, which is reversible [75,78] :

$$HO—ST—OH + h\nu \rightarrow HO—ST—OH^* \rightarrow HO—ST—OH^{\bullet+} \rightarrow O = ST = O + 2H^+$$

Song and coworkers estimate the oxidation potential of excited-state hypericin to be ~1.2 V [77] and use the oxidation potential of dithiodiethanol (0.95 V) for that of a disulfide bridge. (There is considerable uncertainty in these numbers. For example, the oxidation potentials of cystine disulfide and oxidized β-mercaptoethanol are calculated to be 1.7 and 1.5 V, respectively [79]). It is quite possible that such electron transfer processes are occurring in HSA, which has 18 disulfide bridges [80]. Excited-state electron transfer of hypericin bound to poly dG-dC is also feasible (the oxidation potentials of guanine and cytosine are 0.85 V and 1.2 V, respectively [81]. It is also possible that the long-lived (~5.5 ns) excited state of hypericin is quenched by an excited-state *intermolecular* proton transfer process independent of any electron-transfer processes (for example, in myoglobin or micelles, where there are no disulfide bridges). Such excited-state proton transfer to an appropriate acceptor may explain our inability to observe a light-induced pH drop in micelles or bound to HSA (see Experimental Section).

The nonradiative rate processes that are introduced upon binding hypericin (or hypocrellin A) to protein, DNA, or micelles give rise to nonexponential fluorescence decay in hypericin. In the context of what is known for the analogous stentorin chromophore, such nonradiative processes may involve excited-state electron transfer, excited-state proton transfer, or new processes introduced by the presence of surface-bound aggregates. Further work is required to understand the nature and the mechanisms of these pathways. To what

extent they arise from specific or nonspecific binding, interior or surface binding, and aggregation of the chromophore is an important question that we hope to address by studying a more detailed series of target molecules than has been done in the present work where the nature of the chromophore-macromolecule interaction is known or can be predicted.

Acknowledgments

This work was supported in part by NSF grant CHE-9613962 to J.W.P. P.M. was supported by grant 1/3258/96 of the Slovak Ministry of Education. We thank Professor Pierre Jardon and Dr. Anindya Dutta for their extremely careful reading of the manuscript and for their helpful comments.

References

1. Duran, N. and P.-S. Song (1986) Hypericin and its photodynamic action. *Photochem. Photobiol.* **43**, 677-680.
2. Lown, J. W. (1997) Photochemistry and photobiology of perylenequinones. *Can. J. Chem.* **75**, 99-119.
3. Diwu, Z. (1995) Novel therapeutic and diagnostic applications of hypocrellins and hypericins. *Photochem. Photobiol.* **61**, 529-539.
4. Diwu, Z. and J. W. Lown (1990) Hypocrellins and their use in photosensitization. *Photochem. Photobiol.* **52**, 609-616.
5. Kraus, G. A., W. Zhang, M. J. Fehr, J. W. Petrich, Y. Wannemuehler and S. Carpenter (1996) Research at the interface between chemistry and virology, development of a molecular flashlight. Chem. Rev. 96, 523-535.
6. Meruelo, D., G. Lavie and D. Lavie (1988) Therapeutic agents with dramatic antiretroviral activity and little toxicity at effective doses: aromatic polycyclic diones hypericin and pseudohypericin. *Proc. Natl. Acad. Sci. USA.* **85**, 5230-5234.

7. Lenard, J., A. Rabson and R. Vanderoef (1993) Photodynamic inactivation of infectivity of human immunodeficiency virus and other enveloped viruses using hypericin and rose bengal: inhibition of fusion and syncytia formation. *Proc. Natl. Acad. Sci. USA* **90**, 158-162.

8. Hudson, J. B., J. Zhou, J. Chen, L. Harris, L. Yip and G. H. N. Towers (1994) Hypocrellin, from *Hypocrella bambuase*, is phototoxic to human immunodeficiency virus. *Photochem. Photobiol.* **60**, 253-255

9. Lopez-Bazzocchi, I., J. B. Hudson and G. H. N. Towers (1991) Antiviral activity of the photoactive plant pigment hypericin. *Photochem. Photobiol.* **54**, 95-98.

10. Couldwell, W. T., R. Gopalakrishna, D. R. Hinton, S. He, M. H. Weiss, R. E. Law and M. L. J. Apuzzo (1994) Hypericin a potential antiglioma therapy. *Neurosurgery*. **35**, 705-710.

11. Anker, L., R. Gopalakrishna, K. D. Jones, R. E. Law and W. T. Couldwell (1995) Hypericin in adjuvant brain tumor therapy. *Drugs of the Future* **20**, 511-517.

12. Thomas, C. and R. S. Pardini (1992) Oxygen dependence of hypericin-induced phototoxicity to EMT6 mouse mammary carcinoma cells. *Photochem. Photobiol.* **55**, 831-837.

13. Okpanyi, S. N. and M. L. Weischer (1987) Animal experiments on the psychotropic action of hypericum extract. *Arzneilmittel-Forschung* **37**, 10-13.

14. Linde, K., G. Ramirez, C. D. Mulrow, A. Pauls, W. Weidenhammer and D. Melchart (1996) St John's wort for depression—an overview and meta-analysis of randomised clinical trials. *Br. Med. J.* **313**, 253-258.

15. Suzuki, O., Y. Katsumata, M. Oya, S. Bladt and H. Wagner (1984) Inhibition of monoamine oxidase by hypericin. *Planta Medica* **50**, 272-274.

16. Takahashi, I., S. Nakanishi, E. Kobayashi, H. Nakano, K. Suziki and T. Tamaoki (1989) Hypericin and pseudohypericin specifically inhibit protein kinase C: Possible relation to their antiretroviral activity. *Biochem. Biophys. Res. Commun.* **165**, 1207-1212.

17. Utsumi, T., M. Okuma, T. Utsumi, T. Kanno, T. Yashuda, H. Kobuchi, A. A. Horton and K. Utsumi (1995) *Arch. Biochem. Biophys.* **316**, 493-497.

18. Fehr, M. J., S. L. Carpenter and J. W. Petrich (1994) The role of oxygen in the photoinduced antiviral activity of hypericin. *Bioorg. Med. Chem. Lett.* **4**, 1339-1344.

19. Andreoni, A., A. Colasanti, P. Colasanti, M. Mastrocinque, P. Riccio and G. Roberti (1994) Laser photosensitization of cells by hypericin. *Photochem. Photobiol.* **59**, 529-533.

20. Thomas, C., R. S. MacGill, G. C. Miller and R. S. Pardini (1992) Photo-activation of hypericin generates singlet oxygen in mitochondria and inhibits succinoxidase. *Photochem. Photobiol.* **55**, 47-53.

21. De Witte, P., P. Agostinis, P., J. Van Lint, W. Merlevede, J. R. Vandenheede (1993) Inhibition of epidermal growth factor receptor tyrosine kinase activity by hypericin. *Biochem. Pharmacol.* **46**, 1929-1936.

22. Miccoli, L., S. Oudard, F. Sureau, F. Poirson, B. Dutrillaux and M. F. Poupon. (1995) Intracellular pH governs the subcellular distribution of hexokinase in a glioma cell line. *Biochem. J.* **313**, 957-962.

23. Weller, M., M. Trepel, C. Grimmel, M. Schabet, D. Bremen, S. Krajewski and J. C. Reed (1997) Hypericin-induced apoptosis of human malignant glioma cells is light-dependent, independent of bcl-2 expression, and does not require wild-type p53. *Neurological Res.* **19**, 459-470.

24. Mirossay, L., A. Mirossay, E. Kocisova, I. Radvakova, P. Miskovsky and J. Mojzis (1999) Hypericin-induced apoptosis of human leukemic cell line HL-60 is potentiated by omeprazole, an inhibitor of H^+K^+-ATPase and 5'-(N,N-dimethyl)-amiloride, an inhibitor of Na^+/H^+ exchanger. *Physiological Research.* **48**, 135-141.

25. Gai, F., M. J. Fehr and J. W. Petrich (1993) Ultrafast excited-state processes in the antiviral agent hypericin. *J. Am. Chem. Soc.* **115**, 3384-3385.

26. Gai, F., M. J. Fehr and J. W. Petrich (1994) Observation of excited-state tautomerization in the antiviral agent hypericin and identification of its fluorescent species. *J. Phys. Chem.* **98**, 5784-5795.

27. Gai, F., M. J. Fehr and J. W. Petrich (1994) Role of solvent in excited-state proton transfer in hypericin. *J. Phys. Chem.* **98**, 8352-8358.

28. Das, K., D. S. English, M. J. Fehr, A. V. Smirnov and J. W. Petrich (1996) Excited-state processes in polycyclic quinones, the light induced antiviral agent, hypocrellin, and comparison with hypericin. *J. Phys. Chem.* **100**, 18275-18281.

29. Das, K., D. S. English and J. W. Petrich (1997) Deuterium isotope effect on the excited-state photophysics of hypocrellin, evidence for proton or hydrogen atom transfer. *J. Phys. Chem. A.* **101**, 3241-3245.

30. Das, K., D. S. English and J. W. Petrich (1997) Solvent dependence on the intracellular excited-state proton or hydrogen atom transfer in hypocrellin. *J. Am. Chem. Soc.* **119**, 2763-2764.

31. Das, K., E. Dertz, J. Paterson, W. Zhang, G. A. Kraus and J. W. Petrich (1998) Hypericin, hypocrellin, and model compounds: steady-state and time-resolved fluorescence anisotropies. *J. Phys. Chem. B* **102**, 1479-1484.

32. English, D. S., W. Zhang, G. A. Kraus and J. W. Petrich (1997) Excited-state photophysics of hypericin and its hexamethoxy analog, intramolecular proton transfer as a nonradiative process in hypericin. *J. Am. Chem. Soc.* **119**, 2980-2986.

33. English, D. S., K. Das, J. M. Zenner, W. Zhang, G. A. Kraus, R. C. Larock and J. W. Petrich (1997) Hypericin, hypocrellin, and model compounds, primary photoprocesses of light-induced antiviral agent. *J. Phys. Chem. A.* **101**, 3235-3240.

34. English, D. S., K. Das, K. D. Ashby, J. Park, J. W. Petrich and E. W. Castner, Jr. (1997) Confirmation of excited-state proton transfer and ground-state heterogeneity in hypericin by fluorescence upconversion. *J. Am. Chem. Soc.* **119**, 11585-11590.

35. Das, K., A. V. Smirnov, M. D. Snyder and J. W. Petrich (1998) Picosecond linear dichroism and absorption anisotropy of hypocrellin: toward a unified picture of the photophysics of hypericin and hypocrellin. *J. Phys. Chem.* **102**, 6098-6106.

36. Falk, H., J. Meyer and M. Oberreiter (1992) Deprotonation and protonation of hydroxyphenanthroperylenes. *Monatsh. Chem.* **123**, 277-284.

37. Fehr, M. J., M. A. McCloskey and J. W. Petrich (1995) Light-induced acidification by the antiviral agent hypericin. *J. Am. Chem. Soc.* **117**, 1833-1836.

38. Sureau, F., P. Miskovsky, L. Chinsky and P. Y. Turpin (1996) Hypericin-induced cell photosensitization involves an intracellular pH decrease. *J. Am. Chem. Soc.* **118**, 9484-9487.

39. Chaloupka, R., F. Sureau, E. Kocisova and J. W. Petrich (1998) Hypocrellin A photosensitization involves an intracellular pH decrease in 3T3 cells. *Photochem. Photobiol.* **68**, 44-50.

40. Pinto, L. H., L. J. Holsinger and R. A. Lamb (1992) Influenza virus M_2 protein has ion channel activity. *Cell.* **69**, 517-528.

41. Newell, K. J. and I. F. Tannock (1989) Reduction of intracellular pH as a possible mechanism for killing cell in acidic region of solid tumor, effects of carbonylcyanine-3-chlorophenylhydrazone. *Cancer Res.* **49**, 4447-4482.

42. Newell, K. J., P. Wood, I. Stratford and I. Tannock (1992) Effect of agents which inhibit the regulation of intracellular pH on murine solid tumours. *Br. J. Cancer.* **66**, 311-317.

43. Barry, M. A., J. E. Reynold and A. Eastman (1993) Etoposide-induced apoptosis in human HL-60 cells is associated with intracellular acidification. *Cancer Res.* **53**, 2349-2357.

44. Gottlieb, R. A., J. Nordberg, E. Skowronski and B. M. Babior (1996) Apoptosis induced in Jurkat cells by several agents is preceded by intracellular acidification. *Proc. Natl. Acad. Sci. USA* **93**, 654-658.

45. Li, J. and A. Eastman (1995) Apoptosis in an interleukin-2-dependent cytotoxic lymphocyte cell line is associated with intracellular acidification. *J. Biol. Chem.* **270**, 3203-3211.

46. Hudson, J. B., V. Imperial, R. P. Haugland and Z. Diwu (1997) Antiviral activities of photoreactive perylenequinones. *Photochem. Photobiol.* **65**, 352-354.

47. Jardon, P., N. Lazortchak and R. Gautron (1987) Formation d'oxygène singulet $^1\Delta_g$ photosensibilisée par l'hypericine. Caractérisation et étude du mécanisme par spectroscopie laser. *J. Chim. Phys.* **84**, 1141-1145.

48. Racinet, H., P. Jardon and R. Gautron (1988) Formation d'oxygène singulet $^1\Delta_g$ photosensibilisée par l'hypericine étude cinétique en milieu micellaire non ionique. *J. Chim. Phys.* **85**, 971-977.

49. Darmanyan, A. P., L. Burel, D. Eloy and P. Jardon (1994) Singlet oxygen production by hypericin in various solvents. *J. Chim. Phys.* **91**, 1774-1785.

50. Park, J., D. S. English, S. Wannemuehler S. Carpenter and J. W. Petrich (1998) The role of oxygen in the antiviral activity of hypericin and hypocrellin. *Photochem. Photobiol.* **68**, 593-597.

51. Delaey, E. M., A. L. Vandenbogaerde, W. J. Merlevede and P. A. de Witte (1999) Photocytotoxicity of hypericin in normoxic and hypoxic conditions. *J Photochem. Photobiol. B.* (Submitted)

52. Miskovsky, P., F. Sureau, L. Chinsky and P.-Y. Turpin (1995) Subcellular distribution of hypericin in human cancer cells. *Photochem. Photobiol.* **62**, 546-549.

53. English, D. S., R. T. Doyle, J. W. Petrich and P. G. Haydon (1999) Subcellular distributions and excited-state processes of hypericin in neurons. *Photochem. Photobiol.* **69**,.301-305.

54. Peters, T. (1985) Serum albumin. *Advances in Protein Chemistry* **37**, 161-245.

55. Fehske, K. J., W. E. Müller and U. Wollertt (1979) The lone tryptophan residue of human serum.albumin as part of the specific warfarin binding site. *Mol. Pharmacology* **16**, 778-789.

56. Davila, J. and A. Harriman (1990) Photochemical and radiolytic oxidation of a zinc porphyrin bound to human serum albumin. *J. Am. Chem. Soc.* **112**, 2686-2690.

57. Miskovsky, P., D. Jancura, S. Sánchez-Cortés, E. Kocisova, D. Jancura and L. Chinsky (1998) Antiretrovirally active drug hypericin binds the IIA subdomain of human serum albumin: resonance Raman and surface-enhanced Raman spectroscopy study. *J. Am. Chem. Soc.* **120**, 6374-6379.

58. Senthil, V., J. W. Longworth, C. A. Ghiron and L. I. Grossweiner (1992) Photosensitization of aqueous model systems by hypericin. *Biochem. Biophys. Acta* **1115**, 192-200.

59. Köhler, M., J. Gafret, J. Friedrich, H. Falk and J. Meyer (1996) Hole-burning spectroscopy of proteins in external fields: human serum albumin complexed with the hypericinate ion. *J. Phys. Chem.* **100**, 8567-8572.

60. Falk, H. and J. Meyer (1994) On the homo- and heteroassociation of hypericin. *Monatsh. Chem.* **125**, 753-762.

61. Sevenants, M. R. (1965) Pigments of *Blepharisma undulans* compared with hypericin. *J. Protozool.* **12**, 240-245.

62. Lavie, G., Y. Mazur, D. Lavie, A. M. Prince, D. Pascual, L. Liebes, B. Levin and D. Meruelo (1995) Hypericin as an inactivator of infectious viruses in blood components. *Transfusion* **35**, 392-400.

63. Burel, L. and P. Jardon (1996) Homo-association de l'hypéricine dans l'eau et conséquences pour ses propriétés photodynamiques. *J. Chim. Phys.* **93**, 300-316.

64. Huang, C. P., M. T. Asaki, S. Backus, H. Nathel, H. C. Kapteyn and M. M. Murnane (1993) 17-Fs pulses from a mode-locked Ti:sapphire laser. In *Ultrafast Phenomena VIII.* (Edited by J.-L. Martin, A. Migus, G. A. Mourou and A. H. Zewail), pp. 160-162. Springer, Berlin.

65. Jancura, D., S. Sánchez-Cortés, E. Kocisova, A. Tinti, P. Miskovsky and A. Bertoluzza (1995) Surface-enhanced resonance Raman spectroscopy of hypericin and emodin on silver colloids: SERRS and NIR FT SERS study. *Biospectroscopy* **1**, 265-273.

66. Miskovsky, P., L. Chinsky, G. V. Wheeler and P.-Y. Turpin (1995) Hypericin site specific interactions within polynucleotides used as DNA model compounds. *J. Biomol. Str. Dyn.* **13**, 547-552.

67. Sánchez-Cortés, S., P. Miskovsky, D. Jancura and A. Bertoluzza (1996) Specific interactions of antiretroviraly active drug hypericin with DNA as studied by surface enhanced Raman spectroscopy. *J. Phys. Chem.* **100**, 1938-1944.

68. Munro, I., I. Pecht and L. Stryer (1979) Subnanosecond motions of tryptophan residues in proteins. *Proc. Natl. Acad. Sci. U.S.A.* **76**, 56-60.

69. Rich, R. L., F. Gai, J. W. Lane, J. W. Petrich and A. W. Schwabacher (1995) Using 7-azatryptophan to probe small molecule–protein interactions on the picosecond time scale: the complex of avidin and biotinylated 7-azatryptophan. *J. Am. Chem. Soc.* **117**, 733-739.

70. Petrich, J. W., J. W. Longworth and G. R. Fleming (1987) Internal motion and electron transfer in proteins: a picosecond fluorescence study of three homologous azurins. *Biochemistry* **26**, 2711-2722.

71. Avouris, P., L. L. Yang and M. A. El-Bayoumi (1976) Excited state interactions of 7-azaindole with alcohol and water. *Photochem. Photobiol.* **24**, 211-216.

72. Carter, D. C., X.-M. He and S. H. Munson (1989) Three-dimensional structure of human serum albumin. *Science* **244**, 1195-1198.

73. Carter, D. C. (1992) Atomic structure and chemistry of human serum albumin. *Nature* **358**, 209-215.

74. Das, K., K. D. Ashby, J. Wen, and J. W. Petrich (1999) The Temperature Dependence of the Excited-State Intramolecular Proton Transfer Reaction in Hypericin and Hypocrellin A. *J. Chem. Phys. B* **103**, 1581-1585.

75. Dai, R., T. Yamazaki, I. Yamazaki and P.-S. Song (1995) Initial spectroscopic characterization of the ciliate photoreceptor stentorin. *Biochim. Biophys. Acta* **1231**, 58-68.

76. Tao, N., Orlando, M., Hyon, J.-S., Gross, M. and P.-S. Song (1993) A new photoreceptor molecule from *Stentor coeruleus*. *J. Am. Chem. Soc.* **115**, 2526-2528.

77. Wells, T. A., A. Losi, R. Dai, P. Scott, S.-M. Park, J. Golbeck and P.-S. Song (1997) Electron transfer quenching and photoinduced EPR of hypericin and the ciliate photoreceptor stentorin. *J. Phys. Chem. A* **101**, 366-372.

78. Angelini, N., Quaranta, A., Checucci, G., Song, P.-S., Lenci, F. (1998) Electron transfer fluorescence quenching of *Blepharisma japonicum* photoreceptor pigments. *Photochem. Photobiol.* **68**, 864-868.

79. Wardman, P. (1989) Reduction potentials of one-electron couples involving free radicals in aqueous solution. *J. Phys. Chem. Ref. Data* **18**, 1637-1657.

80. Rosenor, V. M., M. Oratz and M. A. Rothschild (1977) In *Albumin Structure, Function and Uses*, p 27. Pergamon Press.

81. Milazzo, G. (1976) In *Topics in Bioelectrochemistry and Bioenergetics* Vol. 1. p. 53. Wiley, London.

CHAPTER IV: ENVIRONMENT OF TRYPTOPHAN 57 IN PORCINE FRUCTOSE-1,6-BISPHOSPHATASE STUDIED BY TIME-RESOLED FLUORESCENCE AND SITE-DIRECTED MUTAGENESIS

A paper published in *Photochemistry and Photobiology*[1]

Jin Wen[2], Scott W. Nelson[3], Richard B. Honzatko[3], Herbert J. Fromm[3], and Jacob W. Petrich[2,4]

Abbreviations: FBPase, fructose-1,6-bisphosphatase; $F16P_2$, fructose 1,6-bisphosphate; F6P, fructose 6-phosphate; $F26P_2$, fructose 2,6-bisphospate; P_i, orthophosphate; CD, circular dichroism; FWHM, full width at half maximum; KDP, potassium dihydrogen phosphate; AMP, adenosine monophosphate; NADP, nicotinamidde adenine dinucleotide phosphate; NADPH, reduced form of nicotinamide adenine dinucleotide phosphate; SDS-PAGE, sodium dodecyl sulfate-polyacrylamide gel electrophoresis.

Abstract

The environment of Trp^{57}, introduced by the mutation of a tyrosine in the dynamic loop of porcine liver fructose-1,6-bisphosphatase, was examined using time-resolved fluorescence and directed mutation. The Trp^{57} enzyme was studied previously by X-ray crystallography and steady-state fluorescence, the latter revealing an unexpected red shift in the wavelength of maximum fluorescence emission for the R-state conformer. The red shift

---

1 Reprinted with permission of *Photochemistry and Photobiology*, **2001**, 74(5), 679-685
[2] Department of Chemistry, Iowa State University, Ames, IA 50011-3111 USA
[3] Department of Biochemistry, Biophysics and Molecular Biology, Iowa State University, Ames, IA 50011-3111 USA
[4] To whom correspondence should be addressed

was attributed to the negative charge of Asp^{127} in contact with the indole side-chain of Trp^{57}. Time-resolved fluorescence experiments here reveal an indole side-chain less solvent exposed and more rigid in the R-state, than in the T-state of the enzyme, consistent with X-ray crystal structures. Replacement of Asp^{127} with an asparagine causes a 6 nm blue shift in the wavelength of maximum fluorescence emission for the R-state conformer, with little effect on the emission maximum of the T-state enzyme. The data here support the direct correspondence between X-ray crystal structures of fructose-1,6-bisphosphatase and conformational states of the enzyme in solution, and provide a clear example of the influence of microenvironment on the fluorescence properties of tryptophan.

Introduction

Fructose-1,6-bisphosphatase (D-fructose-1,6-bisphosphate 1-phosphohydrolase, EC 3.1.3.11; FBPase) catalyzes the hydrolysis of fructose 1,6-bisphosphate ($F16P_2$) to fructose 6-phosphate (F6P) and inorganic phosphate (P_i) [1, 2]. In the absence of a mechanism of regulation, FBPase and fructose-6-phosphate-1-kinase would catalyze a futile cycle in the gluconeogenic/glycolytic pathway. FBPase activity, however, is subject to tight metabolic control, being inhibited synergistically by $F26P_2$ and AMP [3-5]. AMP binds to allosteric sites located 28 Å from the nearest active site [6]. $F26P_2$ binds to the active sites as a substrate analog. FBPase requires divalent cations (Mg^{2+}, Mn^{2+}, or Zn^{2+}), and rates of reaction vary sigmoidally with metal ion concentration (Hill coefficient of 2) [7-9].

FBPase is a homotetramer (subunit M_r of 37,000 [10]), which exists in at least two conformational states designated R and T [11, 12]. AMP, alone or in combination with $F26P_2$, stabilizes the inactive T-state [13-15]. Substrates or products along with metal

cations shift the equilibrium in favor of the R-state [11, 16]. Directed mutations implicate loop 52—72 in the allosteric regulation of FBPase [17, 18]. Product complexes of FBPase in the presence of Mg^{2+} and Zn^{2+} reveal an engaged loop, which makes several important contacts with the active site [16]. In contrast, product complexes with AMP reveal a disengaged loop, well removed from the active site [19]. A proposed mechanism of allosteric regulation of catalysis requires at least these two conformational states (engaged and disengaged) for loop 52—72 [16].

Because of its sensitivity to environment, tryptophan fluorescence can be an excellent probe of protein structure and dynamics [20-24]. As porcine FBPase has no tryptophan, a directed mutation can easily introduce a unique fluorophore. Previously reported are the crystal structures of the R- and T-states, initial rate kinetics, and steady-state fluorescence of the $Tyr^{57} \rightarrow$ Trp mutant [17]. Interestingly, the steady-state fluorescence revealed a red shift in the wavelength of maximum fluorescence emission for the R-state (350 nm) relative to the T-state (340 nm). The typical emission properties of tryptophan as a function of solvent polarity suggest a solvent-exposed environment for Trp^{57} in the R-state, and a more hydrophobic, less exposed environment for Trp^{57} in the T-state. In X-ray crystal structures, however, Trp^{57} of the R-state conformer is in a hydrophobic pocket, whereas Trp^{57} of the T-state is solvent-exposed (Fig.4.1). In this article we consider whether the aforementioned red shift arises from an electrostatic perturbation, due to the proximity of Asp^{127} to the indole of Trp^{57} in the R-state. The electrostatic field produced by the negative charge of Asp^{127} may decrease the energy separation between the ground and excited states of the indole side-chain, thus causing a shift of the fluorescence emission to a lower energy. Another potential

contribution to the red shift is a hydrogen bond between the side-chain of Asp^{127} and the imino hydrogen of the indole group.

The work reported below employs time-resolved fluorescence to achieve greater detail in probing the environment of Trp^{57} and examine the effect of removing the negative charge by mutation of Asp^{127} to asparagine. Solvent accessibility and rotational mobility of Trp^{57} determined in solution is consistent with that deduced from X-ray crystal structures for the R- and T-state conformations. In addition, the double mutant (Asn^{127}/Trp^{57}) exhibits a 6 nm blue-shift in the R-state conformation relative to the λ_{max} of Trp^{57} enzyme.

Materials and Methods

Materials— $F16P_2$, $F26P_2$, $NADP^+$, AMP, ampicillin and IPTG were purchased from Sigma Chemical Co.(St. louis, MO). DNA modifying and restriction enzymes, T4 polynucleotide kinase and ligase came from Promega (Madison, WI). Glucose-6-phophate dehydrogenase and phosphoglucose isomerase came from Roche (Indianapolis, IN). Other chemicals were of reagent grade or the equivalent. *Escherichia coli* strains BMH 71-18 mutS and XL1-Blue came from Clontech (Palo Alto, CA) and Stragene (La Jolla, CA), respectively. FBPase-deficient *E. coli* strain DF 657 was from the Genetic Stock Center at Yale University.

Mutagenesis — The method for generation of the single Trp^{57} mutation is previously described [1]. The $Asp^{127}\rightarrow$ Asn mutation was introduced by changing specific bases in the Trp^{57} double stranded plasmid using the Quickchange™ site-directed mutagenesis method. The forward and reverse primers for the $Asp^{127}\rightarrow$Asn mutation were 5'-CCTCGATGGATCGTCGAACATC<u>AAC</u>TGCCTTGTGTCCATTGG-AACC-3' and

Figure 4.1 Structure of the Trp^{57} Mutant in the R- and T-states. (Top) For clarity only a single subunit of each conformation of the FBPase tetramer is presented. In the orientation shown the subunits would be in the lower left-hand corner of the tetramer (C4). In the R-state, the loop 52-72 (thick Cα trace) is engaged over the active site and Trp^{57} is in proximity to Asp^{127}. In the T-state conformation AMP displaces phosphate from the allosteric site, helix H2 is translated by 0.9Å, and loop 52-72 has little density and is in the disengaged form. (Bottom) Close up views of Trp57 in the R- and T-states. The orientations of the R- and T-state have been changed to better show the interactions between Trp^{57} and other side chains.

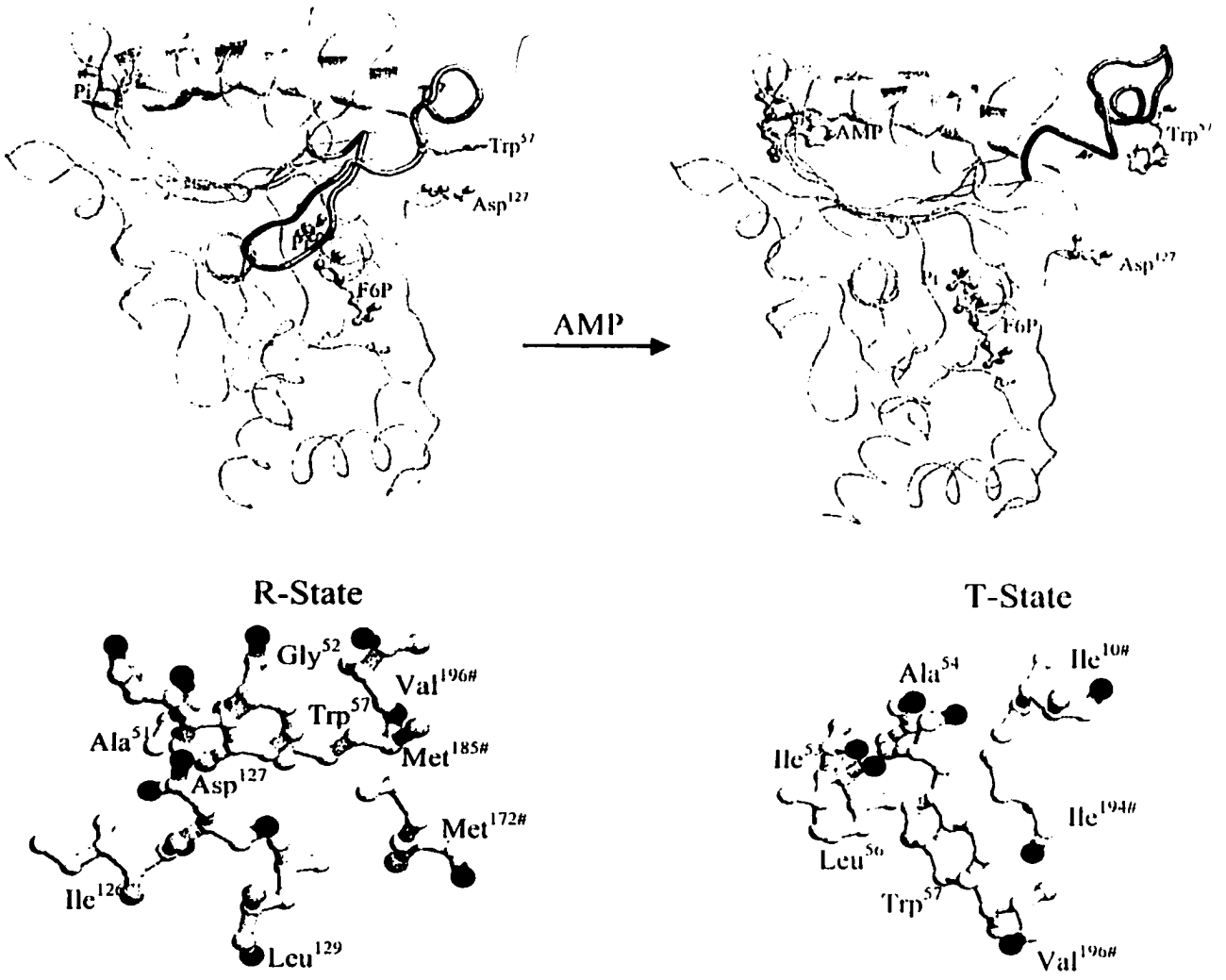
Pi
Trp57
Asp127
F6P
AMP
AMP
Trp57
Asp127
Pi
F6P
R-State
Gly52
Val196#
Trp57
Ala51
Met185#
Asp127
Met172#
Ile126
Leu129
T-State
Ala54
Ile10#
Ile51
Ile194#
Leu56
Trp57
Val196#

5'- GGTTCCAATGGACACAAGGCA**GTT**GATGTTCGACGATCCAT-CGAGG-3' (codon for Asn underlined in bold typeface). Random mutations as a result of the mutagenesis procedure were ruled out by sequencing the entire gene, after which the mutant plasmid was used in the transformation of *E. coli* DF 657 (DE3) cells. The Iowa State University sequencing facility provided DNA sequences, using the fluorescent dye-dideoxy terminator method.

Expression and Purification — Expression and purification of the mutant FBPases were performed as previously described [18]. After cell breakage and centrifugation, the supernatant was loaded directly onto a Cibacron-Blue column and eluted with a NaCl gradient from 0.5—1 M. The active fractions were dialyzed against 20 mM Tris-HCl, pH8.3, loaded onto a DEAE-Sephadex column and eluted with a gradient 0—300 mM in NaCl. FBPase eluted at a salt concentration of 150 mM and its purity confirmed by SDS-PAGE [25]. Protein concentration was determined using the Bradford assay [26] with bovine serum albumin as a standard.

Circular Dichroism (CD) Spectroscopy—Spectra were recorded from 200—260 nm in steps of 1.3 nm on a Jasco J710 spectrometer in a 1 mm cell at room temperature using a protein concentration of approximately 0.25 mg/mL. Each spectrum was blank-corrected using the software provided with the instrument.

Kinetic Experiments — All assays employed the coupling of phosphoglucose isomerase and glucose-6-phosphate dehydrogenase [2]. Specific activity, k_{cat}, and pH 7.5/9.5 activity ratios were determined by directly monitoring the reduction of $NADP^+$ to NADPH at 340 nm. All other kinetic experiments monitored the fluorescence emission from NADPH at 470 nm, using an excitation wavelength of 340 nm [1]. Initial rate data were analyzed using

programs written either in MINITAB [27] or by ENZFITTER [28]. To fit the AMP titration data the Hill equation was used:

$$\frac{\Delta S}{S_o} = \frac{(\Delta S_{max} / S_o) * [AMP]^n}{K_d + [AMP]^n} \qquad (4-1)$$

where ΔS is the change in $\langle\tau_f\rangle_o/\langle\tau_f\rangle$ or S^2 caused by the addition of *AMP*, S_o is the value of $\langle\tau_f\rangle_o/\langle\tau_f\rangle$ or S^2 in the absence of AMP, K_d is the dissociation constant for the enzyme-AMP complex, and n is the Hill coefficient. A Hill coefficient >1 indicates positive cooperativity between AMP binding sites.

Steady-State and Time-Resolved Fluorescence—Steady-state fluorescence spectra were obtained on a SPEX Fluoromax with a 4 nm band-pass. Protein and ligand concentrations are in the figure legends, as are the equations for fitting data.

Apparatus for Time-Correlated Single Photon Counting—A Coherent 701 rhodamine 6 G dye laser is pumped with about 1 W of 532 nm radiation from an Antares 76-s CW mode-locked Nd:YAG laser. The 701 dye laser is cavity-dumped at 3.8 MHz. The pulses have an autocorrelation of about 10 ps FWHM. Excitation of tryptophan at 295 nm is achieved by focusing the dye laser pulses with a 5 cm lens onto a crystal of KDP. Fluorescence is collected at right angles through a polarizer mounted at 54.7° to the excitation polarization and then passed through an ISA H-10 monochromator with a 16 nm band-pass or through cutoff filters. A Hamamatsu R3890u microchannel plate, amplified by a Minicircuits ZHL-1042J, and a FFD 100 EG&G photodiode provide the start and stop signals, respectively. Constant-fraction discrimination of these signals is performed by a Tennelec TC 455, and time-to-amplitude conversion, by an ORTEC 457. Data are stored in a Norland 5500

multichannel analyzer before transfer to and analysis with a PC. The instrument function of this system has a FWHM of 100~150 ps. The polarized fluorescence traces used to obtain fluorescence anisotropy decay parameters are collected to a maximum of 16,000 counts in the peak channel.

Global fitting— Time-resolved fluorescence data, acquired at various wavelengths, are subjected to a global fitting procedure found in Spectra Solve™. The global parameters in this case are time constants and local parameters are amplitudes (pre-exponential factors). The time constants are specified and each curve is fit iteratively varying only the local parameters. A local χ^2 is calculated for each local fit. After all curves are fit (typically 6 to 11), a global χ^2 is calculated as shown below. The global parameters are varied and the whole process is repeated to calculate a new global χ^2. This process is repeated until a minimum is reached for χ^2, which is defined as:

$$\chi^2 = \frac{\sum_{i=1}^{n} \frac{\chi^2_{local,i}}{\chi^2_{best,i}}}{n} \qquad (4-2)$$

where $\chi^2_{best,i}$ is obtained for each curve letting all parameters local and global (that is, amplitudes and time constants) vary; and n is the number of curves. The quality of the fit is determined by visual inspection and residuals.

Results

Expression, Purification and Circular Dichroism Spectroscopy

Wild-type and mutant proteins behaved identically throughout the purification procedure and were at least 95% pure by SDS-PAGE. The CD spectra of wild-type, Trp^{57},

and Trp^{57}/Asn^{127} FBPases are identical from 200 to 260 nm, indicating no major changes in secondary structure of protein fold due to the mutations.

Kinetic Properties of the Trp^{57}/Asn^{127} mutant FBPase

The ratio of catalytic rates at pH 7.5 to 9.5 indicates an intact (non-proteolyzed) enzyme. The addition of the $Asp^{127}\rightarrow Asn$ mutation to the Trp^{57} mutant does not greatly influence kinetic parameters (Table 4.1). The Asn127/Trp57 enzyme exhibits only a 1.2-fold reduction in Mg^{2+}-affinity and a reduction in cooperativity (1.9 to 1.7). Changes in kinetic parameters are not significant. The double mutant has a reduced affinity towards AMP relative to the single mutant (2-fold), but the kinetic mechanism of AMP and $F26P_2$ inhibition are unchanged, as established by inhibition assays. AMP is a non-linear competitive inhibitor with respect to Mg^{2+}, and $F26P_2$ is a linear competitive inhibitor with respect to $F16P_2$.

Fluorescence Properties of the Trp^{57} and Trp^{57}/Asn^{127} Enzymes

The steady-state emission spectra for the R- and T-states of Trp^{57} and Trp^{57}/Asn^{127} are shown in Fig.4.2. The emission maxima for the Trp^{57} single mutant in the R- and T-states are 352 and 340 nm, repectively. The emission maxima for the Trp^{57}/Asn^{127} double mutant in the R- and T-states are 346 and 339 nm, respectively.

The average lifetime for the T-state conformation is shorter than that of the R-state. The change in lifetime as a function of AMP concentration (Fig.4.3) indicates a dissociation constant for AMP of 16.9 μM with a Hill coefficient of 2.0. These values are comparable to those determined from steady-state fluorescence (16 μM and 2.1, respectively) and initial

Table 4.1: Kinetic parameters for Wild-type, Y57W, and Y57W/D127N FBPases.

	Activity ratio pH 7.5/9.5	k_{cat} sec^{-1}	K_m-$F16P_2$ μM	K_a-Mg^{2+} mM^2	Hill-coefficient for Mg^{2+}	K_i-$F26P_2$ μM	I_{50}-AMP[a] μM
Wild-Type	3.3	22.0±0.1	1.75±0.08	0.67±0.04	1.9±0.1	0.264±0.005	1.61±0.05
Trp57	3.3	24.0±0.1	3.39±0.09	0.53±0.06	1.9±0.1	0.84±0.05	8.5±0.4
Trp57/Asn127	3.2	22.5±0.4	2.8±0.2	0.78±0.04	1.7±0.1	0.43±0.03	18±2

[a]Hill coefficient of AMP inhibition is 2.0, as determined from a plot of Mg^{2+} *vs.* AMP at a concentration of 20 μM $F16P_2$.

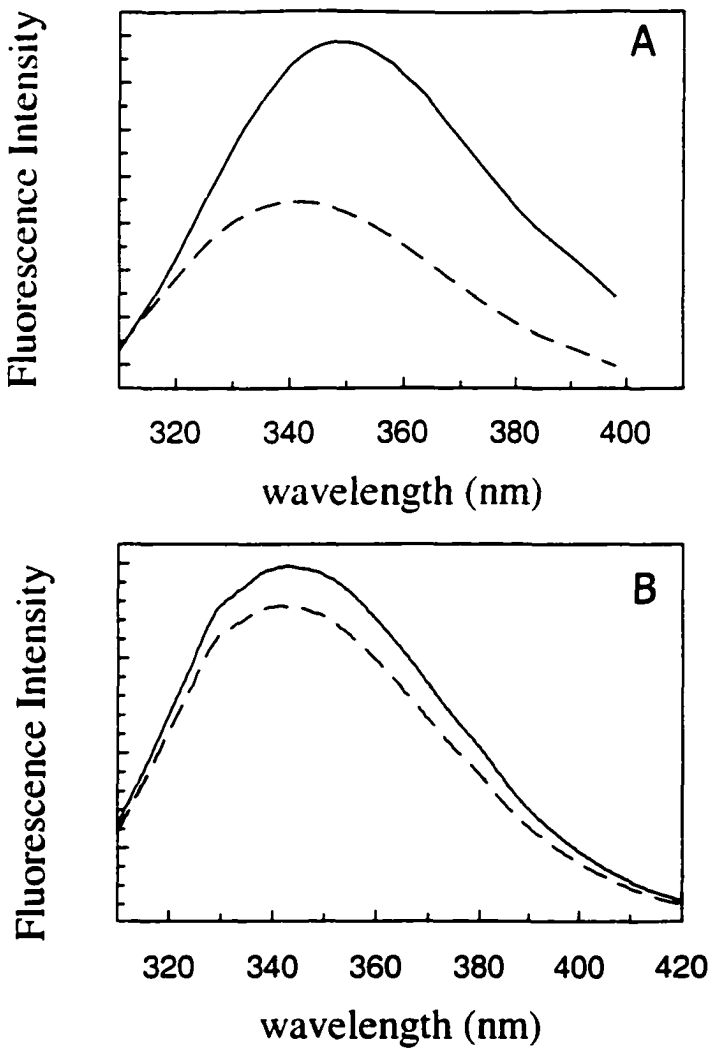

Figure 4.2 (A) Fluorescence spectra of the Trp^{57} mutant. Enzyme under R-state (—) conditions of ligation (5 M F6P and 5 mM KP_i) in the presence of 50 μM Zn^{2+} and enzyme under T-state (----) conditions of ligation (5mM F6P, 5 mM KP_i, and 0.4 mM AMP) in the presence of 50 μM Zn^{2+}.

(B) Fluorescence spectra of $Trp^{57}Asn^{127}$ double mutant. Enzyme under R-state (—) conditions of ligation (5 M F6P and 5 mM KP_i) in the presence of 50 μM Zn^{2+} and enzyme under T-state (----) conditions of ligation (5mM F6P, 5 mM KP_i, and 0.4 mM AMP) in the presence of 50 μM Zn^{2+}.

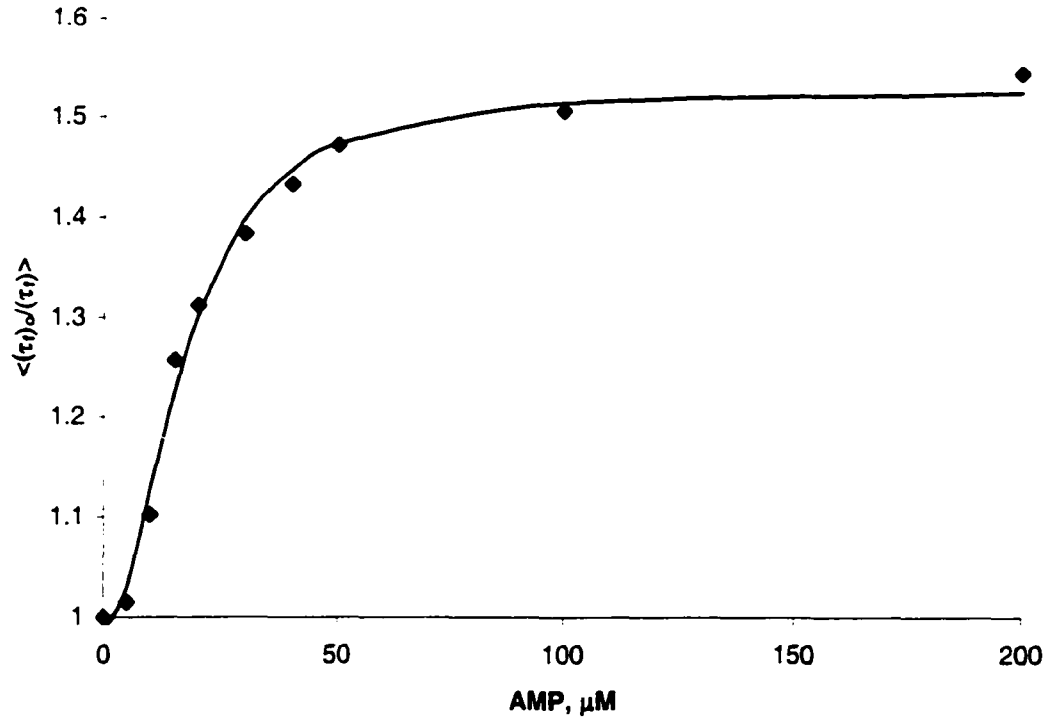

Figure 4.3 Titration curve obtained by plotting $\langle\tau_f\rangle_0/\langle\tau_f\rangle$ vs. [AMP]. For each point, the lifetime decay was fit to a double exponential: $F(t) = a_1\exp(-t/\tau_1) + a_2\exp(-t/\tau_2)$. $\langle\tau_f\rangle$ is the average lifetime ($\langle\tau_f\rangle = a_1 \times \tau_1 + a_2 \times \tau_2$). $\langle\tau_f\rangle_0$ is the average lifetime of the R-state (i.e., without AMP). The fitted line was calculated using the Hill equation.

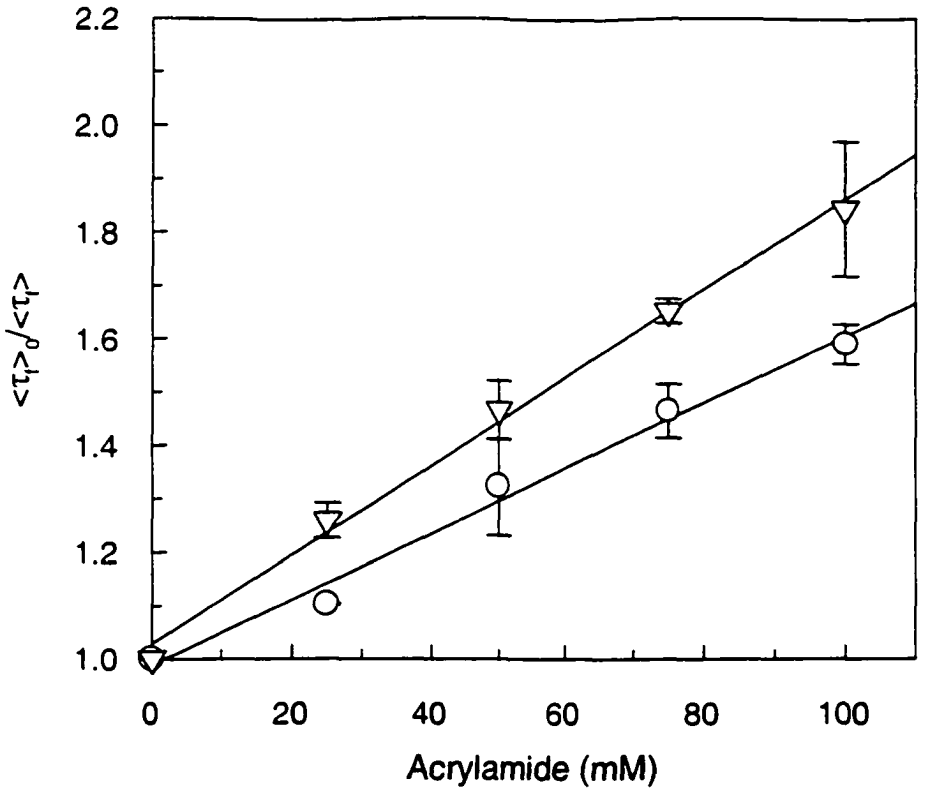

Figure 4.4 Stern-Volmer plot for the acrylamide quenching of Trp^{57} mutant in the presence of 50 μM Zn^{2+}. The Stern-Volmer plot obtained by plotting the ratio of the average lifetime in the absence of quencher over the average lifetime with quencher vs. the concentration of quencher. The solid line is a fit to the equation:

$\frac{<\tau_0>}{<\tau_f>} = 1 + K_{sv}[Q]$, where $K_{sv,R} = 6.2\ M^{-1}$ for the R-state (o), and $K_{sv,T} = 8.4\ M^{-1}$ for the T-state (∇).

Table 4.2: λ_{max}, Quenching Constants, and Order Parameter for the R- and T-state of Y57W.

	λ^{em}_{max} (nm)	K_{sv} (M^{-1})	k_q (x $10^9 M^{-1}s^{-1}$)	S^2
R-state[a]	352	6.2 ± 0.5	1.5 ± 0.1	0.49 ± 0.02
T-state[b]	340	8.4 ± 1.0	2.4 ± 0.3	0.43 ± 0.02

[a]Ligand concentrations are: F6P, 5 mM; Zn^{2+}, 50 μM; KP_i, 5 mM.

[b]Ligand concentrations are identical to those for the R-state with the addition of 200 μM AMP.

Table 4.3: Summary of global fitting parameters for Trp^{57} mutant under R- and T-* state conditions.

λ_{em} (nm)	R-state		T-state	
	a_1	a_2	a_1	a_2
334	0.45	0.55	0.48	0.52
340	0.39	0.61	0.44	0.56
350	0.30	0.70	0.38	0.62
360	0.23	0.77	0.34	0.66
370	0.18	0.82	0.28	0.72
380	0.15	0.85	0.25	0.75

* The functional form used to fit the decays is: $F(t) = a_1 \exp(-t/\tau_1) + a_2 \exp(-t/\tau_2)$. τ_1 and τ_2 were fixed during fitting. R-state: τ_1=1.5ns and τ_2=6.8ns; T-state: τ_1=1.2ns and τ_2=5.8ns.

rate kinetics (22 μM and 2.0, respectively). Evidently, the decrease in fluorescence lifetime is directly related to the conversion of the R-state to the T-state conformer.

Acrylamide quenching is widely used as a measure of solvent accessibility [18]. Slopes of Stern-Volmer plots for the acrylamide quenching of the R- and T-states of Trp^{57} FBPase (Fig.4.4) give the Stern-Volmer constants (K_{sv}). The ratio of slope to average lifetime in the absence of quencher gives the quenching constant (k_q). Quenching constants for the R- and T-states are in Table 4.2.

Fluorescence decays for the Trp^{57} and Trp^{57}/Asn^{127} FBPases under R- and T-state conditions are globally fit to a sum of exponentials (Table 4.3, Table 4.4), where the time constants are fixed and only the amplitudes are permitted to vary (as described above). In all cases the weights of the components change across the emission spectrum, indicating the presence of two distinct environments for each of two lifetimes. The two lifetimes may arise from an equilibrium between the loop-engaged and loop-disengaged states. AMP shifts the

Table 4.4: Summary of global fitting parameters for Trp^{57}/Asn^{127} double mutant under R- and T-* state conditions.

λ_{em} (nm)	R-state		T-state	
	a_1	a_2	a_1	a_2
330	0.60	0.40	0.57	0.43
340	0.57	0.43	0.55	0.45
350	0.54	0.46	0.52	0.48
360	0.51	0.49	0.49	0.51
370	0.48	0.52	0.46	0.54
380	0.46	0.54	0.43	0.57

*The functional form used to fit the decays is: $F(t) = a_1 \exp(-t/\tau_1) + a_2 \exp(-t/\tau_2)$. τ_1 and τ_2 were fixed during fitting. R-state: τ_1=1.6ns and τ_2=6.0ns; T-state: τ_1=1.4ns and τ_2=5.4ns.

equilibrium toward the T-state, but perhaps not all enzyme subunits have disengaged loop. Likewise, the prescence of F6P, KP_i, and $ZnCl_2$ favors the R-state, but some portion of the enzyme ensemble may have disengaged loops. That portion of the Trp^{57} enzyme with the disengaged loop may be responsible for the short lifetime, whereas that portion with the engaged loop might be responsible for the long lifetime. This notion of an equilibrium between the two states is qualitatively consistent with the relative contributions of each lifetime to the R- and T-states.

The mobility of a fluorophore is related to the decay of the fluorescence anisotropy, as well as the order parameter, S^2, where $S^2 = r(0^+)/r_{eff}(0)$. The fluorescence anisotropy decay is fit to a double exponential ($r(t) = r_1(0)\exp(-t/\tau_1) + r_2(0)\exp(-t/\tau_2)$), which allows for rapid motion of tryptophan with respect to the protein, as well as the overall tumbling of the protein itself. $r(0^+)$ comes from a fit of the slow time component of anisotropy decay, which corresponds to overall protein reorientation, and $r_{eff}(0) = r_1(0) + r_2(0)$ [20, 21, 29].

Consequently, S^2 varies from 0 to1, with a value of 1 indicating totally restricted motion of the chromophore. The dependence of mobility (S^2) on AMP concentration is in Fig.4.5. The difference between the R-state (0 μM AMP) and T-state (200 μM AMP) is small, but reproducible. Evidently, the side chain of Trp^{57} is slightly more mobile in the T-state than the R-state. Additionally, the non-linear regression curve of Fig.4.5 results from a Hill coefficient for AMP constrained to a value of 2.0, with an optimized K_d (the dissociation

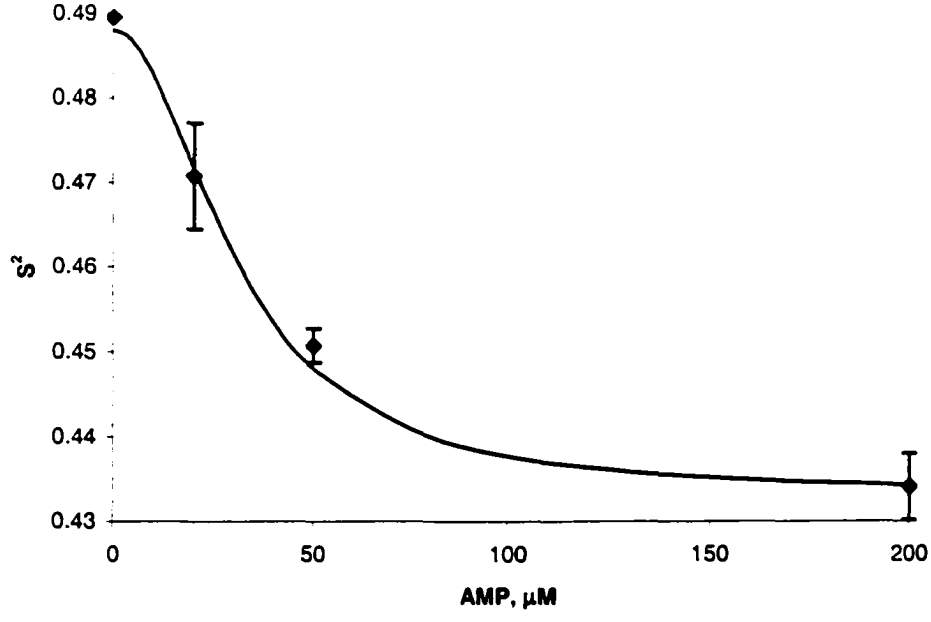

Figure 4.5 Plot of the order parameter (S^2) vs. concentration of AMP. The order parameter was obtained from fitting the anisotropy decay to double exponential ($r(t) = r_1\exp(-t/\tau_{r1}) + r_2\exp(-t/\tau_{r2})$, τ_{r1} and τ_{r2} are the rotation time). The fitted line was calculated using the Hill equation and the same fitting parameter obtained from the titration curve in Figure 4.4. That the same parameters can describe these two sets of data, obtained from different measurements, is evidence that we are probing the mobility of the protein in both experiments.

constant for AMP) of 25 μM, nearly identical to other independent measurements of that dissociation constant.

Discussion

Quenching constants from Stern-Volmer plots reveal that Trp^{57} in the R-state is more protected from solvent than in the T-state, consistent with X-ray crystallographic structures. On the basis of solvent accessibility calculations performed on crystal structures, Trp^{57} has 8.1 and 6.4 $Å^2$ of accessible surface area in the T- and R-states, respectively. A total of 22 proteins compiled by Lakowicz [24] reveal a strong positive correlation between λ_{max}^{em} and k_q. Hence, the *inverse* relationship between k_q and λ_{max}^{em} observed here is *unexpected.* In general, quenching by acrylamide increases with the wavelength of maximum fluorescence emission. The k_q value for the T-state conformer of Trp^{57} FBPase is within the range of quenching constants for other single-tryptophan proteins with emission maxima of 340 nm. In contrast, the k_q value of R-state is anomalous in relation to other proteins with emission maxima of 352 nm. Using the empirical trend between k_q and λ_{max}^{em}, the predicted k_q value for a single-tryptophan protein with an emission maximum of 352 nm is approximately 3.6 x 10^9 $M^{-1}s^{-1}$, almost 250% higher than that determined here.

Anisotropy decay is sensitive to the mobility of the side chain of Trp^{57}. Thermal parameters of Trp^{57} in R- and T-state crystal structures infer more freedom of movement of Trp57 in the T-state than in the R-state. In concurrence with the crystal structures, the order parameter, S^2 (a measure of rotational mobility of a fluorophore), is less in the T-state than in the R-state, indicating a slightly less mobile fluorophore in the R-state (Fig.4.5).

The apparent agreement between the fluorescence and crystallographic analyses, however, does not reveal the cause of the anomalous red shift in the R-state emission spectrum. As noted above, this anomalous behavior may stem from the perturbation of Trp^{57}, by the side chain of Asp^{127} (Fig.4.1). A negative charge correctly placed with respect to Trp^{57} will decrease the energy of separation between ground and excited states and could be responsible for a red-shift in the wavelength of maximum fluorescence emission [30]. As a test of this hypothesis, Asp^{127} was replaced by asparagine. A sequence alignment, using 63 FBPases in Genbank, revealed 93% with aspartate at position 127, and only glutamate or asparagine as alternatives. In addition, the mutation of Asp^{127} to serine significantly alters the kinetics and conformation of FBPase (R. Zhang, Choe, J. Y., R. B. Honzatko, and H. J. Fromm, unpublished results). Hence, the mutation of Asp^{127} to asparagine is the best candidate (and perhaps the only candidate) to remove the electrostatic charge at position 127 and yet retain the functional properties of FBPase. The circular dichroism spectrum of Trp^{57}/Asn^{127} FBPase is identical to that of wild-type and Trp^{57} FBPases, indicating the absence of large changes in secondary structure. Kinetics parameters for enzyme turnover (k_{cat}), Mg^{2+} affinity and cooperativity, $F16P_2$ affinity, and $F26P_2$ inhibition are the same for Trp^{57} and Trp^{57}/Asn^{127} FBPases. The 2-fold increase in K_i-AMP relative to that of Trp^{57} FBPase may arise from a more stabile loop-engaged, R-state conformation, a conformation that putatively cannot bind AMP. Crystal structures reveal the side chain of Trp^{57} in non-bonded contact with the side chain of position 127 in the loop-engaged conformation. The mutation of position 127 to asparagine then, should reduce the thermodynamic penalty associated with the partially buried electrostatic charge of Asp^{127}.

The steady-state fluorescence of the Trp^{57}/Asn^{127} enzyme in the R-state has a wavelength of maximum fluorescence emission of 346 nm, which blue shifted by 6 nm relative to the emission maximum of the Trp^{57} enzyme. Evidently, the side chain of Asp^{127} is responsible for the anomalous red shift in the wavelength of maximum fluorescence emission. As the mutation to asparagine does not shift the emission spectrum to wavelengths shorter than that of the T-state, as would be expected if the charge were wholly responsible for the phenomenon, it is likely that hydrogen bonding also contributes to the anomalous red-shift.

The steady-state fluorescence spectrum of the T-state is insensitive to the mutation of Asp^{127} to asparagine, as Trp^{57} is remote from position 127 in the T-state conformation of the enzyme. The small blue shift of the T-state is probably due to some portion of the enzyme remaining in the R-state even in the presence of 200 μM AMP. This explanation is also consistent with the observation of two distinct lifetimes. Tryptophans in single conformational states, however, also exhibit heterogeneous fluorescence decay [31]. Hence, by itself, hetereogeneity in fluorescence decay is not absolute proof of multiple rotamer populations or conformational states of tryptophan.

Conclusion

Time-resolved fluorescence data presented here are consistent with predictions made on the basis of X-ray crystal structures of Trp^{57} FBPase. The indole side chain of Trp^{57} in the R-state is less mobile and more protected from solvent than in the T-state. In addition, changes in the fluorescence emission spectrum due to the mutation of Asp^{127} to asparagine

support our previous suggestion that the anomalous, red-shifted emission spectrum of the R-state Trp^{57} enzyme is due in part to the electrostatic perturbation of the Asp^{127}.

Acknowledgements

This work was supported in part by National Institutes of Health Research Grant NS 10546 and National Science Foundation Grants MCB-9985565. This is Journal Paper 19476 of the Iowa Agriculture and Home Economic Experiment Station, Ames, IA, Project 3191, and is supported by Hatch Act and State of Iowa funds.

References

1. Benkovic, S.T., and M. M. de Maine (1982) Mechanism of action of fructose 1,6-bisphosphatase. *Adv. Enzymol. Relat. Areas Mol. Biol.* **53,** 45-82.
2. Tejwani, G.A. (1983) Regulation of fructose-bisphosphatase activity. *Adv. Enzymol. Relat. Areas Mol. Biol.* **54,** 121-194.
3. Pilkis, S.J., M. R. El-Maghrabi and T. H. Claus (1988) Hormonal regulation of hepatic gluconeogenesis and glycolysis. *Ann. Rev. Biochem.* **57,** 755-783.
4. Pilkis, S.J., M. R. El-Maghrabi and T. H. Claus (1981) Inhibition of fructose-1,6-bisphosphatase by fructose 2,6-bisphosphate. *J. Biol. Chem.* **256,** 3619-3622.
5. Van Schagtingen, E., and H. G. Hers (1981) Inhibition of fructose-1, 6-bisphosphatase by fructose 2,6-bisphosphate. *Proc. Natl. Acad. Sci. U.S.A.* **78,** 2861-2863.
6. Ke, H., Zhang, Y., Liang, J.-Y., and Lipscomb, W. N. (1991) Crystal structure of the neutral form of fructose-1,6-bisphosphatase complexed with the product fructose 6-phosphate at 2.1 Å resolution. *Proc. Natol. Acad. Sci. U.S.A.* **88,** 2989-2993.
7. Nimmo, H.G., and Tipton, K. F. (1975) The effect of pH on the kinetics of beef-liver fructose bisphosphatase. *Eur. J. Biochem.* **58,** 567-574.

8. Liu, F., and Fromm, H. J. (1988) Interaction of fructose 2,6-bisphosphate and AMP with fructose-1,6-bisphosphatase as studied by nuclear magnetic resonance spectroscopy. *J. Biol. Chem.* **263,** 9122-9128.

9. Stone, S.R., and H. J. Fromm (1980) Investigations of the kinetic mechanism of bovine liver fructose 1,6-bisphosphatase. *Biochemistry* **19,** 620-625.

10. Marcus, F., Edelstein, I., Reardon, I., an dHeinrikson, R. L. (1982) Complete amino acid sequence of pig kidney fructose-1,6-bisphosphatase. *Proc. Natl. Acad. Sci. U.S.A.* **79,** 7161-7165.

11. Zhang, Y., J.-Y. Liang, S. Huang and W. N. Lipscomb (1994) Toward a mechanism for the allosteric transition of pig kidney fructose-1,6-bisphosphatase. *J. Mol. Biol.* **244,** 609-624.

12. Shyur, L.-F., A. E. Aleshin, R. B. Honzatko and H. J. Fromm (1996) Biochemical properties of mutant and wild-type fructose-1,6-bisphosphatases are consistent with the coupling of intra- and intersubunit conformational changes in the T- and R-state transition. *J. Biol. Chem.* **271,** 33301-33307.

13. Ke, H., Zhang, Y., Liang, J.-Y., and Lipscomb, W. N. (1990) Crystal structure of fructose-1,6-bisphosphatase complexed with fructose 6-phosphate, AMP, and magnesium. *Proc. Natl. Acad. Sci. U.S.A.* **87,** 5243-5247.

14. Xue, Y., S. Huang, J.-Y. Liang, Y. Zhang and W. N. Lipscomb (1994) Crystal structure of fructose-1,6-bisphosphatase complexed with fructose 2,6-bisphosphate, AMP, and Zn2+ at 2.0-\overset°A resolution: aspects of synergism between Inhibitors. *Proc. Natl. Acad. Sci. U.S.A.* **91,** 12482-12486.

15. Villeret, V., S. Huang, Y. Zhang and W. N. Lipscomb (1995) Structural aspects of the allosteric inhibition of fructose-1,6-bisphosphatase by AMP: the binding of both the substrate analogue 2,5-anhydro-D-glucitol 1,6-bisphosphate and catalytic metal ions monitored by X-ray crystallography. *Biochemistry* **34,** 4307-4315.

16. Choe, J.-Y., B. W. Poland, H. J. Fromm and R. B. Honzatko (1998) Role of a dynamic Loop in cation activation and allosteric regulation of recombinant porcine fructose-1,6-bisphosphatase. *Biochemistry* **37,** 11441-11450.

17. Nelson, S., W., C. V. Lancu, J. -Y. Choe, R. B. Honzatko and H. J. Fromm (2000) Tryptophan fluorescence reveals the conformational state of a dynamic loop in recombinant porcine fructose-1,6-bisphosphatase. *Biochemistry* **39,** 11100-11106.

18. Nelson, S.W., Choe, J.-Y., Honzatko, R. B., and Fromm, H. J. (2000) Mutations in the hinge of a dynamic loop broadly influence functional properties of fructose-1,6-bisphosphatase. *J. Biol. Chem.* **275,** 29986-29992.

19. Choe, J, -Y., Fromm, H. J., and Honzatko, R. B. (2000) Crystal structures of fructose 1,6-bisphosphatase: mechanism of catalysis and allosteric inhibition revealed in product complexes. *Biochemistry* **39,** 8565-8574.

20. Petrich, J.W., J. W. Longworth and G. R. Fleming (1987) Internal motion and electron transfer in proteins: a picosecond fluorescence study of three homologous azurins. *Biochemistry* **26,** 2711-2722.

21. Smirnov, A.S., D. S. English, R. L. Rich, J. Lane, L. Teyton, A. W. Schwabacher, S. Luo, R. W. Thornburg, and J. W. Petrich (1997) Photophysics and biological applications of 7-azaindole and its analogs. *J. Phys. Chem. B* **101,** 2758-2769.

22. Das, K., K. D. Ashby, A. V. Smirnov, F. C. Reinach, J. W. Petrich, and C. S. Farah. (1999) Fluorescence properties of recombinant tropomyosin containing tryptophan, 5-hydroxytryptophan, and 7-azatryptophan. *Photochem. Photobiol.* **70,** 719-730.

23. Rich, R.L., A. V. Smirnov, A. W. Schwabacher, and J. W. Petrich (1995) Synthesis and photophysics of the optical probe, N1-methyl-7-azatryptophan. *J. Am. Chem. Soc.* **117,** 11850-11853.

24. Lakowicz, J.R., *Principles of fluorescence spectroscopy*. Second Edition ed. 1999, New York: Kluwer Academic/Plenum Publishers.

25. Laemmli, U.K. (1970) Cleavage of structural proteins during the assembly of the head of bacteriophage T4. *Nature* **227,** 680-685.

26. Bradford, M.M. (1976) A rapid and sensitive method for the quantitation of microgram quantities of protein utilizing the principle of protein-dye binding. *Anal. Biochem.* **72,** 248-252.

27. Siano, D.B., J. W. Zyskind and H. J. Fromm (1975) A computer program for fitting and statistically analyzing initial rate data applied to bovine hexokinase type III isozyme. *Arch. Biochem. Biophys.* **319,** 587-600.

28. Leatherbarrow, R.J., *ENAFITTER: A non-linear regression data analysis program for the IBM PC.* 1987, Amsterdam: Elsevier Science Publishers B. V. 13-75.

29. Lipari, G., A. Szabo (1982) Model-free approach to the interpretation of nuclear magnetic resonance relaxation in macromolecules. 2. Analysis of experimental results. *J. Am. Chem. Soc.* **104,** 4559-4570.

30. Callis, P.R. (1997) 1La and 1Lb transitions of tryptophan: applications of theory and experimental observations to fluorescence of proteins. *Methods Enzymol.* **278,** 113-150.

31. Moncrieffe M.C., Juranic N., Kemple M.D., Potter J.D., Macura S., Prendergast F.G. (2000) Structure-fluorescence correlations in a single tryptophan mutant of carp parvalbumin: solution structure, backbone and side-chain dynamics. *J Mol. Biol.* **297,** 147-163.

CHAPTER V: MULTIDIMENSIONAL REACTION COORDINATE FOR THE EXCITED-STATE H-ATOM TRANSFER IN PERYLENE QUINONES: IMPORTANCE OF THE 7-MEMBERED RING IN HYPOCRELLINS A AND B

A paper published in *Photochemistry and Photobiology*[1]

Anindya Dutta[2], Alexandre V. Smirnov[2], Jin Wen[2], and Jacob W. Petrich[2,3]

Abbreviations: DcOH, decanol; DMSO, dimethyl sulfoxide; DT, double tautomer; EtOD, deuterated ethanol; EtOH, ethanol; MeOD, deuterated methanol; MeOH, methanol; NT, normal tautomer; OcOH, octanol.

Abstract

The excited-state intramolecular H-atom transfer reactions of hypocrellins B and A are compared by using time-resolved absorption and fluorescence upconversion techniques. The hypocrellin B photophysics are well described by a simple model involving one ground-state species and excited-state forward and reverse H-atom transfer with a nonfluorescent excited state. We suggest that excited-state conformational changes are coupled to the H-atom transfer in hypocrellin B just as *gauche*/*anti* changes are coupled to the H-atom transfer in hypocrellin A.

---

[1] Reprinted with permission of *Photochemistry and Photobiology*, **2000**, 71(2), 166-172

[2] Department of Chemistry, Iowa State University, Ames, IA 50011-3111 USA

[3] To whom correspondence should be addressed

Introduction

The perylene quinones, hypocrellin, hypericin (Fig.5.1) and their analogs are of interest because of their light-induced biological properties [1-5]. We have argued that they also present a fascinating system with which to study excited-state intramolecular H-atom transfer [6-17] and intermolecular proton transfer [18-20]. In previous articles, we have made detailed comparisons of the photophysics of hypocrellin and hypericin in an attempt to reconcile and to unify their superficially different behavior [16, 17, 21]. In this article, we compare the excited-state H-atom transfer of hypocrellins A and B.

The most significant structural difference of the B form with respect to that of the A form is its double bond in the 7-membered ring. Three significantly populated species are observed for hypocrellin A [17]: two normal, *i.e.* untautomerized, species differing in the orientation of the 7-membered ring (*i.e.* a *gauche* or *anti* conformation about the C14-C13 bond or the C14-C16 bond) and a double tautomer in the *gauche* conformation (Figure 5.2). We have determined in our previous work that conformational changes are coupled to both ground- and excited-state tautomerization in hypocrellin A [17]. Owing to the double bond in its 7-membered ring, hypocrellin B has higher structureal rigidity than hypocrellin A. Consequently, only one tautomer/conformer of hypocrellin B is observed by NMR to be significantly populated in the ground state [17].

Here we present a preliminary comparison of the photophysics of hypocrellin A and B with the aim of understanding how the 7-membered ring and its conformation influences the excited state H-atom transfer. The *gauche* and the *anti* conformers of the 7-membered ring in hypocrellin A are defined in terms of the relative positions of the methyl and the acetyl groups in the Newman projections (Figure 5.2). Because hypocrellin B has lost this

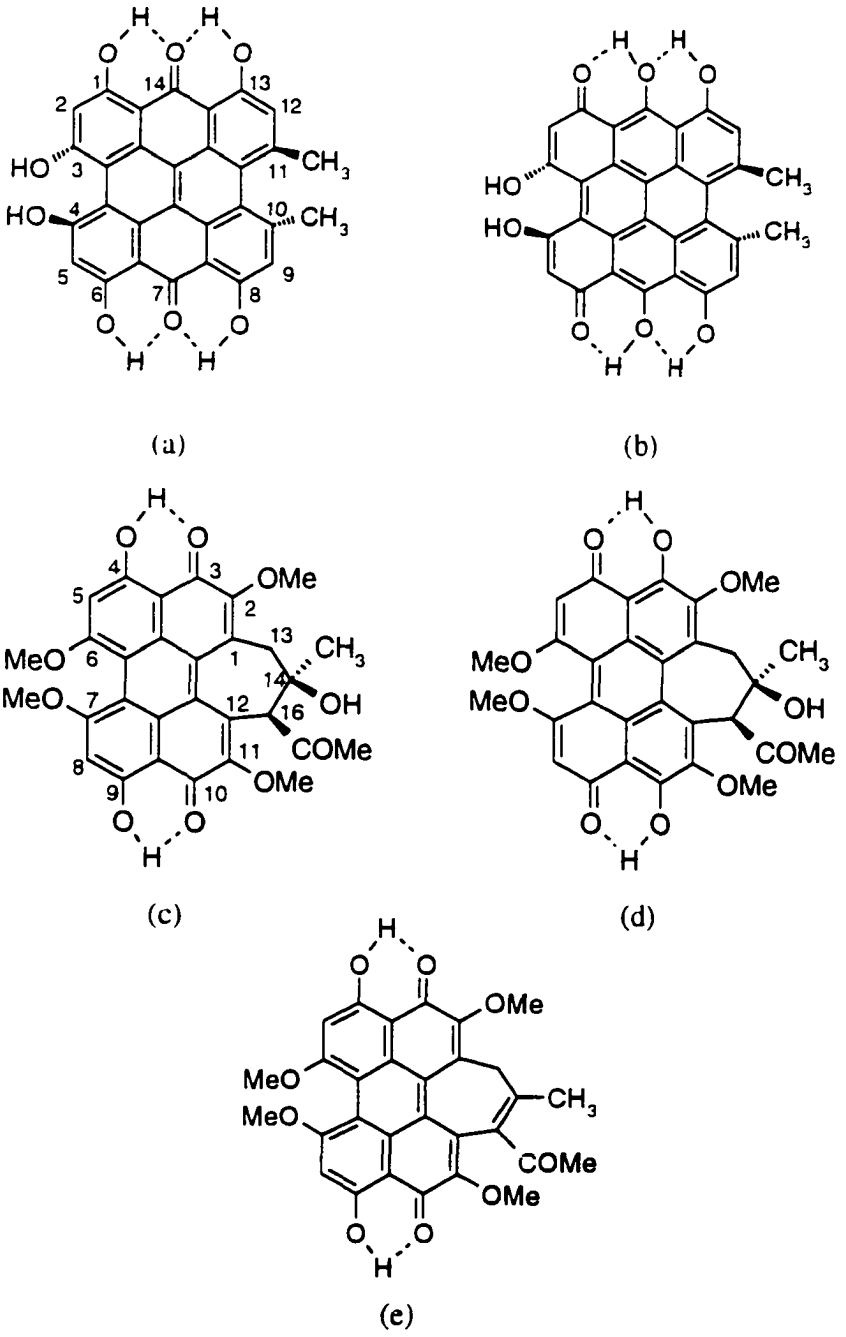

Figure 5.1 Structures of hypericin NT (a) and DT (b) forms; hypocrellin A NT (c) and DT (d) forms and the normal form of hypocrellin B (e).

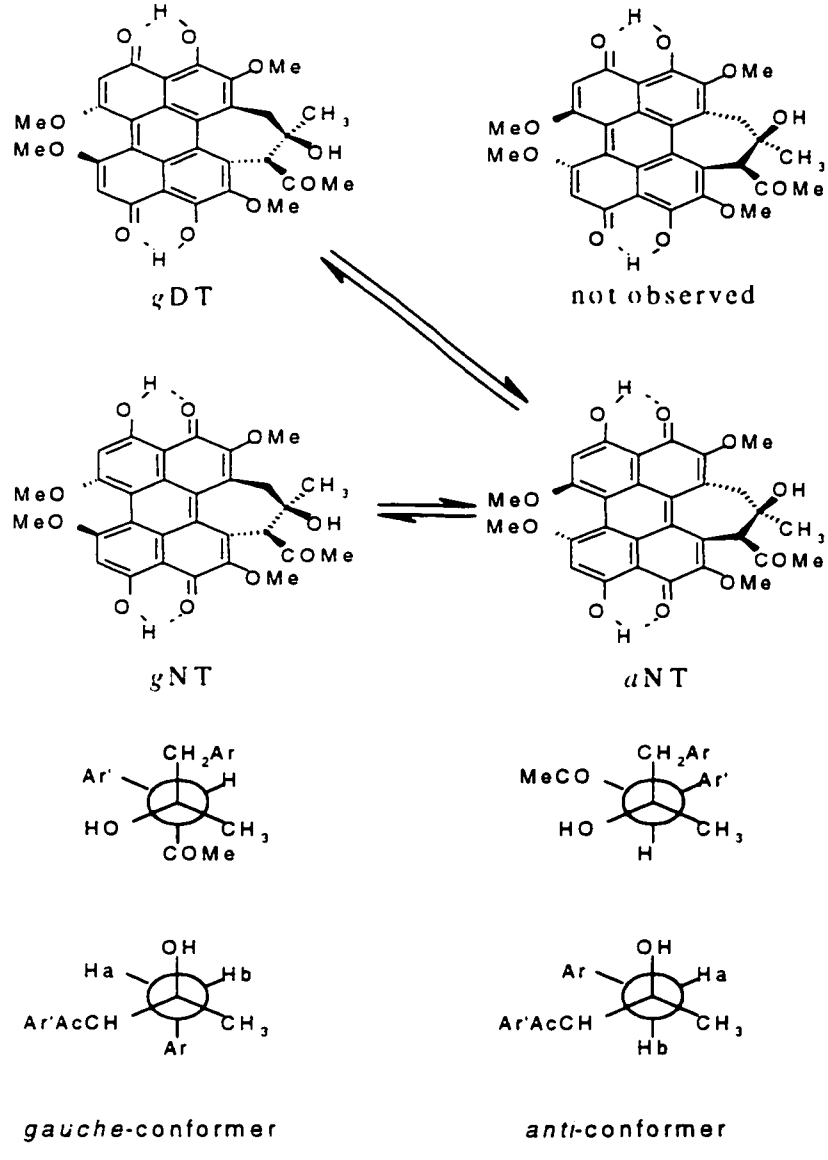

Figure 5.2 Conformational forms of the hypocrellin A NT and DT. The *anti/gauche* nomenclature is based on the relative position of the methyl and acetyl moieties as depicted by the C(14) –C(13) and the C(14) –C(16) Newman projection. The NMR measurements of hypocrellin A indicate that in the ground state there is 60% *gauche* DT (*g*DT), 30% *anti* NT (*a*NT) and 10% *gauche* NT (*g*NT). In the ground state, these species are related sequentially, by the following equilibria: *g*DT ↔*a*NT ↔*g*NT, as indicated in the figure. Based on our model [21], which requires that only the DT is significantly fluorescent, we conclude that in the excited state, the relation among the species is different: *g*NT* →*g*DT* ←*a*NT*.

-OH group by elimination of water, thus forming the dboule bond it is no longer possible to speak of *gauche* and *anti* conformers. The 7-membered ring of hypocrellin B is, however, buckled. Insofar as this double bond is conjugated to the π system of the aromatic skeleton, one might expect that in the excited state the 7-membered ring is able to undergo a conformational change about the double bond. Thus, we suggest that excited-state conformational changes are coupled to the H-atom transfer in hypocrellin B just as *gauche/anti* changes are coupled to the H-atom transfer in hypocrellin A [16, 17].

Materials and Methods

Hypocrellin A and B were obtained from Molecular Probes and were used as received. Anhydrous HPLC-grade solvents (Aldrich) were used as received, except for deuterated ethanol (EtOD) and deuterated methanol (MeOD) that were distilled with CaH_2 and ethanol (EtOH) that was distilled with Mg to ensure that no water was present. Steady-state absorbance spectra were obtained on a Perkin Elmer Lambda 18 double-beam UV–visible spectrophotometer with 1 nm resolution. Steady-state fluorescence spectra were obtained on a Spex Fluoromax with a 4 nm bandpass and corrected for lamp spectral intensity and detector response. Transient absorption [12] and fluorescence upconversion measurements were obtained with the apparatus described in detail elsewhere [15, 16].

Fluorescence upconversion traces were fit with Spectra-Solve for Windows 95/98 data collection and processing software (Ames Photonics, Inc.) employing nonlinear least-squares iterative deconvolution subroutine and assuming a Poisson noise model. Two contributions are generally considered when fitting the data: a short rising component and a

long-lived decaying component (assigned to a time constant of infinity for experiments on time scales up to 50 ps). The data are fit to the following function:

$$F(t) = a_1 [1-\exp(-t/\tau_1)] + a_2 \exp(-t/\tau_2)$$

$$= - a_1 \exp(-t/\tau_1) + (a_1 + a_2) \exp(-t/\infty) \qquad (5\text{-}1)$$

As a matter of convenience the fitting results are reported in a normalized form such that (a_1 + a_2) is equal to unity. A rapid rising component of fluorescence is observed for both hypericin and hypocrellin A. The time constant for this component ranges from 4.5 to 10 ps. For simplicity, we refer to it throughout this article as the ~ 10 ps component.

The transient absorption data were also fit by the same program. For hypocrellin A, the data are fit to the following function:

$$\Delta A(t) = a_1[1- \exp(-t/\tau_1)] + a_2\exp(-t/\tau_2) + a_3\exp(-t/\infty) \qquad (5\text{-}2)$$

For hypocrellin B, however, two exponential components are sufficient to describe the data and the following form is used:

$$\Delta A(t) = a_1[1- \exp(-t/\tau_1)] + a_2\exp(-t/\infty) \qquad (5\text{-}3)$$

In both cases, a_1 is the amplitude of the rising component; and the infinite time constant describes a process that does not decay on the experimental time scales (up to 500 ps full scale) used in this study.

Results

Steady-state absorption and emission spectra of hypocrellins A and B in dimethyl sulfoxide (DMSO) are presented in Fig. 5.3. The most significant difference between the two hypocrellins is the smaller relative intensity of the reddest absorption maxima with respect to the absorption maximum (~ 470 nm) in hypocrellin B.

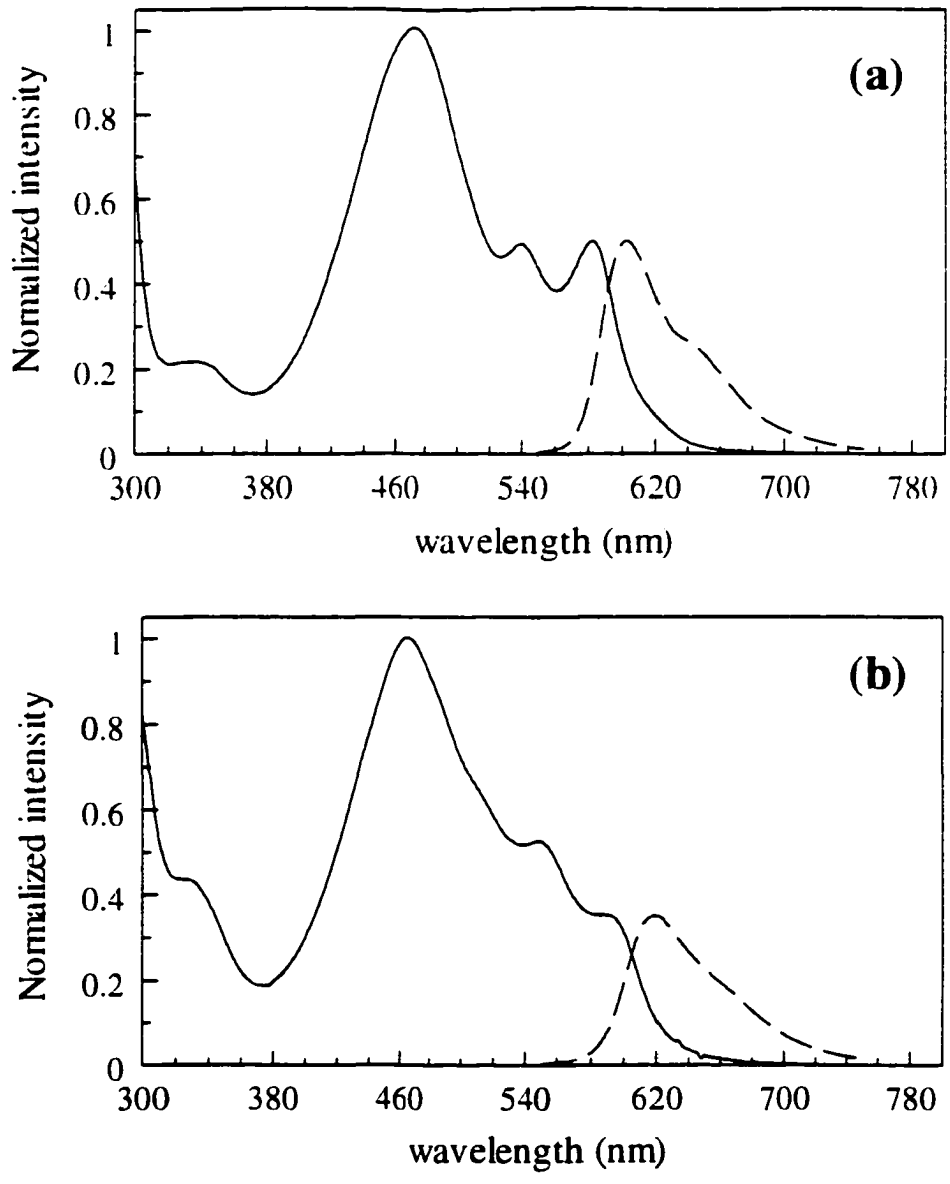

Figure 5.3 Comparison of the absorbance (solid lines) and fluorescence (dashed lines) spectra of hypocrellin A (a) and hypocrellin B (b) in DMSO normalized to the reddest absorption maximum. The emission spectra are independent of the excitation wavelength

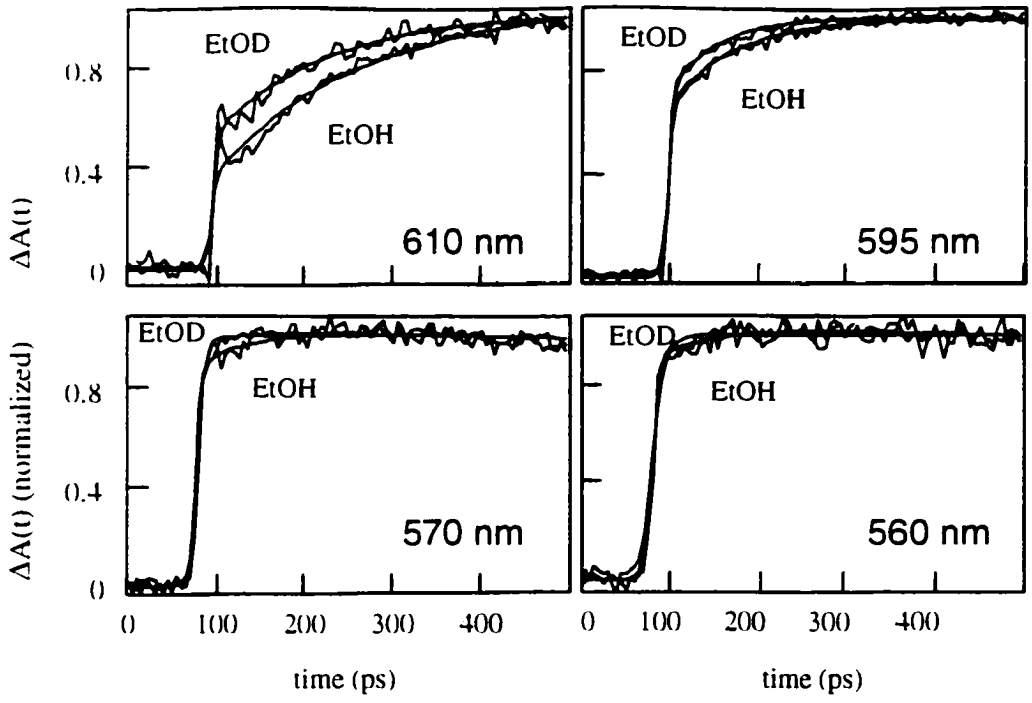

Figure 5.4 Transient absorption traces of hypocrellin B in EtOH and EtOD at probe wavelengths of (a) 610 nm, (b) 595 nm, (c) 570 nm and (d) 560 nm. The global fits to the data are presented in Table 5.1

Transient absorption measurements were performed in C_2H_5OH and C_2H_5OD at several probe wavelengths in order to observe the magnitude of the deuterium isotope effect on the excited-state H-atom transfer reaction in hypocrellin B (Fig. 5.4 and Table 5.1). Four sets of data were simultaneously analyzed by means of a global fitting procedure described in detail elsewhere [22]. Surprisingly, an apparent inverse isotope effect is observed; i.e. $k_H/k_D = 0.75$. Although there is some precedent for inverse isotope effects in ground-state reactions [23], to our knowledge one has never been observed in a subnanosecond excited-state reaction. We propose that our result is a consequence of our inability to interrogate a sufficiently broad spectral range. The signal-to-noise ratio at bluer or redder probe wavelengths than those presented in Fig. 5.4 was unacceptable. Had the kinetic traces in Fig. 5.4 exhibited a more marked difference over the spectral range investigated, we believe that

Table 5.1 Global fitting parameters for transient absorption traces of hypocrellin B in EtOH and EtOD*

Solvent	λ_{probe} (nm)	a_1	a_2
EtOH	610	0.35	0.11
	595	0.28	0.51
	570	0.02	0.33
	560	0.06	0.44
EtOD	610	0.35	0.25
	595	0.27	0.69
	570	0.05	0.28
	560	0.04	0.24

*The data were fit to the functional form: $\Delta A(t)=a_1[1-\exp(-t/\tau_1)]+a_2\exp(-t/\tau_2)$, where τ_1=84 ps, $\tau_2=\infty$ for EtOH; and τ_1=63 ps, $\tau_2=\infty$ for EtOD

an isotope effect greater than unity would have been obtained from the analysis. As an example we cite the case of hypocrellin A in CH_3OH and CH_3OD (Fig.5.5 and Table 5.2) [22]. Global analysis of the data at four probe wavelengths yields a normal isotope effect: $k_H/k_D = 1.4$. On the other hand, examination of these data at only one probe wavelength gives aberrant results. For example, analysis of the hypocrellin A data at only λprobe = 570 nm yields a perfectly acceptable fit (Fig. 5.6) but gives $k_H/k_D = 0.71$.

The data presented in Figs. 5.4-5.6 and Tables 5.1 and 5.2 demonstrate very vividly the potential complications in analyzing kinetic data (especially transient absorbance data), the importance of employing global analysis procedures whenever possible and the necessity of employing complementary techniques, for example, fluorescence measurements that only detect emission from excited-state singlets [15, 16].

Transient absorption data were obtained in a range of solvents of different type and viscosity (Figs.5.7 and 5.8). Figure 5.8 indicates that the viscosity dependence of the H-atom

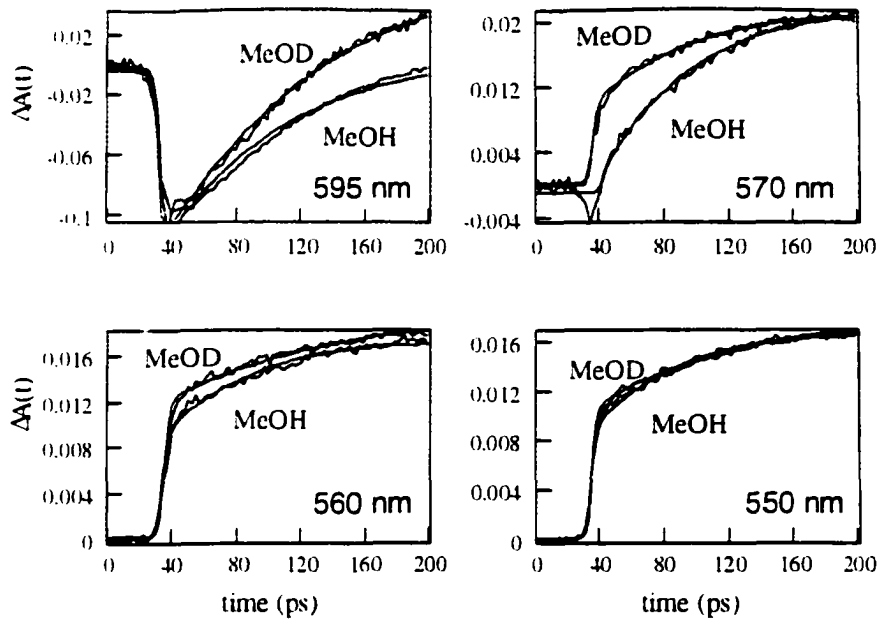

Figure 5.5 Transient absorption traces of hypocrellin A in methanol (MeOH) and MeOD probe wavelengths of (a) 595 nm, (b) 570 nm, (c) 560 nm and (d) 550 nm. The global fits to the data are presented in Table 5.2

Table 5.2 Global fitting parameters for transient absorption traces of hypocrellin A in MeOH and MeOD*

Solvent	λ_{probe} (nm)	a_1	a_2	a_3
MeOH	595	0.24	-0.19	0.07
	570	0.13	0.16	0.12
	560	0.11	0.16	0.07
	550	0.11	0.19	0.10
MeOD	595	0.21	0.20	0.04
	570	0.14	0.01	0.13
	560	0.10	0.15	0.02
	550	0.08	0.03	0.09

* The data were fit to the functional form: $\Delta A(t)=a_1[1-\exp(-t/\tau_1)]+a_2\exp(-t/\tau_2)+a_3\exp(-t/\tau_3)$, where τ_1=68 ps, τ_2=1290 ps and $\tau_3=\infty$ for MeOH; and τ_1=98 ps, τ_2=1250 ps and $\tau_3=\infty$ for MeOD.

transfer in hypocrellin B is very similar to that for hypocrellin A. The results presented are based on a global fit of the kinetics obtained at 595 and 610 nm for hypocrellin B and at 550, 560, 570 and 600 nm for hypocrellin A.

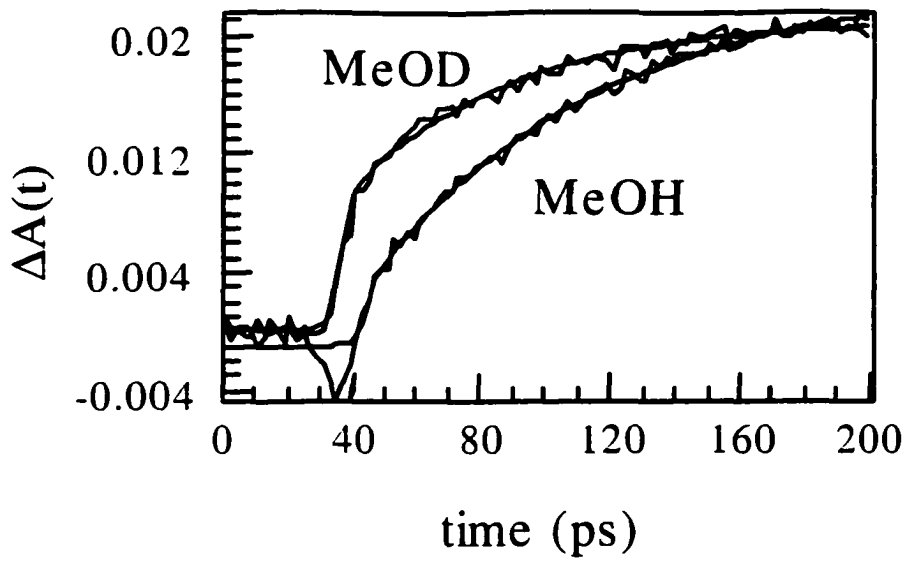

Figure 5.6 Transient absorption traces of hypocrellin A in (a) MeOH and (b) MeOD at 570 nm, fit nonglobally. For MeOH: 0.40[1 −exp(−t/74 ps)] + 0.09exp(−t/1480 ps) + 0.001 exp(−t/∞) and for MeOD: 0.23[1 −exp(−t/53 ps)] + 0.11 exp(−t/1980 ps) + 0.06 exp(−t/∞).

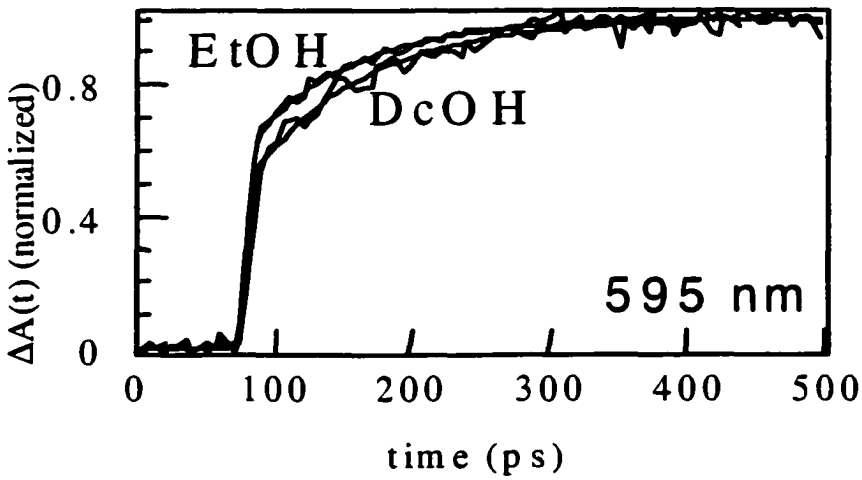

Figure 5.7 Transient absorption traces of hypocrellin B in (a) EtOH and (b) decanol (DcOH). λ_{ex} = 588 nm, λ_{em} = 595 nm. The fits to the data are: (a) ΔA(t) = 0.59[1 −exp(−t/80 ps)] + 0.99exp(−t/∞) and (b) ΔA(t) = 0.52[1 −exp(−t/120 ps)] + 0.64exp(−t/∞). In the figure, the traces are normalized to have a value of 1.0 at their maximum.

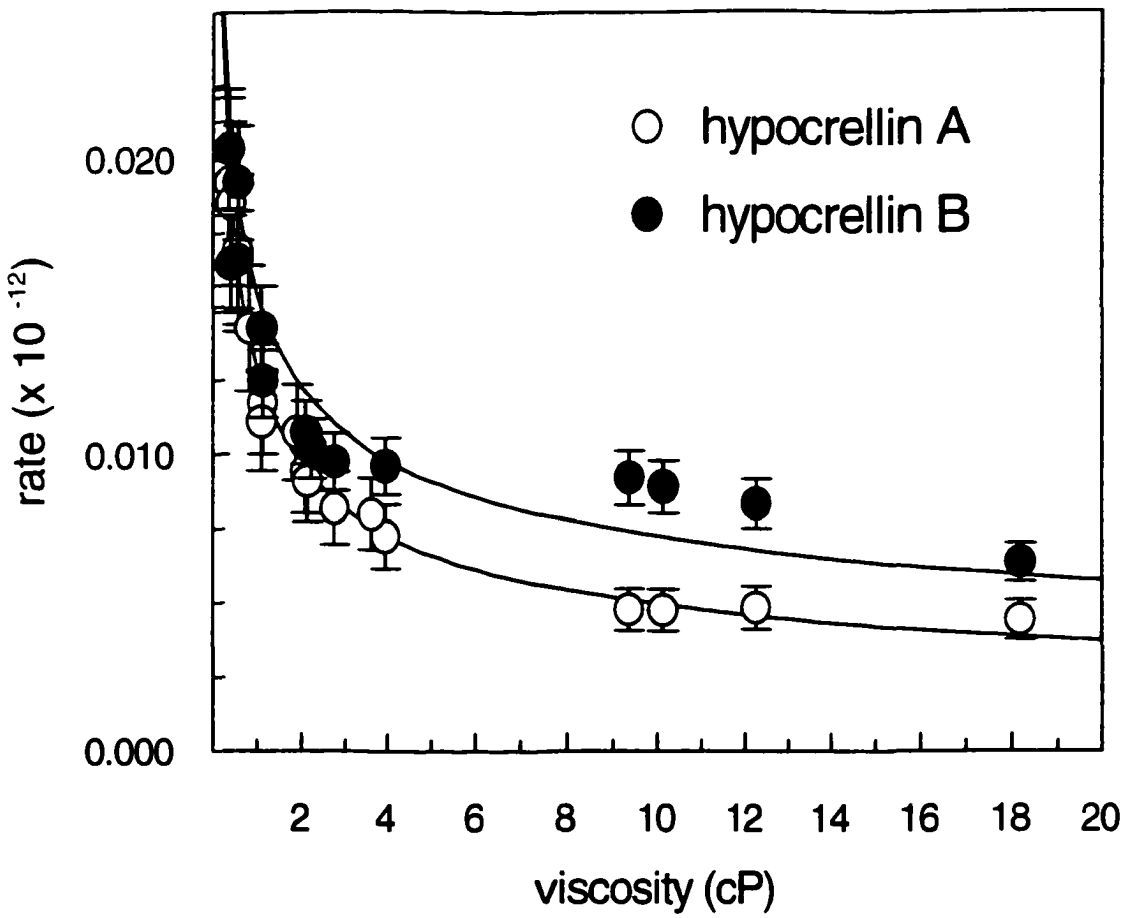

Figure 5.8 Intramolecular H-atom transfer rate of millimolar hypocrellin B and hypocrellin A in various solvents of different viscosity at 22°C. The data are fit to a phenomenological expression $k = (C/\eta^a)\exp(-E_0/RT)$ where $C = 2.17 \times 10^{12}$ s^{-1}, $a = 0.33$ and $E_0 = 2.92$ kcal mol^{-1} for hypocrellin B and 1.9×10^{12} s^{-1}, 0.42 and 3.0 kcal mol^{-1} for hypocrellin A, respectively. An iterative nonlinear least-squares fit is used to obtain the parameters in both the cases. The solvents used in this study are MeOH, EtOH, propanol, pentanol, octanol (OcOH), nonanol, DcOH, ethylene gycol, DMSO, formamide, dimethylformamide, acetonitrile, butyronitrile, 2,2,2-trifluoroethanol and cyclohexanone. Viscosity data are obtained from the text by Viswanath and Natarajan [24]. The data points represent an average of from two to four measurements. The error bars represent an estimated error of 10%.

The most surprising result we have obtained is that for hypocrellin B there is no obvious, significant <100 ps decay or rise in the fluorescence upconversion data (on time scales ranging from 50 ps to 1 ns), whereas for hypocrellin A there is a distinct ~10 ps rising component (Fig.5.9). This result is satisfactorily explained in terms of the kinetic model presented below.

Discussion

Our argument for intramolecular excited-state H-atom transfer in hypericin is as follows. The deshydroxy analog of hypericin, mesonaphthobianthrone, is nonfluorescent except in strong acids [7, 8, 11] (e.g. sulfuric acid) where it produces a fluorescence spectrum that has nearly the same shape as that of hypericin in DMSO. These results demonstrate the importance of a protonated carbonyl group for producing hypericin-like fluorescence. The hypericin emission spectrum grows on a 6–12 ps time scale in all solvents except in sulfuric acid where it is instantaneous. Based on the results for mesonaphthobianthrone, the rise time for the appearance of the hypericin emission is taken as evidence for an excited-state H-atom transfer [7]. It is an assumption of our developing model for the excited-state photophysics of these perylene quinones that only the tautomer, not the normal species is significantly fluorescent.

This assumption has proved to be quite useful in analyzing the complicated photophysics of these molecules [16, 21] although it is, however, very likely too rigid [21]. A question that arises is what we mean by tautomer. There is no particular problem when comparing the two forms of hypericin illustrated in Fig. 5.1a,b. For hypericin, the double

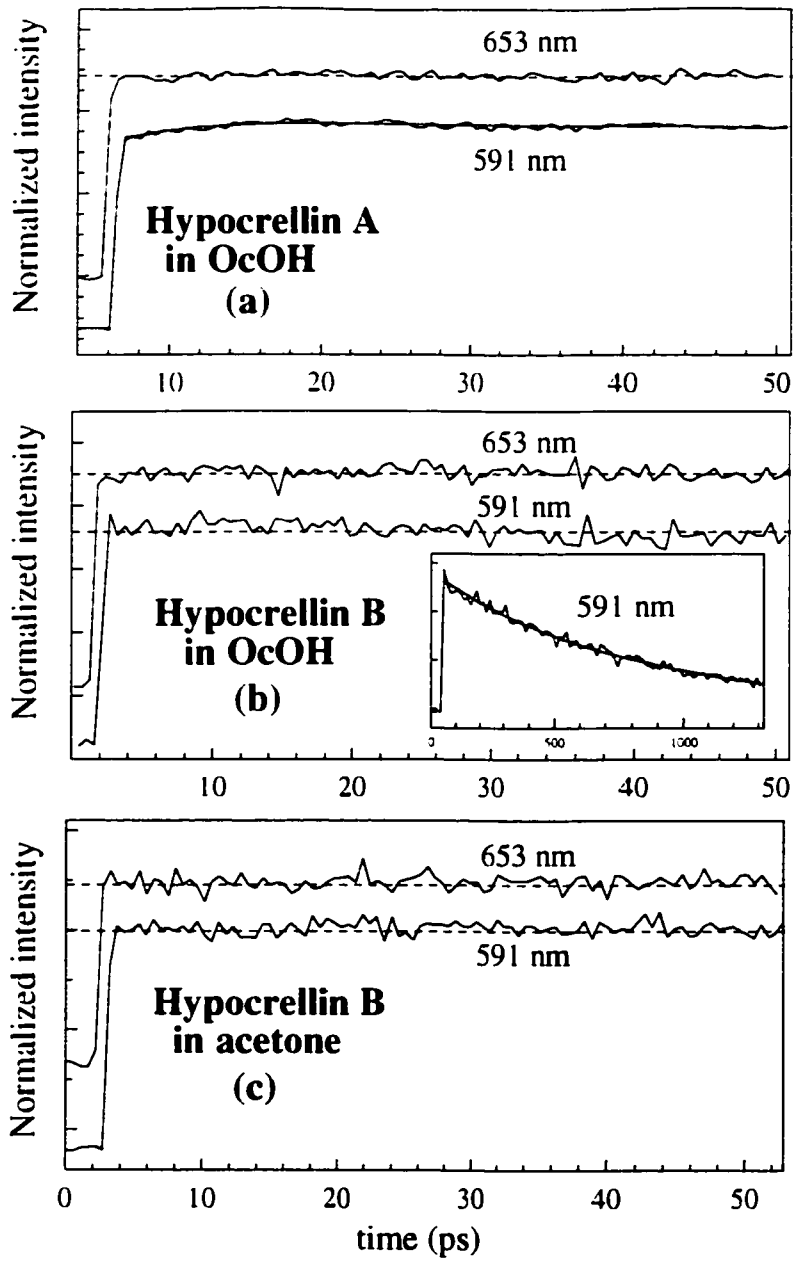

Figure 5.9. Fluorescence upconversion traces of hypocrellin A in OcOH (a) and hypocrellin B in OcOH (b) and acetone (c) collected at blue (591 nm) and red (653 nm) emission wavelengths. A fit of the hypocrellin A rising emission yields $F(t) = -0.10\exp(-t/4.1\text{ ps}) + 1.00\exp(-t/\infty)$. Dashed lines are included to help evaluate trace flatness. The inset of panel b shows the hypocrellin fluorescence decay on a nanosecond timescale, which is fit to $F(t) = 1.0\exp(-t/814\text{ ps})$.

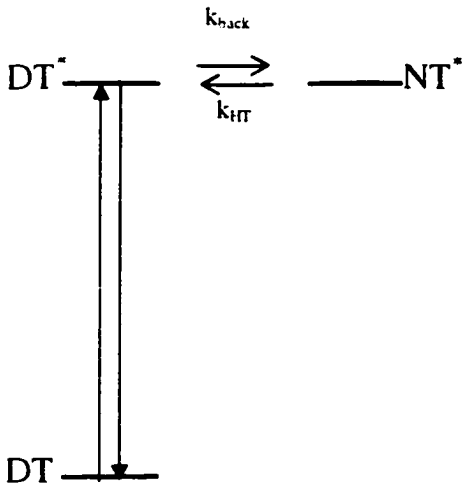

Figure 5.10. Schematic for the hypocrellin B excited-state kinetics. The only species populated in the ground state, as determined by NMR measurements [17], is the DT. The NT* is the normal excited state of the normal species; k_{back} is the rate constant of tautomerization from DT* to NT*; and k_{HT} is the rate constant to reform DT* from NT*. The NT* is assumed to be nonfluorescent

tautomer is the species that has both carbonyl groups on the same side of the molecule, i.e. the 1,6- or 8,13-dioxo species. (There is a possible double tautomer that has the two carbonyl groups on either side of the molecule, the 1,8-dioxo form, but this species has not been determined to present a minimum on the ground-state potential energy surface [25]). On the other hand, the structural differences between what we refer to as the normal and the tautomer species are much more subtle when we compare these forms of hypocrellin (Fig.5.1c,d).

Based on the NMR results for hypocrellin B, only one species exists in the ground state [17]. It is assigned, by the fundamental assumption enumerated above, to the double tautomer, DT (whose structure is, in turn, assigned based on analogy to that proposed for hypocrellin A [17]) because fluorescence is instantaneous, with no apparent rise time, in hypocrellin B (Fig. 5.9). The rise time in the transient absorption data for hypocrellin B is attributed to the formation of the normal tautomer, NT*, from DT*.

A model of textbook simplicity can be constructed to rationalize qualitatively the photophysics of hypocrellin B. In this model (Fig.5.10), DT* can tautomerize to NT* with rate constant, k_{back}. Again, by the fundamental assumption, NT* is nonfluorescent, but it can undergo H-atom transfer to reform DT* with rate constant k_{HT}. The concentrations of DT* and NT* can be determined easily analytically or can be simply obtained from Chapter 7 of Birks' text [26]:

$$[DT^*](t) = \frac{[DT^*]_o}{(\lambda_2 - \lambda_1)}\left\{(\lambda_2 - X)e^{-\lambda_1 t} + (X - \lambda_1)e^{-\lambda_2 t}\right\} \qquad (5-4)$$

$$[NT^*](t) = \frac{k_{back}[DT^*]_o}{(\lambda_2 - \lambda_1)}\left\{e^{-\lambda_1 t} - e^{-\lambda_2 t}\right\} \qquad (5-5)$$

Where

$$\lambda_{1,2} = \frac{1}{2}\left[X + Y \mp \left\{(Y - X)^2 + 4\,k_{back}\,k_{HT}\right\}^{1/2} \right] \qquad (5-6)$$

$$X = \frac{1}{\tau_{F,D^*}} + k_{back}\,; \quad Y = \frac{1}{\tau_{F,N^*}} + k_{HT} \qquad (5-7)$$

τ_{F,D^*} and τ_{F,N^*} are the fluorescence lifetimes of the DT and the normal form in the absence of H-atom transfer. Figure 5.11 presents simulated upconversion and transient absorption traces. The τ_{F,D^*} was fixed at 1 ns, which is the fluorescence lifetime of hypocrellin B, as measured by the upconversion experiment (Fig. 5.9b, inset). The τ_{F,N^*} was set to be infinitely large, because the normal excited state is assumed to be nonfluorescent. The k_{HT} was fixed at 0.02 $\times 10^{12}$ s^{-1} (the inverse of the time constant for H-atom transfer in methanol, 50 ps [Fig. 5.7]). The only adjustable parameter in the simulation is k_{back}, for which the optimal value was approximately 0.0013 $\times 10^{12}$ s^{-1}. The agreement between the experimental data and the

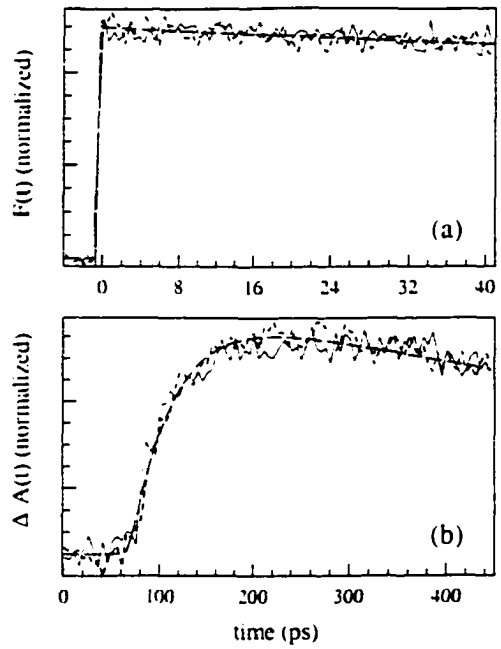

Figure 5.11. (a) Plot of simulated fluorescence upconversion data obtained from the kinetic scheme presented in Fig. 10. The solid line represents the experimental data for hypocrellin B in OcOH at an emission wavelength of 591 nm (Fig. 5.9b). The fluorescence lifetime of hypocrellin B is rather insensitive to solvent, as in the cases of hypocrellin A and hypericin [7-10]. The long dashed line represents the simulated data convoluted with an appropriate instrument response function and the short dashed line represents the simulated data with a 5% Poisson noise added to it. (Poisson noise is added because this is the type of noise inherent to the photon counting experiment.) The functional form of the simulated fluorescence upconversion data is given by $F(t) \sim [DT^*](t) = 0.93\exp(-t/1070\text{ ps}) + 0.07\exp(-t/50\text{ ps})$, where the prefactors are normalized such that the fluorescence intensity is unity at time zero.

(b) Plot of simulated transient absorption data obtained from the kinetic scheme. The solid line represents experimental data for hypocrellin B in MeOH at a probe wavelength of 595 nm. The long dashed line represents simulated data convoluted with an appropriate instrument response function and the short dashed line represents the simulated data with a 5% level of Gaussian noise added to it. The functional form of the simulated transient absorption data is: $\Delta A(t) = (\varepsilon_{D^*} - \varepsilon_D)[DT^*](t)l + (\varepsilon_{N^*} - \varepsilon_D)[NT^*](t)l$, where ε_{D^*}, ε_D and ε_{N^*} are the molar extinction coefficients for DT*, DT and NT*, respectively; and l is the pathlength of the sample. It is assumed that $\varepsilon_{N^*} > \varepsilon_{D^*}$, that $\varepsilon_{D^*} \sim \varepsilon_D$ and that NT is not present in the ground state. This equation thus reduces to $\Delta A(t) \propto [NT^*](t) = 3.4[1 - \exp(-t/50\text{ ps})] + 0.1\exp(-t/1070\text{ ps})$. The experimental data are fit to: $\Delta A(t) = 0.46[1 - \exp(-t/52)] + 0.30\exp(-t/\infty)$. The curves are normalized to unity at 500 ps.

simulation is excellent. As noted above, the simplest and most constrained assumption is that NT* is nonfluorescent and hence that $\tau_{F,N^*} \sim \infty$. Nevertheless, the experimental data are qualitatively reproduced even if $\tau_{F,N^*} \sim 1$ ns, i.e. approximately the measured fluorescence lifetime of hypocrellin B (Fig. 5.9b).

Conclusions

The crucial observation that permitted the unification of the hypocrellin A and hypericin photophysics is the observation of a ~10 ps transient that lacks a deuterium isotope effect, in time-resolved absorption and fluorescence upconversion measurements [16, 21]. This component is absent in the hypocrellin B data because in terms of our model, it exists in only one ground-state conformer/tautomer that does not correspond to the gauche normal form of hypocrellin A that exhibits the ~10 ps component (Fig. 5.2. The longer-lived transients of hypocrellin B are similar in magnitude and solvent dependence to those of hypocrellin A (Figs. 5.7 and 5.8).

The similarity of these long-lived transients is surprising. Although the double bond in the 7-membered ring of hypocrellin B constrains it to exist in one conformational and tautomeric form [16], it appears that in the excited state this is not the case. As suggested in the introduction, if these double bonds are conjugated with the aromatic system of the hypocrellin B skeleton, then optical π–π^* excitation would result in a relaxation of the constraint and would permit the 7-membered ring to execute the type of *gauche/anti* structural changes that we propose occur in hypocrellin A and that are the origin of the strong viscosity dependence [17].

The hypocrellin B photophysics are well described by a simple model involving one ground-state species and excited-state forward and reverse H-atom transfer with a nonfluorescent state. These results suggest that careful fluorescence measurements with high signal-to-noise ratio (such as those provided by the time-correlated single photon counting technique rather than the fluorescence upconversion technique (Fig. 5.9) may reveal two exponentially decaying components for the fluorescence decay of hypocrellin B. If this is the case, knowledge of the second, shorter-lived, low-amplitude component, not resolved by our fluorescence upconversion measurements, can permit us to estimate k_{HT} as defined in terms of the kinetic scheme presented in Fig. 5.7.

Acknowledgements

This work was supported by NSF grant CHE-9613962 to J.W.P.

References

1. Diwu, Z.; Lown, J. W. (1990) Hypocrellins and their use in photosensitization. *Photochem. Photobiol.* **52**, 609-616.
2. Diwu, Z. (1995) Novel therapeutic and diagnostic applications of hypocrellins and hypericins. *Photochem. Photobiol.* **61**, 529-539.
3. Durán, N.; Song, P. S. (1986) Hypericin and its photodynamic action. *Photochem. Photobiol* **43**, 677-680.
4. Kraus, G. A.; Zhang, W.; Fehr, M. J.; Petrich, J. W.; Wannemuehler, Y.; Carpenter, S. (1996) Research at the Interface between Chemistry and Virology: Development of a Molecular Flashlight. *Chem. Rev.* **96**, 523-535.
5. Lown, J. W. (1997) 1996 Hoffman-LaRoche Award Lecture. Photochemistry and phobiology of perylenequinones. *Can. J. Chem.* **75**, 99-119.
6. Gai, F.; Fehr, M. J.; Petrich, J. W. (1993) Ultrafast excited-state processes in the antiviral agent hypericin. *J. Am. Chem. Soc.* **115**, 3384-3385.

7. Gai, F.; Fehr, M. J.; Petrich, J. W. (1994) Observation of Excited-State Tautomerization in the Antiviral Agent Hypericin and Identification of Its Fluorescent Species. *J. Phys. Chem.* **98**, 5784-5795.

8. Gai, F.; Fehr, M. J.; Petrich, J. W. (1994) Role of Solvent in Excited-State Proton Transfer in Hypericin. *J. Phys. Chem.* **98**, 8352-8358.

9. English, D. S.; Zhang, W.; Kraus, G. A.; Petrich, J. W. (1997) Excited-State Photophysics of Hypericin and Its Hexamethoxy Analog: Intramolecular Proton Transfer as a Nonradiative Process in Hypericin. *J. Am. Chem. Soc.* **119**, 2980-2986.

10. English, D. S.; Das, K.; Zenner, J. M.; Zhang, W.; Kraus, G. A.; Larock, R. C.; Petrich, J. W. (1997) Hypericin, Hypocrellin, and Model Compounds: Primary Photoprocesses of Light-Induced Antiviral Agents. *J. Phys. Chem. A* **101**, 3235-3240.

11. English, D. S.; Das, K.; Ashby, K. D.; Park, J.; Petrich, J. W.; Castner, E. W. J. (1997) Confirmation of Excited-State Proton Transfer and Ground-State Heterogeneity in Hypericin by Fluorescence Upconversion. *J. Am. Chem. Soc.* **119**, 11585-11590.

12. Das, K.; English, D. S.; Fehr, M. J.; Smirnov, A. V.; Petrich, J. W. (1996) Excited-State Processes in Polycyclic Quinones: The Light-Induced Antiviral Agent, Hypocrellin, and a Comparison with Hypericin. *J. Phys. Chem.* **100**, 18275-18281.

13. Das, K.; English, D. S.; Petrich, J. W. (1997) Solvent Dependence on the Intramolecular Excited-State Proton or Hydrogen Atom Transfer in Hypocrellin. *J. Am. Chem. Soc.* **119**, 2763-2764.

14. Das, K.; Dertz, E.; Paterson, J.; Zhang, W.; Kraus, G. A.; Petrich, J. W. (1998) Hypericin, hypocrellin, and model compounds: steady-state and time-resolved fluorescence anisotropies. *J. Phys. Chem. B* **102**, 1479-1484.

15. Das, K.; Smirnov, A. V.; Wen, J.; Miskovsky, P.; Petrich, J. W. (1999) Photophysics of hypericin and hypocrellin A in complex with subcellular components: interactions with human serum albumin. *Photochem. Photobiol.* **69**, 633-645.

16. Smirnov, A. V.; Das, K.; English, D. S.; Wan, Z.; Kraus, G. A.; Petrich, J. W. (1999) Excited-State Intramolecular H Atom Transfer of Hypericin and Hypocrellin A Investigated by Fluorescence Upconversion. *J. Phys. Chem. A* **103**, 7949-7957.

17. Smirnov, A.; Fulton, D. B.; Andreotti, A.; Petrich, J. W. (1999) Exploring Ground-State Heterogeneity of Hypericin and Hypocrellins A and B: Dynamic and 2D ROESY NMR Study. *J. Am. Chem. Soc.* **121**, 7979-7988.

18. Fehr, M. J.; McCloskey, M. A.; Petrich, J. W. (1995) Light-Induced Acidification by the Antiviral Agent Hypericin. *J. Am. Chem. Soc.* **117**, 1833-1836.

19. Sureau, F.; Miskovsky, P.; Chinsky, L.; Turpin, P. Y. (1996) Hypericin-Induced Cell Photosensitization Involves an Intracellular pH Decrease. *J. Am. Chem. Soc.* **118**, 9484-9487.

20. Chaloupka, R.; Sureau, F.; Kocisova, E.; Petrich, J. W. (1998) Hypocrellin A photosensitization involves an intracellular pH decrease in 3T3 cells. *Photochem. Photobiol.* **68**, 44-50.

21. Das, K.; Smirnov, A. V.; Snyder, M. D.; Petrich, J. W. (1998) Picosecond Linear Dichroism and Absorption Anisotropy of Hypocrellin: Toward a Unified Picture of the Photophysics of Hypericin and Hypocrellin. *J. Phys. Chem. B* **102**, 6098-6106.

22. Das, K.; English, D. S.; Petrich, J. W. (1997) Deuterium Isotope Effect on the Excited-State Photophysics of Hypocrellin: Evidence for Proton or Hydrogen Atom Transfer. *J. Phys. Chem. A* **101**, 3241-3245.

23. Collins, C. J. a. B., N. S. *Isotope Effect in chemical Reactions*; Van Nostrand Reinhold Co.: New York, **1970**.

24. Viswanath, D. S.; Natarajan, G. *Data book on the viscosity of liquids*; Hemisphere Pub. Corp.: New York, **1989**.

25. Petrich, J. W.; Gordon, M. S.; Cagle, M. (1998) Structure and Energetics of Ground-State Hypericin: Comparison of Experiment and Theory. *J. Phys. Chem. A* **102**, 1647-1651.

26. Birks, J. B. *Photophysics of aromatic molecules*; Wiley-Interscience: London, New York, **1970**.

CHAPTER VI: COPLING OF LARGE-AMPLITUDE SIDE CHAIN MOTIONS TO THE EXCITED-STATE H-ATOM TRANSFER OF PERYLENE QUINONES: APPLICATION OF THEORY AND EXPERIMENT TO CALPHOSTIN C

A paper published in *Journal of Physical Chemistry*[1]

Anindya Datta[2], Pradipta Bandyopadhyay[2], Jin Wen[2], Jacob W. Petrich[2,3], and Mark S. Gordon[2,3]

Abstract

The excited-state intramolecular H-atom transfer reactions of hypocrellins B and A are compared with those of calphostin C. Based on the results of transient absorption measurements and *ab initio* quantum mechanical calculations, it is concluded that large-amplitude conformational changes are coupled to the H-atom transfer in calphostin C, just as they are in hypocrellins A and B. The calculations on this very large molecule with a very complex ground electronic state potential energy surface were made possible by the use of highly scalable electronic structure theory codes on large parallel computers.

---

[1] Reprinted with permission of *J. Phys. Chem. A*, **2001**, 105, 1057-1060

[2] Department of Chemistry, Iowa State University, Ames, IA 50011-3111 USA

[3] To whom correspondence should be addressed

Introduction

The nearly symmetrical perylene quinones, hypericin, hypocrellins A and B, and calphostin C (Figure 6.1), are of interest because of their light-induced biological properties [1-5]. We have argued that they also present a fascinating system with which to study excited-state intramolecular H-atom transfer [6-20].

Hypericin executes an intramolecular excited-state H-atom transfer in ~10 ps [20]. This reaction is independent of solvent. In this respect, hypericin distinguishes itself from the other perylene quinones such as hypocrellins A and B, which both undergo excited-state H-atom transfer that is strongly viscosity dependent. Their H-atom transfer times in ethanol and octanol range from 50 to 100 ps (Table 6.1). The origin of this dependence lies in the presence of the 7-membered ring in the hypocrellin "bay region."

Three significantly populated species are observed in the ground state for hypocrellin A [19]: two "normal," that is untautomerized, species differing in the orientation of the 7-membered ring (i.e., a *gauche* or *anti* conformation about the C14-C13 bond or the C14-C16 bond) and a double tautomer in the *gauche* conformation (Figure 6.2). Conformational changes are coupled to both ground- and excited-state tautomerization in hypocrellin A [19]. Owing to the double bond in its 7-membered ring, hypocrellin B, has higher structural rigidity in the ground state than does hypocrellin A. Consequently, only one tautomer/conformer of hypocrellin B is observed by NMR to be significantly populated in the ground state [19]. On the other hand, insofar as the double bond of hypocrellin B's 7-membered ring is conjugated

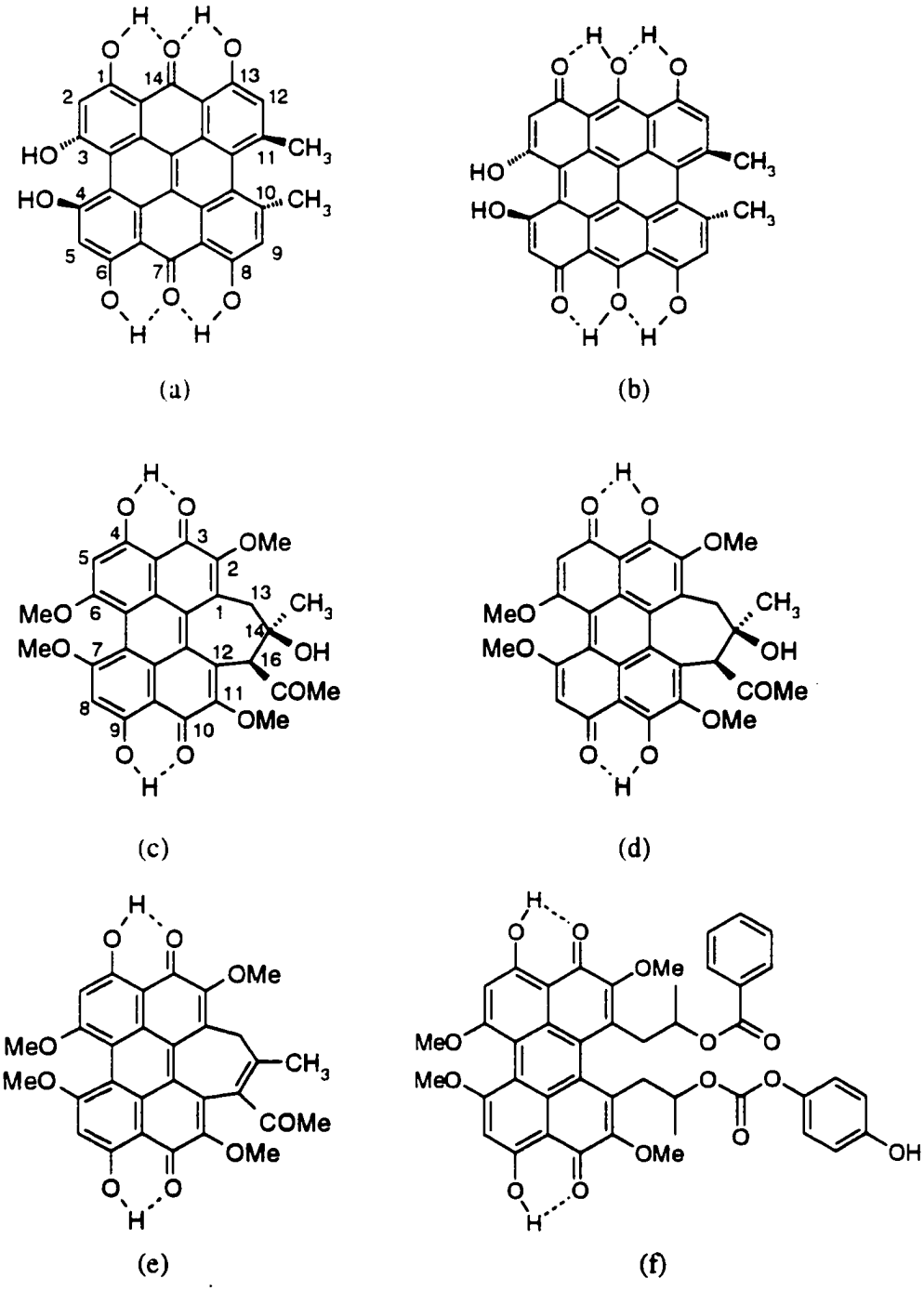

Figure 6.1 Structures of hypericin "normal" (a) and double tautomer (b) forms; hypocrellin A "normal" (c) and double tautomer (d) forms; hypocrellin B (e) and calphostin C (f).

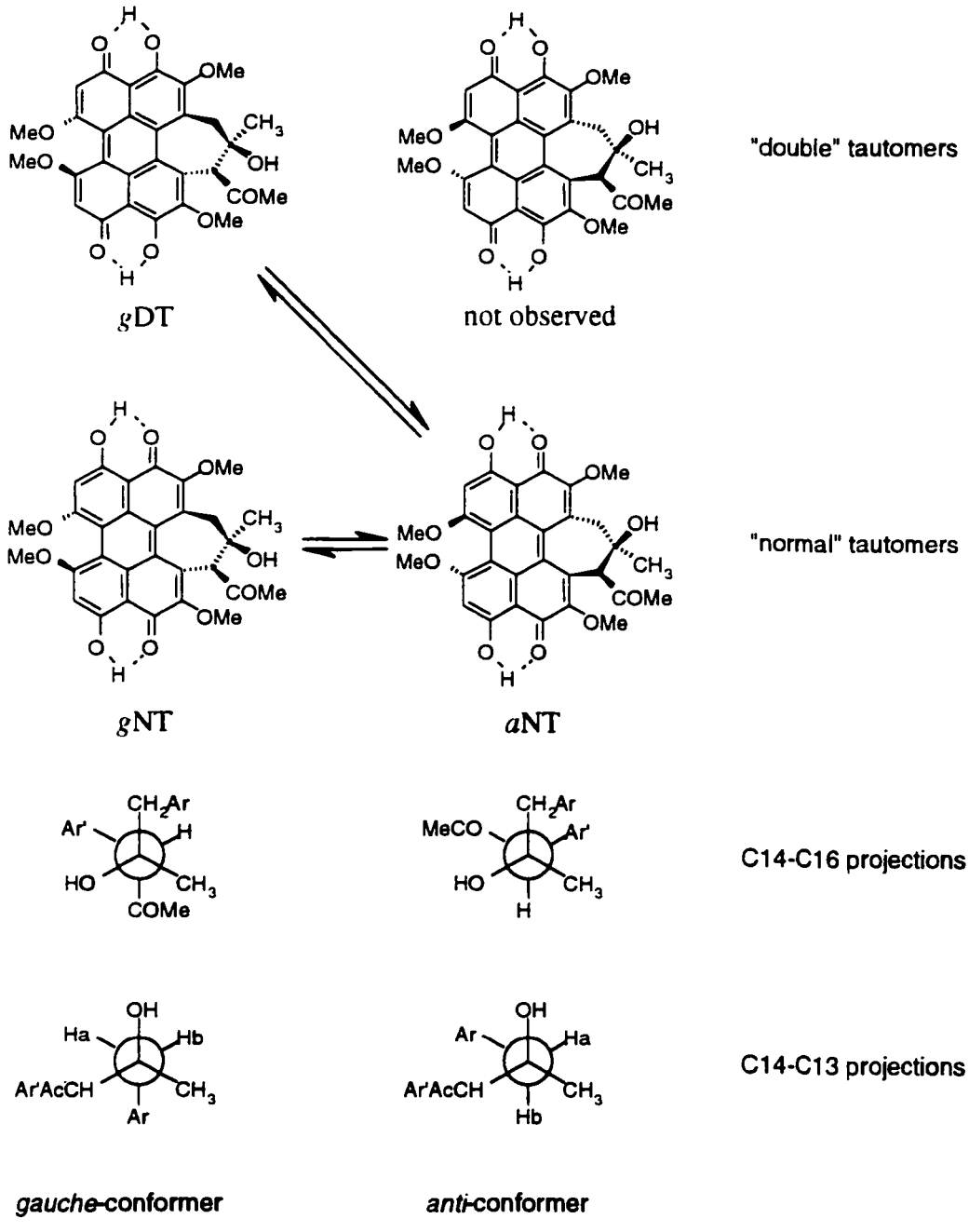

Figure 6.2 Conformational forms of the hypocrellin A normal and double tautomers. The *anti/gauche* nomenclature is based on the relative position of the methyl and acetyl moieties as depicted by the Newman projection: *gauche* double tautomer, *g*D, 60% of the ground-state population; *anti* normal tautomer, *a*N, 30%; *gauche* normal tautomer, *g*N, 10%.

Table 6.1: Kinetic Parameters for Hypocrellin A, Hypocrellin B, and Calphostin C at 595nm in Ethanol and Octanol[a]

Probe molecule	Solvent	a_1	τ_1 (ps)	a_2	τ_2 (ps)	a_3	τ_3 (ps)
Hypocrellin A	EtOH	0.23	55	-0.46	1010	0.09	∞
	OcOH	0.02	103	-0.72	1060	0.47	∞
Hypocrellin B	EtOH	0.28	84	0.51	∞	-	-
	OcOH	0.26	109	0.14	∞	-	-
Calphostin C	EtOH	0.37	104	0.01	∞	-	-
	OcOH	0.16	147	0.05	∞	-	-

[a] The data are fit to the following function: $\Delta A(t) = a_1 [1-\exp(-t/\tau_1)] + a_2 \exp(-t/\tau_2) + a_3 \exp(-t/\infty)$, where a_1 is the amplitude of the rising component; and the infinite time constant describes a process that does not decay on the experimental time scales (up to 500 ps full scale) used in this study.

to the π system of the aromatic skeleton, one might expect that in the excited state the 7-membered ring is able to undergo a conformational change about the double bond. Thus, we suggest that excited-state conformational changes are coupled to the H- atom transfer in hypocrellin B just as *gauche/anti* changes are coupled to the H-atom transfer in hypocrellin A [19,20].

Calphostin C is a perylene quinone isolated from *Cladosporium cladosporides*. It is a potent and specific inhibitor of protein kinase C [21]. To our knowledge, ours are the first time-resolved measurements obtained for calphostin C. Aside from the biological importance of investigating calphostin C, we were motivated by fundamental photophysical considerations. We originally hypothesized that if, as we suggest above, the viscosity dependent time constants in hypocrellins A and B are a result of conformational changes of their 7-membered rings that are coupled to the H-atom transfer, then breaking this 7-membered ring ought to afford hypericin-like, viscosity independent, time constants of

~10 ps.

The results presented here indicate that contrary to our expectation, calphostin C, in which there is no 7-membered ring, behaves qualitatively very similarly to hypocrellins A and B. In order to rationalize this behavior, it is necessary to propose that there is some interaction of the bulky side chains in the bay region that retard the H-atom transfer reaction. Justification of this proposal is demonstrated by *ab initio* quantum mechanical calculations.

Materials and Methods

Hypocrellin A and B were obtained from Molecular Probes and were used as received. Calphostin C was obtained from Sigma and used without further purification. Anhydrous HPLC grade solvents (Aldrich) were used as received. Steady-state absorbance spectra were obtained on a Perkin Elmer Lambda 18 double-beam UV-Vis spectrophotometer with 1-nm resolution. Steady state fluorescence spectra were obtained on a Spex Fluoromax with a 4-nm bandpass and corrected for lamp spectral intensity and detector response. Transient absorption measurements were obtained with the apparatus described in detail elsewhere [12].

For hypocrellin A, the data are fit to the following function:

$$\Delta A(t) = a_1 [1-\exp(-t/\tau_1)] + a_2 \exp(-t/\tau_2) + a_3 \exp(-t/\infty) \qquad (6\text{-}1)$$

For hypocrellin B and calphostin C, however, two exponential components are sufficient to describe the data and the following form is used:

$$\Delta A(t) = a_1 [1-\exp(-t/\tau_1)] + a_2 \exp(-t/\infty) \qquad (6\text{-}2)$$

In both cases, a_1 is the amplitude of the rising component; and the infinite time constant describes a process that does not decay on the experimental time scales (up to 500 ps full scale) used in this study.

Geometry optimizations for various possible isomers of calphostin C in its electronic ground state were performed using restricted Hartree-Fock (RHF) wave functions with the 3-21G* basis set. Various starting points for the geometry optimization were tried, including "flat" structures in which the side group and the H-atom transfer region are well separated, but all searches led to one of the two structures shown in Figure 6.1. Given the complexity of the potential energy surface (more than 50 heavy atoms and many low frequency torsional modes), it is certainly possible that other local minima exist. Nonetheless, it is likely that the structures given here are among the lowest energy isomers.

Once the optimized geometries were obtained, single point energy calculations were performed with the 6-31G(d) basis set, at both stationary points and at selected points along the linear least motion (LLM) path connecting the two. All calculations were carried out using the electronic structure code GAMESS [22].

Results and Discussion

Steady state absorption and emission spectra of hypocrellins A and B and of calphostin C in ethanol are presented in Figure 6.3. Their excited-state H-atom transfer in octanol and ethanol, as monitored by transient absorbance, is illustrated in Figure 6.4 and summarized in Table 6.1. As indicated above, calphostin C lacks the 7-membered ring, which we have attributed to origin of the viscosity dependence of the H-atom transfer in hypocrellins A and B. The crucial feature revealed by the data is that its H-atom transfer

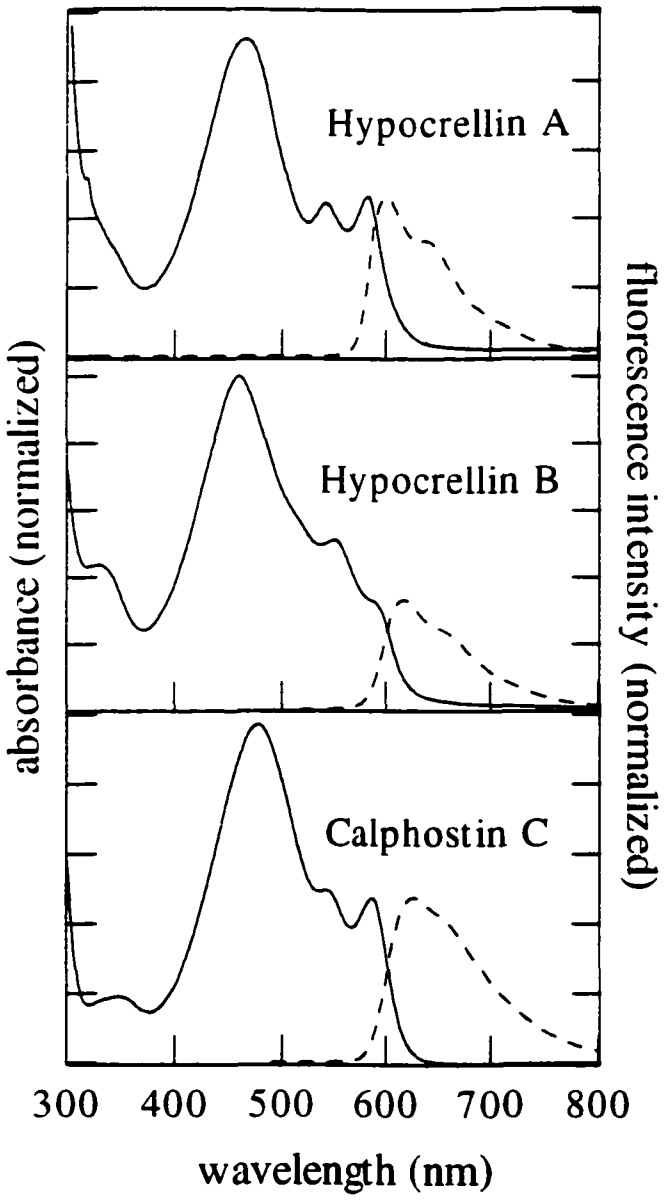

Figure 6.3 Absorption (——) and emission (- - -) spectra of hypocrellin A, hypocrellin B and calphostin C in ethanol. The spectra are normalized to the reddest absorption maximum. The excitation wavelength for the emision spectra is 477 nm.

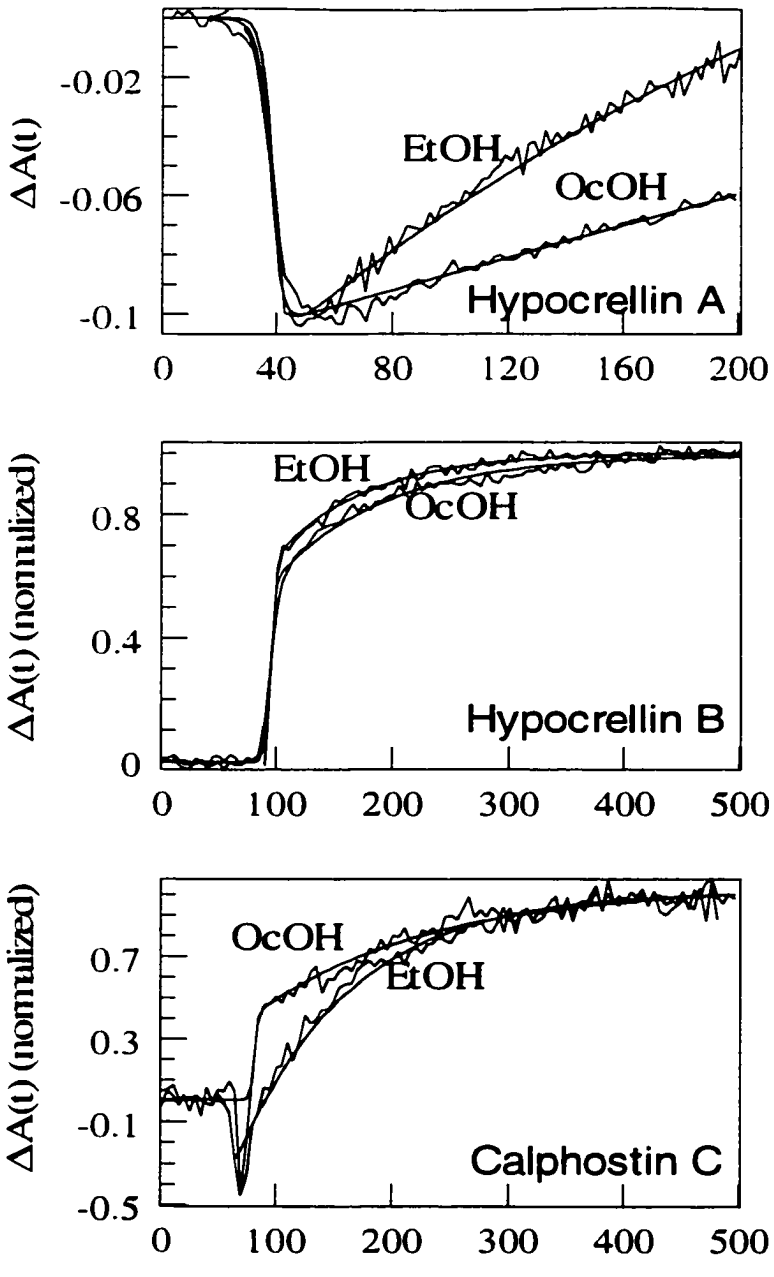

Figure 6.4 Transient absorbance traces of hypocrellin A, hypocrellin B and calphostin C in ethanol and octanol at probe wavelength of 595 nm. The global fits to the data are presented in Table 6.1.

reaction, nevertheless, exhibits a similar viscosity dependence, which we initially expected to be absent.

To rationalize this behavior, we hypothesized that there is some interaction of the bulky side chains that retard the H-atom transfer reaction. By means of *ab initio* calculations, we have discovered structures (Figure 6.5) in which the hydroxyl group of the phenolic side chain of calphostin C hydrogen bonds to the carbonyl and hydroxyl groups of the perylene quinone moiety. We propose that the large amplitude motion required for the displacement of this side chain from the carbonyl group is responsible for the slow H-atom transfer kinetics of calphostin C. We anticipate that analogs of the fundamental hypocrellin unit, 4,9-dihydroxyperylene-3,10-quinone, lacking bulky side chains, will exhibit hypericin-like 10-ps, viscosity independent time constants for H-atom transfer.

The two optimized structures both exhibit significant hydrogen bonding. The OH---OH distance in structure **1** is 1.995 Å, while the OH---O= distance in structure **2** is 1.991 Å. The O---O distances are 2.84 and 2.79 Å, respectively. At the RHF/6-31G(d) level of theory, **1** is predicted to be about 4 kcal/mol lower in energy than **2**, but the two isomers should be considered to be approximately equal in energy, given the level of theory used here. The upper limit for the H-atom transfer barrier, obtained from the LLM path is about 23 kcal/mol. Both correlation corrections and a proper transition state search would be expected to lower this estimate.

In conclusion, the similarity of the viscosity dependence of the excited-state H-atom transfer reaction of calphostin C with that of hypocrellins A and B can be explained by the interaction of its side chain and carbonyl group. This interaction, in turn, is predicted by the results of *ab initio* quantum mechanical calculations. We note that these are vacuum

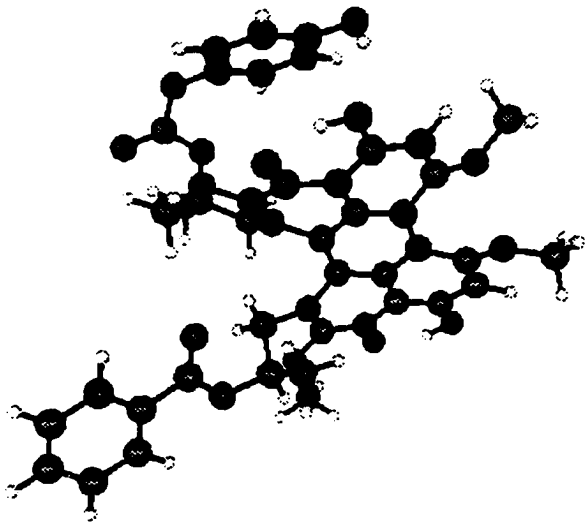

Structure **1**

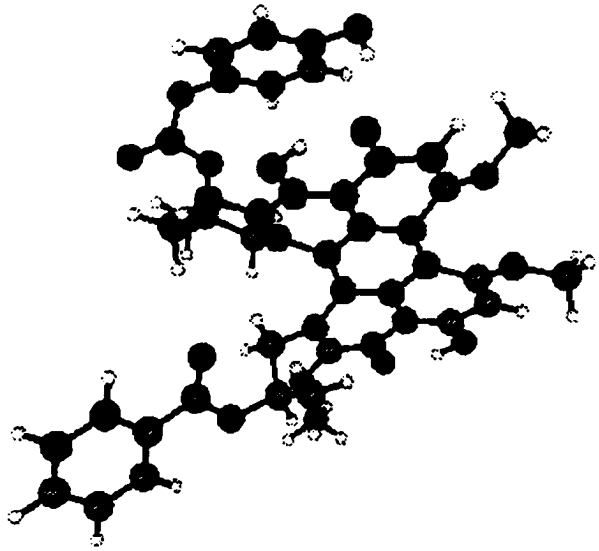

Structure **2**

Figure 6.5 Optimized structures for calphostin C. White, black and red atoms represent hydrogen, carbon and oxygen respectively.

calculations, and consequently they do not take into account any additional complications introduced by possible hydrogen bonding interactions of the phenolic side chain with the hydrogen bonding solvents used in this investigation. We note, for example, that the gas-phase dipole moments for structures **1** and **2** in Figure 6.5 are predicted to be 9.8 and 10.6 D, respectively. On the basis of a simple eletrostatic model (probably reasonable given the large dipoles, polar solvents are therefore expected to stabilize both isomers and to favor structure **2** relative to structure **1**.

Acknowledgements

This work was supported by NSF grant CHE-9613962. The calculations were performed, via a DoD Grand Challenge grant, on 256 nodes of the Cray T3E at the DoD ERDC and on 96 nodes of the IBM SP at the Maui High Performance Computation Center.

References

1. Durán, N.; Song, P. S. *Photochem. Photobiol* **1986**, *43*, 677-680.

2. Diwu, Z.; Lown, J. W. *Photochem. Photobiol.* **1990**, *52*, 609-616.

3. Diwu, Z. *Photochem. Photobiol.* **1995**, *61*, 529-539.

4. Lown, J. W. *Can. J. Chem.* **1997**, *75*, 99-119.

5. Kraus, G. A.; Zhang, W.; Fehr, M. J.; Petrich, J. W.; Wannemuehler, Y.; Carpenter, S. *Chem. Rev.* **1996**, *96*, 523-535.

6. Gai, F.; Fehr, M. J.; Petrich, J. W. *J. Am. Chem. Soc.* **1993**, *115*, 3384-3395.

7. Gai, F.; Fehr, M. J.; Petrich, J. W. *J. Phys. Chem.* **1994**, *98*, 5784-5795.

8. Gai, F.; Fehr, M. J.; Petrich, J. W. *J. Phys. Chem.* **1994**, *98*, 8352-8358.

9. English, D. S.; Zhang, W.; Kraus, G. A.; Petrich, J. W. *J. Am. Chem. Soc.* **1997**, *119*, 2980-2986.

10. English, D. S.; Das, K.; Zenner, J. M.; Zhang, W.; Kraus, G. A.; Larock, R. C.; Petrich, J. W. *J. Phys. Chem. A* **1997**, *101*, 3235-3240.

11. English, D. S.; Das, K.; Ashby, K. D.; Park, J.; Petrich, J. W.; Castner, E. W. J. *J. Am. Chem. Soc.* **1997**, *119*, 11585-11590.

12. Das, K.; English, D. S.; Fehr, M. J.; Smirnov, A. V.; Petrich, J. W. *J. Phys. Chem.* **1996**, *100*, 18275-18281.

13. Das, K.; English, D. S.; Petrich, J. W. *J. Phys. Chem. A* **1997**, *101*, 3241-3245.

14. Das, K.; English, D. S.; Petrich, J. W. *J. Am. Chem. Soc.* **1997**, *119*, 2763-2764.

15. Das, K.; Smirnov, A. V.; Snyder, M. D.; Petrich, J. W. *J. Phys. Chem. B* **1998**, *102*, 6098-6106.

16. Das, K.; Dertz, E.; Paterson, J.; Zhang, W.; Kraus, G. A.; Petrich, J. W. *J. Phys. Chem. B* **1998**, *102*, 1479-1484.

17. Das, K.; Ashby, K.; Wen, J.; Petrich, J. W. *J. Phys. Chem. B* **1999**, *103*, 1581-1585.

18. Das, K.; Smirnov, A. V.; Wen, J.; Miskovsky, P.; Petrich, J. W. *Photochemistry and Photobiology* **1999**, *69*, 633-645.

19. Smirnov, A. V.; Fulton, D. B.; Andreotti, A.; Petrich, J. W. *J. Am. Chem. Soc.* **1999**, *121*, 7979 - 7988.

20. Smirnov, A. V.; Das, K.; English, D. S.; Wan, Z.; Kraus, G. A.; Petrich, J. W. *J. Phys. Chem. A* **1999**, *103*, 7949 - 7957.

21. Kobayashi, E.; Nakano, H.; Morimoto, M.; Tamaoki, T. *Biochem. Biophys. Res. Commun.* **1989**, *159*, 548-553.

22. Schmidt, M. W.; Baldrdige, K. K.; Boatz, J. A.; Elbert, S. T.;Gordon, M. S.; Jensen, J. H.; Koseki, S.; Matsunaga, N.; Nguyen, K. A.; Su, S. J.; Windus, T. L.; Dupuis, M.; Montogomery, J. A. *J. Comput. Chem.* **1993**, *14*, 1347-1363.

CHAPTER VII: TOWARDS THE MOLECULAR FLASHLIGHT: PREPARATION, PROPERTIES, AND PHOTOPHYSICS OF A HYPERICIN-LUCIFERIN TETHERED MOLECULE

A research note accepted by *Photochemistry and Photobiology*

Jin Wen[1], Pramit Chowdhury[1], Nick J. Wills[2], Yvonne Wannemuehler[2],

Jaehun Park[1], Sarathy Kesavan[1],

S. Carpenter[23], G. A. Kraus[1,3], and J. W. Petrich[1,3]

Abstract

The synthesis of a molecule containing hypericin and luciferin moieties joined by a tether is reported. The light induced (*in vitro*) antiviral activity as well as the photophysical properties of this new compound are measured and compared to those of the parent compounds, hypericin and pseudohypericin. This tethered molecule exhibits excited-state behavior that is very similar to that of its parent compounds and antiviral activity that is identical, within experimental error, to that of its most closely related parent compound, pseudohypericin. The implications for a photodynamic therapy that is independent of external light sources are discussed.

---

[1] Department of Chemistry, Iowa State University, Ames, IA 50011-3111 USA
[2] Department of Veterinary Microbiology and Preventive Medicine, Iowa State University, Ames, IA 50011-3111 USA
[3] To whom correspondence should be addressed

Introduction

The light induced biological activity of hypericin (Figure 7.1) and its analogs, in particular their antiviral and anti tumor activities, as well as the rich photophysics they exhibit are gaining increasing notice and appreciation and have already been the subject of several reviews [1-6].

The traditional method of exploiting the light-induced activity of photosensitizers is to administer the drug to the patient and to illuminate the target area by introducing fiber optics [7-9] or to depend on external light sources to penetrate the tissue efficiently enough to excite the chromophore [10-12]. The first of these methods is invasive and only effective for localized tumors. The latter depends critically on the absorption spectrum of the photosensitizer and the spectrum intensity, and penetration efficiency of the external light source.

We have proposed an alternative method of exciting the phototherapeutic properties of hypericin, namely, by inducing a chemiluminescent reaction *in* the patient [13, 4]. We have demonstrated that the chemiluminescence produced by the reaction of luciferin and the enzyme luciferase is sufficient to induce the antiviral activity of hypericin *in vitro* [13]. Chemiluminescent activation of hypericin, however, resulted in only a tenfold reduction of viral activity under the conditions investigated, whereas illumination by ambient light provided by fluorescent bulbs resulted in greater than 10,000-fold reduction of infectious virus. It was suggested that a first step in augmenting the activity is to ensure the proximity of the light source, luciferin, and the antiviral or antitumor agent, hypericin. Here we report

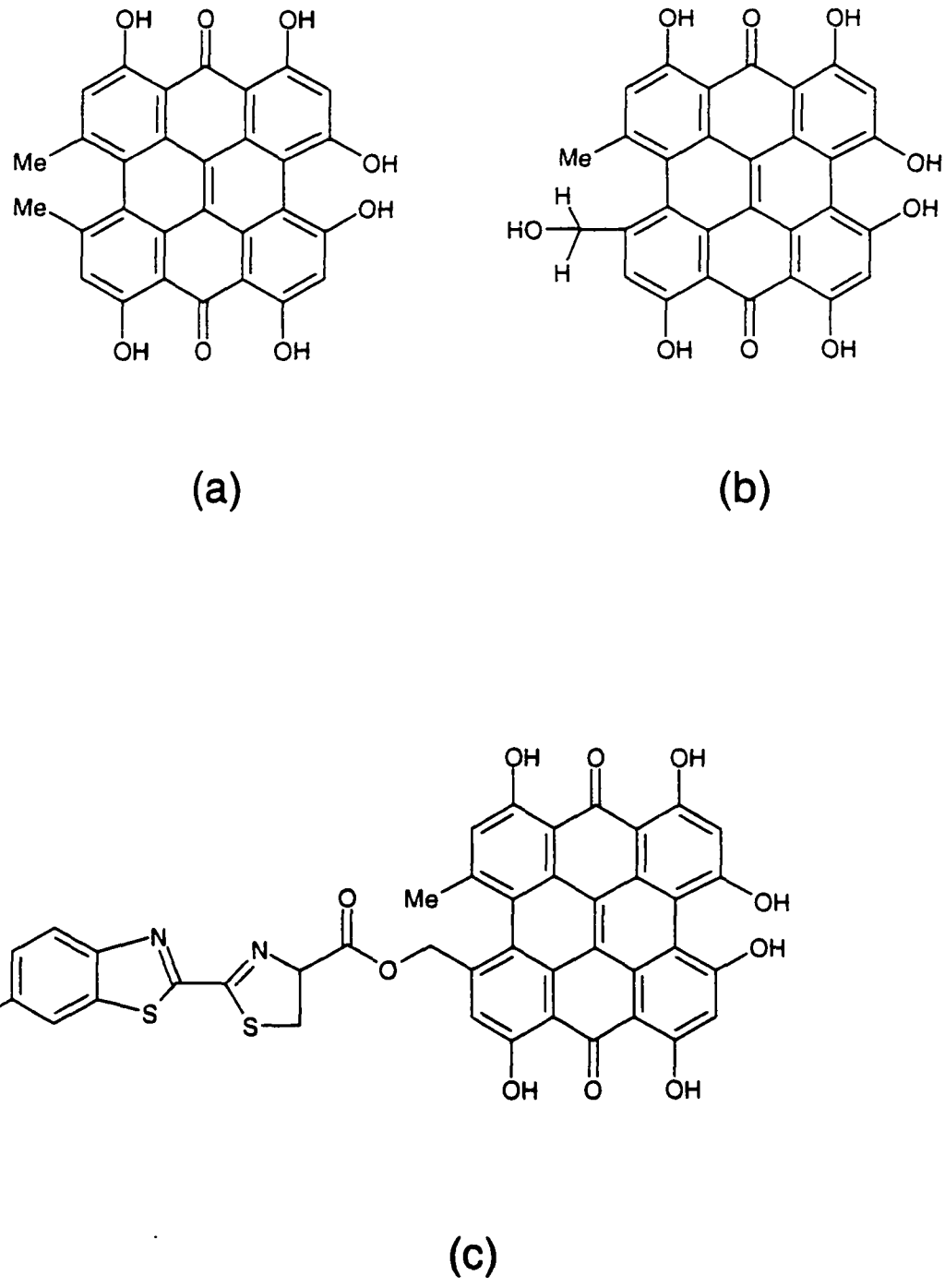

Figure7.1 Structures of (a) hypericin, (b) pseudohypericin, (c) tethered pseudohypericin – luciferin molecule.

the synthesis of such a tethered pseudo hypericin-luciferin compound (Figure 7.1) and cite some of its biological and photophysical properties. In particular, our main concern is to verify that the pseudohypericin-luciferin tethered molecule not only exhibits the same excited-state photoprocesses as its parent compounds, such as steady-state absorption and emission spectra, excited-state singlet kinetics, triplet lifetime, and singlet oxygen yield; but also, and most importantly, the same light-induced antiviral activity. In this preliminary study, the antiviral activity of the tethered molecule is excited by ambient light.

Materials and Methods

Materials: Hypericin was purchased from Molecular Probes (Eugene, OR) and was used as received. Pseudohypericin was purchased from Calbiochem (La Jolla, CA) and was used as received. Brij 35 was purchased from Aldrich (Milwaukee, WI) and was recrystallized from ethanol before use.

Preparation of Brij-35 solution: Samples were dissolved in 100 CMC Brij-35 (240 mg Brij-35 in 10 mL of pH 7.0 buffer) and sonicated for 20~40 min because of their low solubility in Brij. The concentration of the solution was ~ 10^{-6} M for steady-state and time resolved fluorescence lifetime measurements, while that for the transient absorption measurements was ~10^{-5}M. Because the tethered molecule has low solubility in Brij-35, 10^{-5}M-tethered in Brij-35 solution was prepared by adding 40uL of ~2 mM tethered molecule in DMSO into 1.2 mL Brij-35, amounting to a solution that is 3% by volume in DMSO. Doping the solution in this manner does not influence the form of the kinetic traces but significantly improves the signal-to-noise.

Synthesis of the tethered molecule: To a solution of luciferin (6 mg, 0.0214 mmol) in anhydrous methylene chloride (2 mL) at -15 °C was added N-methylmorpholine (5 mg, 0.049 mmol). The solution was stirred for 5 minutes at this temperature, after which benzylchloroformate (8 mg, 0.046 mmol) was added to get a bright yellow solution. The yellow solution was stirred at -15 °C for 15 minutes before 1-hydroxybenzotriazole (3mg, 0.022 mmol) was added. The reaction mixture was stirred for an additional 20 minutes before pseudohypericin (11 mg, 0.0213 mmol) dissolved in DMF(0.2 mL) was added, resulting in a deep red solution. The deep red solution was allowed to warm to room temperature and was stirred at room temperature for an additional 12 h. After 12 h the solvent was evaporated and the crude mixture was purified by TLC using 5:1 mixture of ethyl acetate and methanol to get 7 mg of the tethered molecule (Rf in 5:1 ethyl acetate:MeOH is 0.65). The integrity of the tethered molecule was regularly ensured by monitoring steady-state optical spectra, NMR spectra, fluorescence lifetimes, and TLC. NMR (D6-DMSO) 8.10-8.20 (M, 1 H), 7.78 (s, 1 H), 7.3-7.55 (m, 4 H), 6.55-6.60 (m, 1 H), 5.20-5.42 (m, 2 H), 4.85-5.0 (m, 2 H), 4.25-4.35 (m, 1 H), 2.7 (s, 3 H). IR 9KBr) 2957, 2923, 2854, 1584, 1186, 1100. UV 213, 286, 327, 546, 589 nm.

Singlet oxygen assay: A 1-kHz Nd: YLF (Quantronix) was used to excite samples at 527nm. The excitation irradiance at samples was 13 mW/cm^2. Fluorescence and scattered light were blocked by a 1270 ± 40 nm interference filter fastened to a liquid nitrogen cooled charge-coupled device (North Coast EO-817L). The excitation beam was chopped at 400 Hz and the output of the detector was fed to a lock-in amplifier (Standford Research SR510), which provided the signal, S, proportional to the intensity of the singlet oxygen luminescence. Unless otherwise indicated, rose bengal in DMSO was used as the standard

for the singlet oxygen yield, $\Phi = 0.162$ (14). The relative quantum yield and the quantum yield of singlet oxygen were calculated as below:

$$\Phi_{rel} = \frac{S^{sample}}{S^{standard}} \frac{1-10^{-OD_{527nm}^{standard}}}{1-10^{-OD_{527nm}^{sample}}} \qquad (7-1)$$

$$\Phi = \Phi_{rel} \times 0.162 \qquad (7-2)$$

where the optical density, OD, was measured at the excitation wavelength of 527 nm. The OD of compounds was ~0.2. The measured Φ values reported in Table 1 represent the average of three experiments.

Flash photolysis: Flash photolysis measurements were performed with a system based on a 10 Hz Surelite (Continuum, Santa Clara, CA) Nd:YAG laser with 100 mW of 532-nm radiation and an Arc lamp (Photon Technology International, Lawrenceville, NJ). Fluorescence and scattered light were blocked by an 8-nm band-pass monochromator at 520 nm before the photomultiplier. Triplet transient absorbance data were collected by a two channel, 100 MHz oscilloscope (Tektronix, TDS 220, Beaverton, OR) and analyzed by Igor Pro software (WaveMetrics Inc., Lake Oswego, OR).

Time-resolved Pump-Probe Absorption Spectroscopy. The apparatus used for ultrafast kinetic measurements is described in detail elsewhere [15, 16].

Anitviral Assays. The MA-1 isolate of equine infectious anemia virus (EIAV) [17] was used for antiviral assays as previously described [13]. Briefly, cell free virus was diluted to approximately 10^5 focus forming units (FFU) in Hanks buffered saline solution, treated with a 20-μM final concentration of tethered molecule, hypericin, pseudohypericin, or luciferin and incubated for 30 minutes in light (or dark). The total light exposure was

equivalent to 16.3 J/cm^2. Serial ten-fold dilutions of treated virus were then inoculated onto equine dermal cells (ATCC CCL57) and the titer of infectious virus was quantified by a focal immunoassay as described previously [13]. Results are expressed as reduction in infectious virus as compared to the DMSO control.

Results and Discussion

The photophysical properties of hypericin, pseudohypericin, and the tethered molecule are studied in two systems, DMSO and Brij-35 micelles, in order to compare them in bulk solvent and in organized media crudely mimicking a cell. Figure 7.2 and figure 7.3 present the absorption and emission spectra of the three hypericin derivatives considered here in DMSO and in Brij-35 micelles. The spectra are in general quite similar, but there are some notable differences: the enhanced absorption at ~400 nm for pseudohypericin in micelles and the lack of fluorescent emission from the luciferin moiety of the tethered molecule in micelles. (The latter is the result of the environment on the emission of the luciferin (inset to Figure 7.3c). In micelles, the maximum is more intense at ~550 nm rather than at ~440 nm in DMSO. That the 550-signal is significantly attenuated in the tethered molecule may partially be attributed to energy transfer to pseudohypericin; although it is not clear why energy transfer is not as effective in DMSO.) Figure 7.4 presents a comparison of the transient absorption at a probe wavelength of 600 nm, for all the three compounds in both DMSO and Brij. The parameter obtained from fitting these data are summarized in Table 7.3. In both solvents the rise time of stimulated emission that we have attributed to excited-state intramolecular H-atom transfer is present. The possible biological significance of this process is discussed in much detail elsewhere [6, 18-20].

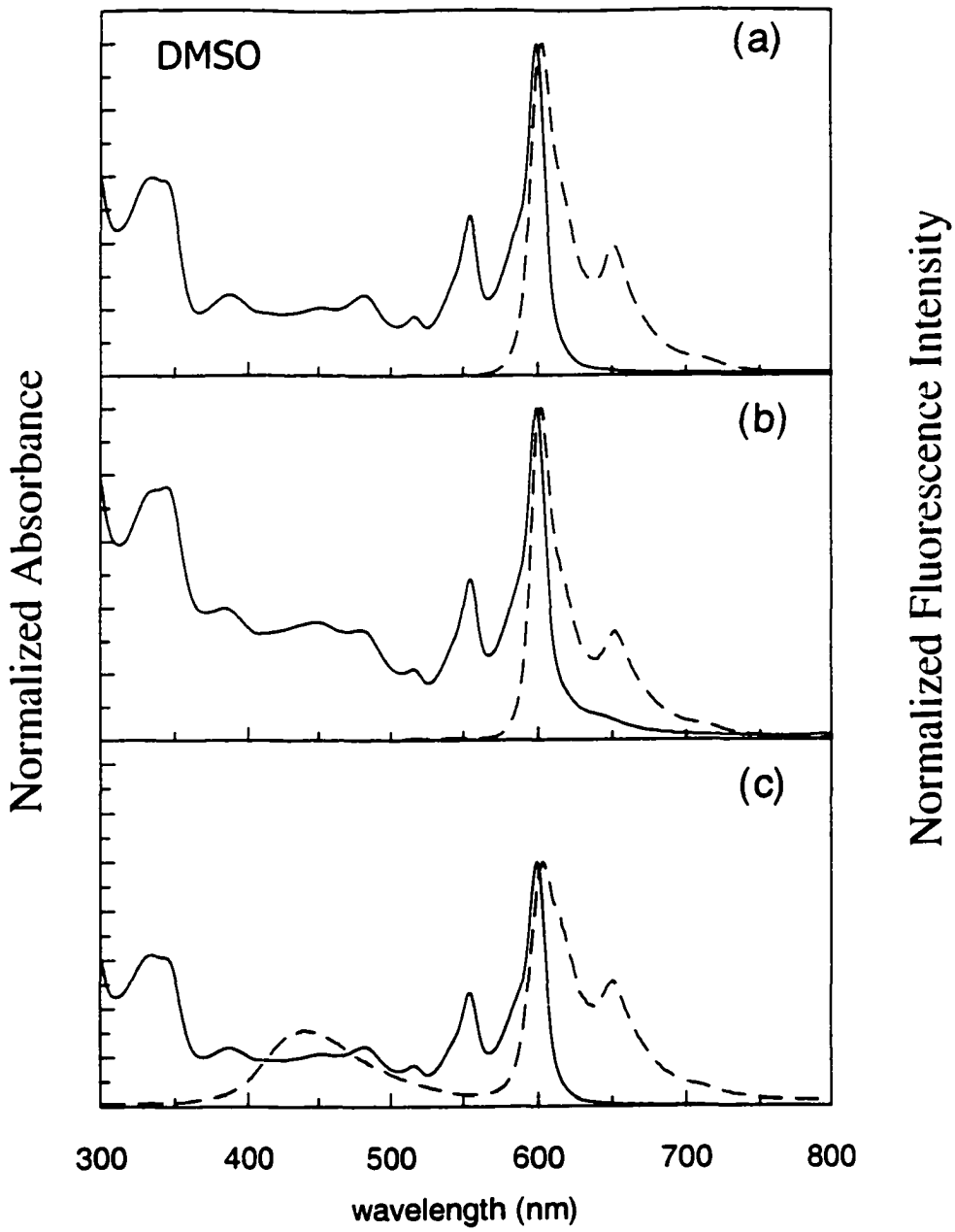

Figure 7.2. Comparison of the absorption (solid lines) and fluorescence emission(dashed lines) spectra of (a) hypericin, (b) pseudohypericin and (c) tethered pseudo hypericin – luciferin molecule in DMSO. The excitation wavelength for (a) and (b) was 500 nm; and for (c) it was 290 nm.

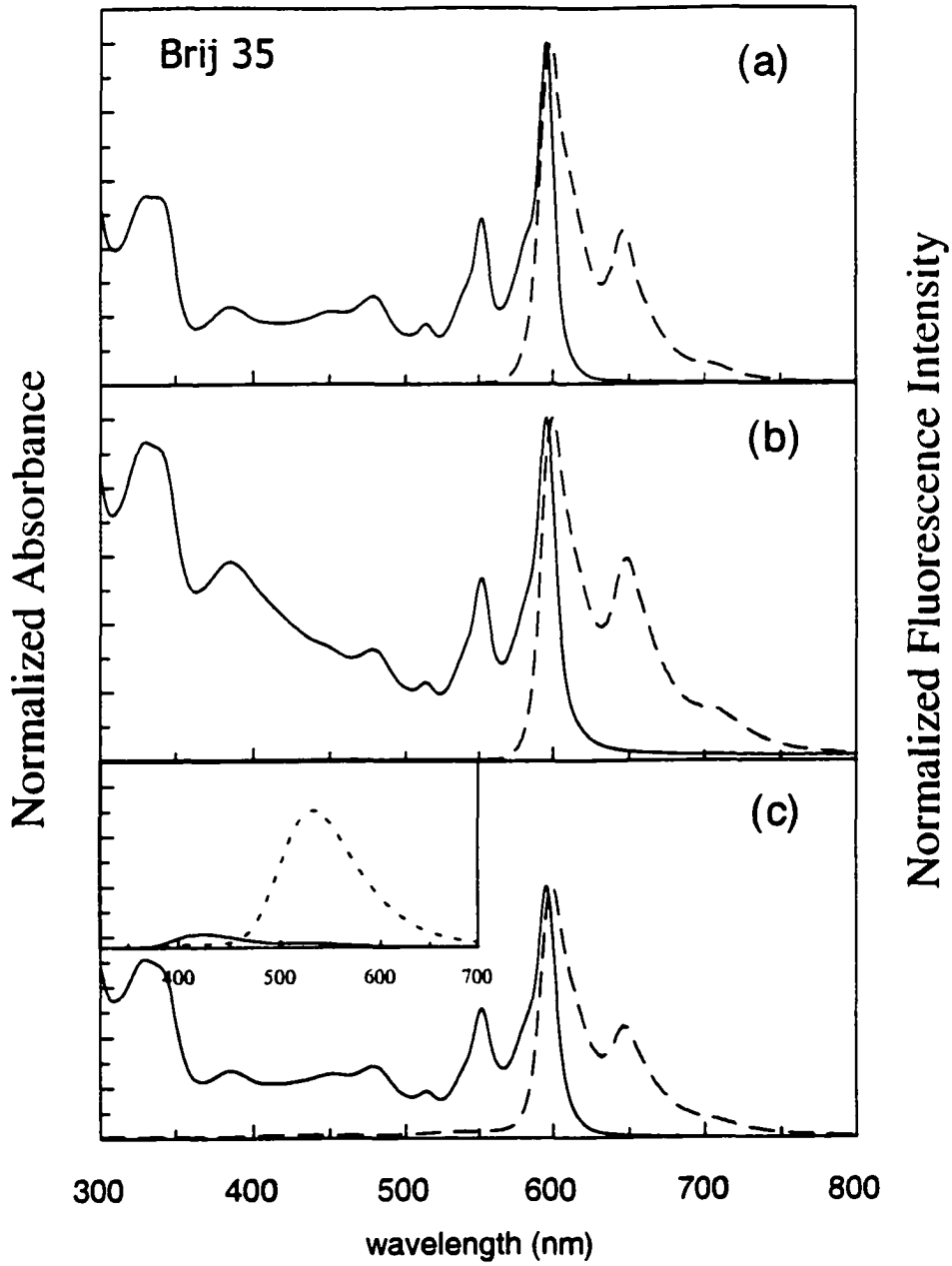

Figure 7.3 Comparison of the absorption (solid lines) and fluorescence emission (dashed lines) spectra of (a) hypericin, (b) pseudohypericin and (c) tethered pseudo hypericin – luciferin molecule in Brij-35. Excitation wavelength for (a) and (b) was 500 nm and for (c) was 290 nm. Inset of panel (c): emission spectra of luciferin in DMSO (—) and in Brij35 (- - -), λex = 290nm. The concentration of luciferin is the same for both solvents, ~4×10^{-5} M.

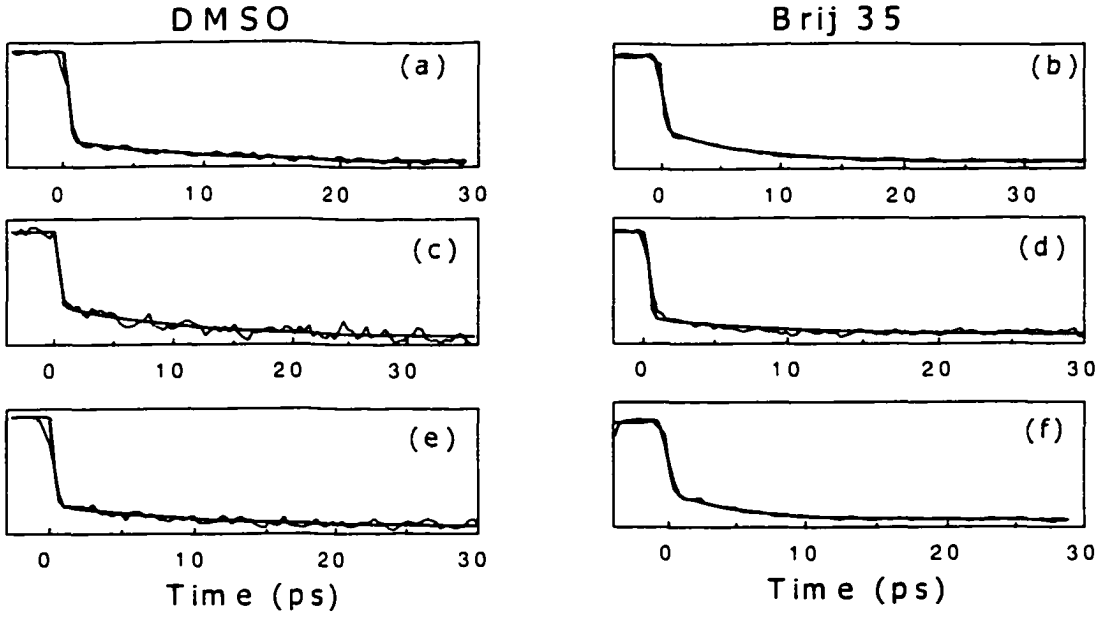

Figure 7.4 Transient absorption traces (ΔA vs. time) of hypericin (a), hypericin in DMSO (b) hypericin in Brij doped with 3% DMSO (by volume), (c) pseudohypericin in DMSO, (d) pseudohypericin in Brij, (e) tethered molecule in DMSO and (f) tethered molecule in Brij doped with 3% DMSO (by volume). λ_{pump}(for all samples) = 407 nm; probe wavelength for all the samples was 600 nm. The fitting parameters are reported in Table7.3.

Table 7.3: Parameters obtained from the fit of the transient absorption data[a].

sample	a_1	τ_1(ps)	a_2
Hypericin in DMSO	0.19	8.2	-1.00
Hypericin in Brij (3% DMSO)	0.32	8.0	-1.00
Pseudohypericin in DMSO	0.30	10.3	-1.00
Pseudohypericin in Brij	0.17	9.6	-1.00
Tethered molecule in DMSO	0.20	10.3	-1.00
Tethered molecule in Brij (3% DMSO)	0.30	4.9	-1.00

[a] Transient absorption data are fit to the function: $\Delta A(t) = a_1 \exp(-t/\tau_1)+a_2 \exp(-t/\tau_2)$. In all cases, $\tau_2 = \infty$ since the time scale on which the experiment is performed does not permit the determination of this longer-lived component. For all the samples λ_{pump} = 407 nm and λ_{probe} = 600 nm.

Table 7.1: Fluorescence lifetime parameters

Sample	a_1	τ_1 (ps)	a_2	τ_2 (ps)	a_3	τ_3 (ps)
Hypericin in DMSO[(a)]	1.0	5600 ± 200				
Pseudo Hypericin in DMSO[(a)]	1.0	5200 ± 300				
Tethered Molecule in DMSO[(a)]	1.0	5040 ± 40				
Hypericin in Brij-35[(a)]	0.92 ± 0.02	6600 ± 100	0.08 ± 0.02	820 ± 50		
Pseudo Hypericin in Brij-35[(a)]	0.90 ± 0.02	5590 ± 60	0.10 ± 0.02	970 ± 40		
Tethered Molecule in Brij-35[(a)]	0.91 ± 0.02	5700 ± 100	0.09 ± 0.02	780 ± 50		
Luciferin in DMSO[(b)]	0.06 ± 0.02	2690 ± 10	0.59 ± 0.02	210 ± 10	0.36 ± 0.01	75 ± 10
Luciferin in Brij35[(b)]	0.23 ± 0.03	4900 ± 300	0.18 ± 0.01	610 ± 80	0.59 ± 0.03	90 ± 5

(a) The sample was excited at 580nm and the emission was collected after 610 nm through a cut-off filter. Fluorescence lifetimes were fit to a sum of up to two exponentially decaying components: $F(t) = a_1 \exp(-t/\tau_1) + a_2 \exp(-t/\tau_2)$. The absence of values for a_2 and τ_2 indicates that the lifetime was adequately described by a single exponential decay. The data were the average of 3 data sets. $\chi^2 \leq 1.2$ for all data presented in the table.
(b) The sample was excited at 290 nm and the emission was collected after 370 nm through a cut-off filter. Fluorescence lifetimes were fit to a sum of three exponentials: $F(t) = a_1 \exp(-t/\tau_1) + a_2 \exp(-t/\tau_2) + a_3 \exp(-t/\tau_3)$. The data were the average of 3 data sets. $\chi^2 \leq 1.2$ for all data presented in the table.

The most important result to be obtained from this comparative study, however, is that as indicated by the kinetics measured with subpicosecond resolution, the primary photoprocess in these three compounds appear to be the same. Table 7.1 compares the behavior of the longer lived singlet states of these molecules by comparing their fluorescence lifetimes. It is interesting that in going from DMSO to Brij-35, the lifetimes all acquire a shorter-lived subnanosecond component that represents about 10% of the fluorescence intensity. The shorter component most likely does not arise from quenching interactions from nearby or aggregated hypericin chromophores because at the concentrations used there is only 1 hypericin molecule for every 250 micelles. This behavior is not unprecedented. We have observed the generation of shorter lived fluorescence lifetime components in all the hypericin complexes we have investigated, whether they be with Brij micelles, human serum albumin, myoglobin, or DNA [21]. An important point to resolve is the origin of the nonradiative processes that are induced upon binding to larger macromolecules. The lifetimes of the hypericin moieties reported in Table 7.1 are obtained using 580-nm, visible, excitation instead of bluer or ultraviolet wavelengths in order to avoid stimulating fluorescence either from trace impurities that may be contained in the Brij preparation or from the luciferin partner of the tethered molecule. (The last two entries of Table 7.1 are control experiments demonstrating that luciferin emission does not contribute to the hypericin fluorescence lifetimes we quote. The fluorescence lifetime of luciferin is well described by 3 decaying components, in agreement with other results [22]. What is interesting is that the weights and duration of the lifetime components change significantly on introduction to the micellar environment. Excitation of Brij35 only at 290 nm affords no detectable fluorescence.)

Table 7.2: Singlet Oxygen Yields and Triplet Lifetimes

Compound [a]	solvent	Φ ($^1O_2$)	Triplet Lifetime (μs)
Hypericin	DMSO	0.34 ± 0.02 [b]	73 ± 15
Hypericin	Brij-35	0.72 [c]	2.15 ± 0.05
Pseudohypericin	DMSO	0.44 ± 0.03 [b]	71 ± 18
Pseudohypericin	Brij-35	0.96 ± 0.03 [c]	2.60 ± 0.15
Tethered molecule	DMSO	0.36 ± 0.02 [b]	52 ± 15
Tethered molecule	Brij-35	1.04 ± 0.03 [c]	3.00 ± 0.17

[a] Molecular oxygen concentrations are determined by atmospheric pressure. Samples were not degassed for triplet lifetime measurements.
[b] Singlet oxygen yields are taken relative to that of rose bengal in DMSO, $\Phi = 0.162$ (14)
[c] Hypericin in Brij-35 was used as a standard for singlet oxygen yields: $\Phi = 0.72$; [Brij35] = 1.25 mM. pH = 7.0 (25).

Reactive oxygen species are generated through the triplet species of the photosensitizing drug. Table 7.2 summarizes both the triplet lifetimes and the quantum yields of singlet oxygen. In all cases, the triplet lifetime decreases roughly one hundred fold in going from DMSO to micelles, corresponding to an increase in singlet oxygen yield of a factor of two to three. In Brij-35, the singlet oxygen yield of pseudohypericin and of the tethered molecule is unity, within experimental error.

Treatment of virus with the tethered molecule resulted in a significant reduction in virus infectivity (Figure 7.5). The antiviral activity of the tethered molecule is equivalent to that of pseudohypericin, which is to be expected since pseudohypericin is the base molecule for the synthesis of the tethered species. However, both pseudohypericin and the tethered molecule were about 1000 times less effective than hypericin in reducing virus infectivity. The $-CH_2OH$ group in the bay region of pseudohypericin (Figure 7.1b), which affords pseudohypericin a "handle" for the tethering of luciferin, is absent on hypericin and may

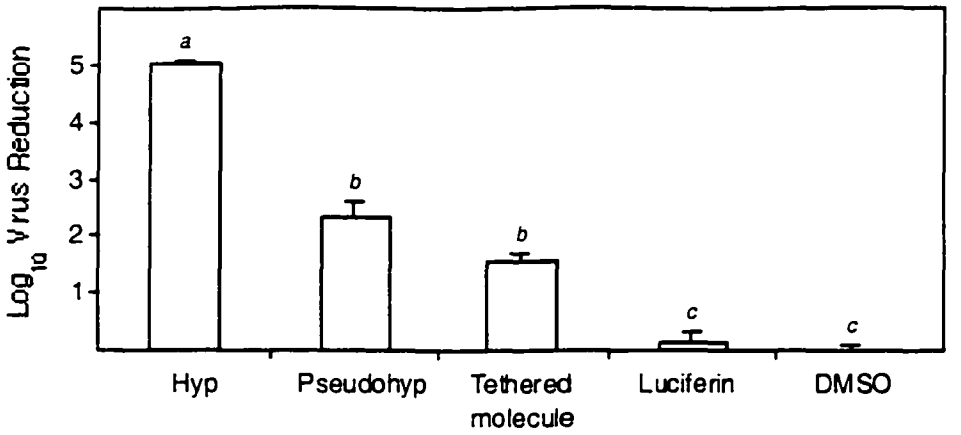

Figure 7.5 Antiviral activity of the tethered molecule and related compounds. Light induced antiviral activity of tethered molecule. Virus infectivity was assayed following treatment with tethered molecule and related compounds. DMSO and luciferin samples were used as negative controls. Results are expressed as the mean $\log_{10}$ virus reduction as compared to DMSO, with error bars representing the standard error of the mean. Results were analyzed by Student's t-test. Treatments with the same letter above the bar are not statistically significant from each other.

contribute to the reduced antiviral activity of pseudohypericin as compared to hypericin. The factors contributing to the relative antiviral and antitumor activities of photoactive compounds are rather complicated to assess, as indicated in two recent articles dealing with cytotoxicity [23, 24]. In particular, a proper comparison of a series of such analogs must carefully consider their: 1) association with the target; 2) absorption spectrum; 3) and excited-state photochemistry [24]. It has been proposed that this lower activity can be attributed to the lower extinction coefficient of pseudohypericin with respect to that of hypericin [24].

Conclusion

We have demonstrated the synthesis of pseudohypericin-luciferin tethered molecule, which we ultimately intend to be employed as part of our proposed "molecular flashlight"

[13]. An important preliminary to any studies employing chemiluminescence or the expression of bioluminescent molecules in cellular systems is to ensure that the presence of the tethered luciferin moiety does not adversely affect the photoprocesses of its hypericin partner, which are known or suggested to be responsible for its biological and medicinal activity. That such should be the case is not obvious. For example, it could reasonably be argued that the proximity of the luciferin moiety in the tethered molecule might scavenge singlet oxygen species. This work has demonstrated that in bulk solvent and in micelles, which crudely mimic a cell, the relevant photophysical parameters of the tethered molecule are very similar or identical within experimental error those of hypericin and pseudohypericin. Finally, we have shown that the tethered molecule maintains the antiviral activity of its most closely related parent compound, pseudohypericin.

Acknowledgements

This work was funded by NSF grant CHE-9613962 (JWP, GAK), and NIH grant R21 GM57351 (SC, JWP, GAK). We thank Dr. Andreja Bakac and Professor William Jenks for the loan of their infrared detectors, which we used for measurements of singlet oxygen yields.

References

1. Duran, N., and P. S. Song. (1986). Hypericin and its photodynamic action. *Photochem. Photobiol.* **43**, 677-680.
2. Lown, J. W. (1997). Photochemistry and photobiology of perylenequinones. *Can. J. Chem.* **75**, 99-119.
3. Diwu, Z. (1995). Novel therapeutic and diagnostic applications of hypocrellins and hypericins. *Photochem. Photobiol.* **61**, 529-539.

4. Kraus, G. A., W. Zhang, M. J. Fehr, J. W. Petrich, Y. Wannemuehler, and S. Carpenter. (1996). Research at the Interface between Chemistry and Virology: Development of a Molecular Flashlight. *Chem. Rev.* **96**, 523-535.

5. Falk, H. (1999). From the Photosensitizer Hypericin to the Photoreceptor Stentorin--The Chemistry of Phenanthroperylene Quinones. *Angew. Chem. Int. Ed.* **38**, 3116-3136.

6. Petrich, J. W. (2000). Excited-State Intramolecular H-Atom Transfer in Nearly Symmetrical Perylene Quinones: Hypericin, Hypocrellin, and their Analogs. *International Reviews in Physical Chemistry.* **19**, 479-500.

7. D'Hallewin, M. A., L. Baert, J. P. A. Marijnissen, and W. M. Star. (1992). Whole bladder wall photodynamic therapy with *in situ* light dosimetry for carcinoma in situ of the bladder. *J. Urol.* **148**, 1152-1155.

8. Kriegmair, M., R. Baumgartner, L. R. Waidelich, and A. Hofstetter. (1996). Early clinical experience with 5-aminolevulinic acid for the photodynamic therapy of superficial bladder cancer. *Brit. J. Urol.* **77**, 667-671.

9. Nseyo, U. O., J. DeHaven, T. J. Dougherty, W. R. Potter, D. L. Merrill, S. L. Lundahl, and D. L. Lamm. (1998). Photodynamic therapy (PDT) in the treatment of patients with resistant superficial bladder cancer: A long term experience. *Journal of Clinical Laser Medicine & Surgery.* **16**, 61-68.

10. Dougherty, T. J., C. J. Gomer, B. W. Henderson, G. Jori, D. Kessel, M. Korbelik, J. Moan, and Q. Peng. (1998). Photodynamic therapy. *J. Nat. Cancer. Inst.* **90**, 889-905.

11. Xie, X., J. B. Hudson, and E. S. Guns. (2001). Tumor-specific and photodependent cytotoxicity of hypericin in the human LNCaP prostate tumor model. *Photochem. Photobiol.* **74**, 221-225.

12. Alecu, M., C. Ursaciuc, F. Halalau, G. Coman, W. Merlevede, E. Waelkens, and P. de Witte. (1998). Photodynamic treatement of basal cell carcinoma and squamous cell carcinoma with hypericin. *Anticancer Res.* **18**, 4651-4654.

13. Carpenter, S., M. J. Fehr, G. A. Kraus, and J. W. Petrich. (1994). Chemiluminescent activation of the antiviral activity of hypericin: a molecular flashlight. *Proc. Natl. Acad. Sci. U. S. A.* **91**, 12273-12277.

14. Redmond, R. W., and J. N. Gamlin. (1999). A compilation of singlet oxygen yields from biologically relevant molecules. *Photochem. Photobiol.* **70**, 391-475.

15. English, D. S., K. Das, J. M. Zenner, W. Zhang, G. A. Kraus, R. C. Larock, and J. W. Petrich. (1997). Hypericin, Hypocrellin, and Model Compounds: Primary Photoprocesses of Light-Induced Antiviral Agents. *J. Phys. Chem. A.* **101**, 3235-3240.

16. English, D. S., W. Zhang, G. A. Kraus, and J. W. Petrich. (1997). Excited-State Photophysics of Hypericin and Its Hexamethoxy Analog: Intramolecular Proton Transfer as a Nonradiative Process in Hypericin. *J. Am. Chem. Soc.* **119**, 2980-2986.

17. Carpenter, S., L. H. Evans, M. Sevoian, and B. Chesebro. (1987). Role of the host immune response in selection of equine infectious anemia virus variants. *J. Virol.* **61**, 3783-3789.

18. Showalter, B. M., A. Datta, P. K. Chowdhury, J. Park, P. Bandyopadhyay, P. K. Choudhury, S. Kesavan, Y. Zeng, G. A. Kraus, M. S. Gordon, J. P. Toscano, and J. W. Petrich. (2001). Identification of a vibrational frequency corresponding to H-atom translocation in hypericin. *Photochem. Photobiol.* **74**, 157-163.

19. Chaloupka, R., F. Sureau, E. Kocisova, and J. W. Petrich. (1998). Hypocrellin A photosensitization involves an intracellular pH decrease in 3T3 cells. *Photochem. Photobiol.* **68**, 44-50.

20. Fehr, M. J., M. A. McCloskey, and J. W. Petrich. (1995). Light-Induced Acidification by the Antiviral Agent Hypericin. *J. Am. Chem. Soc.* **117**, 1833-1836.

21. Das, K., A. V. Smirnov, J. Wen, P. Miskovsky, and J. W. Petrich. (1999). Photophysics of hypericin and hypocrellin A in complex with subcellular components: Interactions with human serum albumin. *Photochemistry and Photobiology.* **69**, 633-645.

22. Grishanin, B. A.; A.Y. Chikishev, N. I. Koroteev, V. D.Vachev, and V. N. Zadkov. (1994) Fast (pico- and femtosecond) reaction dynamics in the excited states of large molecules: Fluorescence studies and computer simulations. *Verh. - K. Ned. Akad. Wet., Afd. Natuurkd., Eerste Reeks.* **42**, 169-195.

23. Delaey, E. M., R. Obermueller, I. Zupko, D. De Vos, H. Falk, and P. A. M. de Witte. (2001). *In vitro* study of the phototoxicity of some hypericin analogs on different cell lines. *Photochem. Photobiol.* **74**, 164-171.

24. Wills, N. J., J. Park, J. Wen, S. Kesavan, G. A. Kraus, J. W. Petrich, and S. Carpenter. (2001). Tumor cell toxicity of hypericin and related analogs. *Photochem. Photobiol.* **74**, 216-220.

25. Racinet, H., P. Jardon, and R. Gautron. (1988). Formation d'oxygène sigulet photosensibilisée par l'hypericine étude cinétique en milieu micillaire non ionique. *J. Chim. Phys.* **85**, 971-977.

CHAPTER VIII: SUMMARY AND CONCLUSIONS

This dissertation illustrates diverse laser techniques and their applications in photochemical and biophysical studies. Picosecond time-correlated single photon counting provides a powerful tool to study the fluorescence lifetime of most molecules and to investigate the dynamics of proteins. The ultrafast pulses of the 30Hz transient spectrometer allow us to investigate primary photoprocess in picosecond time scale, for example excited-state H-atom transfer.

In chapter III, time-resolved fluorescence and absorption measurements are performed to compare the photophysics of hypericin and hypocrellin A in complex with subcellular components, for example human serum albumin. Energy transfer from the tryptophan residue of HSA to hypericin is very efficient and is characterized by a critical distance of 94 Å, from which we estimate a time constant for energy transfer of $\sim 3\times10^{-15}$ s. There is no evidence for energy transfer from tryptophan to hypocrellin. The result is consistent with Raman studies that suggest the carbonyl oxygen of hypericin interacts with the N_1-H of the single tryptophan residue present in IIA subdomain of HSA [1].

In chapter IV, we have exploited the fluorescence properties of the tryptophan chromophore to investigate the structure conformation of porcine fructose-1,6-bisphosphatase (Trp^{57}FBPase). The sensitivity of tryptophan chromophore to the polarity of its environment allows us to elucidate protein dynamics and structure. The results from time-resolved fluorescence measurement are consistent with the predictions made on the basis of X-ray crystal structures of Trp^{57}FBPase.

Our previous studies [2-5] provided some evidence for the excited-state H-atom transfer in hypericin and hypocrellin. Hypericin was observed to perform an intramolecular excited-state H-atom transfer in ~10ps [6] and this reaction is independent of solvent. On the other hand, the excited H-atom transfer in hypocrellin was observed to be strongly viscosity dependent. In chapter V, a comparison of the photophysics of hypocrellin A and B provides a base to understand the importance of the 7-membered ring and how its conformation influences the excited state H-atom transfer. A simple model is proposed to describe the hypocrellin B photophysics. In chapter VI, the results of transient absorption measurements and *ab initio* quantum mechanical calculations on calphostin C gives more evidence that the viscosity dependence of the excited state H-atom transfer reaction of calphostin C with that of hypocrellins can be explained by the interaction of its side chain and carbonyl group. The perylene quinines, hypocrellin, hypericin and their analogs are of interest because of their light-induced biological properties, i.e. antiviral and antitumor activity.

In chapter VII, a new compound, a hypericin-luciferin tethered molecule, is proposed as a potential photosensitizer in photodynamic therapy. This new molecule provides an alternative method of exciting the phototherapeutic properties of hypericin by inducing a chemiluminescent reaction in the patient. This study indicates that the tethered molecule exhibits similar excited-state behavior and antiviral activity as its parent compound, hypericin.

References

1. Miskovsky, P.; Jancura, D.; Sanchez-Cortes, S.; Kocisova, E.; Chinsky, L. (1998) Antiretrovirally Active Drug Hypericin Binds the IIA Subdomain of Human Serum Albumin: Resonance Raman and Surface-Enhanced Raman Spectroscopy Study. *J. Am. Chem. Soc.* **120**, 6374-6379.
2. Gai, F.; Fehr, M. J.; Petrich, J. W. (1993) Ultrafast excited-state processes in the antiviral agent hypericin. *J. Am. Chem. Soc.* **115**, 3384-3385.
3. Gai, F.; Fehr, M. J.; Petrich, J. W. (1994) Role of Solvent in Excited-State Proton Transfer in Hypericin. *J. Phys. Chem.* **98**, 8352-8358.
4. Fehr, M. J.; McCloskey, M. A.; Petrich, J. W. (1995) Light-Induced Acidification by the Antiviral Agent Hypericin. *J. Am. Chem. Soc.* **117**, 1833-1836.
5. English, D. S.; Das, K.; Zenner, J. M.; Zhang, W.; Kraus, G. A.; Larock, R. C.; Petrich, J. W. (1997) Hypericin, Hypocrellin, and Model Compounds: Primary Photoprocesses of Light-Induced Antiviral Agents. *J. Phys. Chem. A* **101**, 3235-3240.
6. Smirnov, A. V.; Das, K.; English, D. S.; Wan, Z.; Kraus, G. A.; Petrich, J. W. (1999) Excited-State Intramolecular H Atom Transfer of Hypericin and Hypocrellin A Investigated by Fluorescence Upconversion. *J. Phys. Chem. A* **103**, 7949-7957.

ACKNOWLEDGMENTS

First and foremost, I would like to thank my major professor, Jacob W. Petrich, for his encouragement and patience throughout my graduate studies. Without his support, little of this dissertation would exist.

I wish to acknowledge all the group members who contribute support, insight and encouragement to me throughout the past five years. Kaustuv Das led me into the LASER world. Thanks for his patience and time he took to explain things in the way I could understand. I also would like to thank Anindya Dutta, Kyle Ashby, Jaehun Park and Pramit Chowdhury for their friendship and assistance. I especially want to thank Dr. Joseph Burnett, for his friendship and kindness.

Finally, I would like to thank my mom and dad for their love, patience and support throughout my education. I thank my husband, Shuquan, for his love and encouragement all the time, especially during I wrote this dissertation. I appreciated your support.